

## COMPUTATIONAL CHALLENGES IN ESS

H. Danared, M. Eshraqi, E. Laface, R. Miyamoto, S. Molloy and A. Ponton,  
European Spallation Source, Box 176, SE-221 00 Lund, Sweden

### Abstract

The European Spallation Source, ESS, will be based on a 2.5-GeV, 50-mA superconducting proton linac delivering 5 MW of beam power to a rotating tungsten target. ESS is a challenging project in many respects, not the least with respect to RF power and RF sources. Because of the high power, relative beam losses must be very small to avoid activation and allow hands-on maintenance of accelerator components. The beam-dynamics calculations required to ensure these low beam losses are thus another challenge. This paper gives an introduction to ESS and the ESS linac, discusses briefly computational aspects in general, and presents specific examples of computational problems from beam dynamics and RF cavity design as well as efforts initiated to benchmark beam-dynamics codes for beam parameters relevant to ESS.

### ESS AND THE ESS LINAC

Lund was selected as the site for the European Spallation Source, ESS, in 2009, and a year later, the ESS Accelerator Design Update, ADU, Project was launched. This project is a collaboration between universities and institutes in five European countries with additional participation and support from accelerator laboratories in many countries inside and outside of Europe. One of the primary outputs from the ADU Collaboration and of the ESS design effort as a whole will be a Technical Design Report at the end of 2012. This will be accompanied by a cost report, time schedule and other documents needed for the final approval of the construction of ESS.

Many of the parameters of the current ESS project [1] are similar to those of the ESS Design Study from 2003/2004 [2]. A major change is that the short-pulse source has been abandoned, based on studies showing that a large fraction of the science foreseen at ESS can be done as well or better with a long-pulse source [3]. Thus, no accumulator ring is required, and the linac can accelerate protons instead of  $H^-$  ions. Significant progress has also been made in the field of superconducting RF since 2003. As a consequence, the CCL copper cavities have been replaced by superconducting spoke cavities, and the output energy of the linac has increased while the

Table 1: Selected ESS Top-level Parameters

Parameter	Unit	Value
Average beam power	MW	5
Proton kinetic energy	GeV	2.5
Average macro-pulse current	mA	50
Macro-pulse length	ms	2.86
Pulse repetition rate	Hz	14
Maximum cavity surface field	MV/m	40

current has decreased.

Top-level parameters of the ESS linac are summarized in Table 1. The linac will accelerate 50 mA of protons to 2.5 GeV in pulses that are 2.86 ms long and come with a repetition rate of 14 Hz. This implies that the average beam power on the target will be 5 MW, as in the 2003 ESS study, and the peak power will be 125 MW. The linac will have a normal-conducting front-end up to 79 MeV followed by three families of superconducting cavities and a high-energy beam transport to the spallation target which will consist of a rotating tungsten wheel.

A go-ahead for construction is expected in early 2013. Then will follow an intense period of detailed design and prototyping. The most critical components are cry-modules and RF sources, where worldwide production capacity will be a limiting factor. Acceptance tests at the site in Lund and installation work in the linac tunnel and the klystron gallery will also be time-consuming. Nevertheless, the current plan calls for first neutrons from the spallation target in 2019.

### LINAC DESIGN

The configuration of the current, May 2012 Baseline linac is shown schematically in Fig. 1, and selected linac parameters are listed in Table 2 [4]. The warm linac has contributions from INFN Catania, CEA Saclay, ESS-Bilbao and INFN Legnaro, the superconducting cavities and their cryomodules are designed at IPN Orsay and CEA Saclay, and the HEBT will come from ISA in Aarhus.

The 50-mA proton beam is produced in a pulsed microwave-discharge source on a platform at 75 kV. A low-energy beam transport, LEBT, with two solenoid



Figure 1: Schematic layout of the ESS linac [4]. Blue colour represents superconducting sections and green arrows locations where the beam could be extracted at intermediate energies.

# PROJECT OVERVIEW AND COMPUTATIONAL NEEDS TO MEASURE ELECTRIC DIPOLE MOMENTS AT STORAGE RINGS

A. Lehrach<sup>#</sup> on behalf of the JEDI collaboration\*, Forschungszentrum Jülich, Germany

## Abstract

Different approaches to measure Electric Dipole Moments (EDMs) of proton, deuteron and light nuclei are pursued at Brookhaven National Laboratory (BNL) and Forschungszentrum Jülich (FZJ) with an ultimate goal to reach a sensitivity of  $10^{-29}$  e-cm in a dedicated storage ring. As an intermediate step, a first direct EDM measurement of protons and deuterons at  $10^{-24}$  e-cm sensitivity level will be carried out in a conventional storage ring, the Cooler Synchrotron COSY at FZJ [1].

Full spin-tracking simulations of the entire experiment are absolutely crucial to explore the feasibility of the planned storage ring EDM experiments and to investigate systematic limitations. For a detailed study of particle and spin dynamics during the storage and buildup of the EDM signal, one needs to track a large sample of particles for billion of turns.

## INTRODUCTION

Permanent EDMs of fundamental particles violate both time invariance  $\mathcal{T}$  and parity  $\mathcal{P}$ . Assuming the  $CPT$  theorem this implies  $CP$  violation. The Standard Model (SM) predicts non-vanishing EDMs, their magnitudes, however, are expected to be unobservably small in the near future. Hence, the discovery of a non-zero EDM would be a signal for “new physics” beyond the SM. It is mandatory to measure EDMs on different species of particles in order to disentangle various sources of  $CP$  violation. While neutron EDM experiments are pursued at many different places worldwide, no such direct measurements have been conducted yet for protons and other light nuclei due to special difficulties of applying electric fields on charged particles. EDM experiments with charged particles are only possible at storage rings.

As a first step towards EDM searches in storage rings we proposed R&D work to be carried out at the Cooler Synchrotron COSY [2,3], then perform a first direct EDM measurement of a charged particle in a storage ring at the Cooler Synchrotron COSY, and on a longer time scale construct a dedicated storage ring [3,4].

The COSY Infinity simulation program [5] and its updates are used to simulate beam and spin motion in storage rings. To study subtle effects and simulate the particle and spin dynamics during the storage and buildup of the EDM signal, one needs custom-tailored fast trackers capable of following up to 100 billion turns for samples of up to  $10^6$  particles. Given the complexity of the tasks, particle and spin dynamics simulations

performed with COSY Infinity must be benchmarked with other simulation programs and experiments performed at the Cooler Synchrotron COSY, to ensure the required accuracy of the obtained simulation results.

## EDM MEASUREMENTS AT STORAGE RINGS

### Principle

The principle of every EDM measurement (e.g., neutral and charged particles, atom, molecule) is the interaction of an electric field with the dipole moment of the particle. In the center-of-mass system of a particle electric dipole moments  $\vec{d}$  couple to electric fields, whereas magnetic dipole moments  $\vec{\mu}$  couple to magnetic fields. The spin precession in the presence of both electric and magnetic fields is given by:

$$\frac{d\vec{S}}{dt} = \vec{d} \times \vec{E}^* + \vec{\mu} \times \vec{B}^*. \quad (1)$$

Here,  $\vec{E}^*$  and  $\vec{B}^*$  denote the electric and magnetic fields in the particle rest frame. In case of moving particles in a circular accelerator or storage ring, the spin motion is covered by the Thomas-BMT equation and its extension for EDM:

$$\frac{d\vec{S}}{dt} = \vec{\Omega} \times \vec{S} \quad (2)$$

$$\vec{\Omega} = \frac{e\hbar}{mc} \left\{ G\vec{B} + \left( G - \frac{1}{\gamma^2 - 1} \right) (\vec{v} \times \vec{E}) + \frac{\eta}{2} (\vec{E} + \vec{v} \times \vec{B}) \right\}.$$

$\vec{E}$  and  $\vec{B}$  denote the electric and magnetic fields in the laboratory system, with the constraint, that the electric and magnetic fields are perpendicular to the velocity vector  $\vec{v}$  of the particle beam:  $\vec{v} \cdot \vec{B} = \vec{v} \cdot \vec{E} = 0$ .

The gyromagnetic anomaly  $G$ , magnetic and electric dipole moments are given by:

$$G = \frac{g-2}{2}, \vec{\mu} = 2(G+1) \frac{e\hbar}{2mc} \vec{S}, \text{ and } \vec{d} = \eta \frac{e\hbar}{2mc} \vec{S}. \quad (3)$$

### Methods

Starting from equation 2, different approaches are possible to excite spin rotations via the electric dipole moment:

\*JEDI spokespersons: A. Lehrach, J. Pretz, and F. Rathmann

<sup>#</sup>a.lehrach@fz-juelich.de

# SIMULATING THE LHC COLLIMATION SYSTEM WITH THE ACCELERATOR PHYSICS LIBRARY MERLIN, AND LOSS MAP RESULTS

J.G. Molson\*, R.B. Appleby, M. Serluca, A. Toader  
The University of Manchester and the Cockcroft Institute, UK  
R.J. Barlow, University of Huddersfield, UK

## Abstract

We present large scale simulations of the LHC collimation system using the MERLIN code for calculations of loss maps, currently using up to  $1.5 \times 10^9$  halo particles. In the dispersion suppressors following the collimation regions, protons that have undergone diffractive interactions can be lost into the cold magnets. This causes radiation damage and could possibly cause a magnet quench in the future with higher stored beam energies. In order to correctly simulate the loss rates in these regions, a high statistics physics simulation must be created that includes both accurate beam physics, and an accurate description of the scattering of a 7 TeV proton in bulk materials. The current version includes the ability to simulate new possible materials for upgraded collimators, and advances to beam-collimator interactions, including proton-nucleus interactions using the Donnachie-Landshoff Regge-Pomeron scattering model. Magnet alignment and field errors are included, in addition to collimator jaw alignment errors, and their effects on the beam losses are systematically estimated. Collimator wakefield simulations are now fully parallel via MPI, and many other speed enhancements have been made.

## INTRODUCTION

The LHC is a superconducting 7 TeV proton-proton collider with a high nominal stored beam energy (360MJ) and a low quench limit on the superconducting magnets ( $4.5\text{mW}/\text{cm}^3$ ) [1]. To protect the machine from this high stored energy, the LHC is equipped with an efficient collimation system to collimate halo particles and prevent quenching, in addition to reducing the background at the experimental regions and preventing radiation damage to sensitive electronics. There exist two collimation regions - one in interaction region 7 (IR7) which contains a series of betatron collimators for transverse collimation. The primary collimators in this regions are the aperture restriction in the machine. In IR3 there is a region of beam dispersion to perform momentum collimation.

Of critical importance are regions known as the dispersion suppressors, which match the long straight section (LSS) optics to the periodic optics of the arcs. In these regions, the dispersion rises rapidly, and any protons that have undergone any interactions in the collimators that causes them to lose momentum may be lost in a localised region, see Figure 4. Due to this, one must have an accurate

simulation of the accelerator optics, the machine physical aperture, and the scattering physics of a proton inside a collimator jaw.

Merlin is a C++ accelerator physics library [2] initially developed for the ILC beam delivery system [3, 4], then later extended to model the ILC damping rings. Merlin has been extended to be used for large scale proton collimation simulations, with the aim of providing an accurate simulation of the Large Hadron Collider (LHC) collimation system, and any future upgrades. In this paper we describe the developments of the Merlin code to enable study of the LHC collimation system and present beam loss maps for 2012 running.

## THE MERLIN ACCELERATOR PHYSICS LIBRARY

The Merlin library consists of a large number of classes designed to simulate a particle accelerator, and any additional systems required. The classes can be split into three main categories.

The *AcceleratorModel* and associated classes deal with the creation and storage of an accelerator lattice. The lattice is stored as a series of *AcceleratorComponent* classes, which contain information about each element. Different types of accelerator component are child classes of the main *AcceleratorComponent* class. These contain pointers to classes describing specific properties of the element: *EMField* describes any electromagnetic fields inside the element, *AcceleratorGeometry* describes any geometric transforms that the element has undergone, *Aperture* describes the experimental beam pipe, and *WakePotentials* describe any wake fields that exist for this element class. Input can take place via multiple methods: the direct creation and addition of elements, via the MAD-X [5] TFS output (*MADInterface*), or tape format (*XTFFInterface*), both of which create an *AcceleratorModel* as output.

The *ParticleTracker* and associated classes deal with the transport of particles along the accelerator optical lattice, including stepping between elements, and within individual elements, whilst applying additional physics processes at appropriate locations. These create integrator sets for tracking, and individual integrators can be overridden for selected class types, e.g. crab cavities. The *ParticleTracker* takes as its input a *ParticleBunch* class, and a *Beamline*, where the *ParticleBunch* can be one of many different types, e.g. gaussian, flat and ring amongst others. The *Beamline* is a subsection of an *AcceleratorModel*, and bunches can be passed between multiple trackers, allowing

\* james.molson@hep.manchester.ac.uk

# AUTOMATIC COMPUTER ALGORITHMS FOR BEAM-BASED SETUP OF THE LHC COLLIMATORS\*

G. Valentino<sup>†</sup>, N. Sammut

CERN, Geneva, Switzerland and University of Malta, Msida, Malta  
 R.W. Assmann, R. Bruce, S. Redaelli, B. Salvachua, D. Wollmann  
 CERN, Geneva, Switzerland

## Abstract

Beam-based setup of the LHC collimators is necessary to establish the beam centers and beam sizes at the collimator locations and determine the operational settings during various stages of the LHC machine cycle. Automatic software algorithms have been successful in reducing the costly beam time required for the alignment, as well as significantly reducing human error. In this paper, the beam-based alignment procedure is described, and the design of algorithms such as a BLM feedback loop, parallel collimator alignment, pattern recognition of BLM loss spikes, automatic loss threshold selection and coarse BPM-interpolation guided alignment is explained. A comparison on the alignment results from the 2010 to the 2012 LHC runs is presented to illustrate the improvements achieved with the automatic algorithms.

## INTRODUCTION

The Large Hadron Collider (LHC) located at CERN is designed to collide two counter-rotating particle beams with an energy of 7 TeV each [1]. Machine protection systems are installed to prevent damage to the LHC in the event of beam loss scenarios. The collimation system protects the collider against unavoidable losses, which may cause quenches in the superconducting magnets, damage to beam pipe equipment or cause electronics degradation as a result of radiation effects [2].

At present, the collimation system is made up of over 100 collimators which are arranged in four levels of retraction from the beam in the form of a hierarchy. The LHC consists of 8 arcs and 8 straight sections, called insertion regions (IRs). The collimators are located mainly in IR3 and IR7 to scatter and absorb particles with large momentum and betatron offsets respectively.

Each collimator providing cleaning of normal beam losses consists of two blocks, known as jaws, of graphite or tungsten. In order to ensure maximum cleaning efficiency and protection, the jaws must be positioned symmetrically around the beam with the correct gap in units of beam standard deviations (sigmas). The jaw positioning accuracy is 5 μm, and a three-tier control system allows the upstream and downstream edges of each jaw to be moved separately via four motors [3].

The beam centers and beam sizes at the collimator lo-

cations are determined from beam-based alignments. The setup procedure relies on feedback from beam loss monitors (BLMs) [4], which consist of ionization chambers placed downstream of the collimators. The BLMs capture beam loss showers caused by primary beam particles impacting on the collimators. A collimator jaw is aligned to the beam halo when a clear spike is observed in the BLM signal.

In 2010, the setups were performed ‘manually’, meaning that human feedback was required to determine when the jaw is aligned to the beam. This was achieved by observing the BLM signal on a screen following a jaw movement. A disadvantage of this method is the setup time required, which is data lost for the experiments and beam time for other users. Human error results in incorrect jaw movements, causing high losses and beam dumps, therefore contributing to the setup time. In order to speed up the collimator alignment and minimize the intervention required from the operator, a set of automatic algorithms has been implemented in the top-layer of the LHC software architecture in Java.

## COLLIMATOR SETUP PROCEDURE

Each collimator is aligned in a four-step procedure, as established in [5]. The setup procedure is illustrated in Fig. 1. The first step is to align the left and right jaws of a reference collimator to form a reference cut in the beam halo. This collimator is taken to be the primary collimator (TCP) in the same plane (horizontal, vertical or skew) as the collimator to be aligned, called collimator  $i$ . As a particular jaw can be declared to be aligned only if it was the only jaw moving when the BLM signal spike occurs, the left and right jaws are moved towards the beam separately. After aligning the reference collimator, the same procedure is performed for the collimator  $i$  (2), and the reference collimator is aligned once again (3). The beam center can then be determined from the final measured left and right jaw positions  $x_i^{L,m}$  and  $x_i^{R,m}$  of collimator  $i$ :

$$\Delta x_i = \frac{x_i^{L,m} + x_i^{R,m}}{2} \tag{1}$$

A full derivation of the calculation for the inferred beam size at collimator  $i$  is available in [6], and can be calculated from the jaw half gap and the average cut  $n_1$  in units of sigma at the reference collimator:

\* Work supported by FP7 EuCARD

<sup>†</sup> gianluca.valentino@cern.ch

# LINAC BEAM DYNAMICS SIMULATIONS WITH PY-ORBIT

A. Shishlo\*, ORNL, Oak Ridge, TN 37830, USA

## Abstract

Linac dynamics simulation capabilities of the PyORBIT code are discussed. PyORBIT is an open source code and a further development of the original ORBIT code that was created and used for design, studies, and commissioning of the SNS ring. The PyORBIT code, like the original one, has a two-layer structure. C++ is used to perform time-consuming computations, and the program flow is controlled from a Python language shell. The flexible structure makes it possible to use PyORBIT also for linac dynamics simulations. A benchmark of PyORBIT with Parmila and the XAL Online model is presented.

## INTRODUCTION

The negative hydrogen ion SNS linac was designed [1] by using the Parmila accelerator simulation code [2]. In addition to envelope tracking codes, such as the XAL online model that is used routinely in the SNS control room, particle in cell (PIC) simulation codes like Parmila are valuable tools for halo growth calculations and beam loss estimation in heavy ion linear accelerators. Unfortunately, the Parmila code is not actively supported today, and a large project, such as SNS, cannot afford to lose PIC simulation capabilities for any part of the accelerator. During the search performed by the SNS accelerator physics group, we could not find an accelerator code that satisfies the necessary conditions of the full control over the source code, the underlying physical models, and possible modifications. To solve this problem we started the development of a home-grown open source linac accelerator code on an existing platform, namely the PyORBIT code.

## PY-ORBIT AND ORBIT CODES

PyORBIT is a PIC code developed from the original ORBIT code [3]. ORBIT has been used for the design of the SNS ring and transfer lines, simulations of collective effects for SNS, and for other projects. PyORBIT, like the original ORBIT, has a two-language structure. Time-consuming calculations are performed at the C++ language level, and a simulation flow control is implemented in a scripting language. In PyORBIT the outdated and unsupported SuperCode is replaced by Python, an interpreted, interactive, object-oriented, extensible programming language. The PyORBIT project was started not only to replace the old programming technologies, but to perform calculations for the laser stripping experiment [4] which could not be performed by the original ORBIT. At this moment, PyORBIT does not have all features of the original code, but we are in the process of transferring the old ORBIT modules to the new

code. It is not a straightforward process because of ubiquitous SuperCode dependencies in ORBIT. On the other hand, this provides the opportunity to restructure the modules in a more efficient and clear way.

The structure of the PyORBIT code was described in Ref. [3]. From the beginning the code has been developing as a loose structure capable of accommodating many weakly or completely unrelated projects. We took advantage of this feature of PyORBIT when the linac simulation part was included into the code.

## LINAC PART OF PY-ORBIT CODE

The new linear accelerator lattice package in PyORBIT is a concrete implementation of abstract accelerator lattice classes described in [3]. Therefore, right now we have two types of the lattices – one for rings and transfer lines, which is similar to the lattice of the original ORBIT code, and another for the linear accelerators. The new implementation was necessary because the energy of a synchronous particle changes along the linac lattice, and the parameters of the lattice elements must be changed accordingly. In addition to this feature of the linear accelerator lattice, we implemented a more complicated structure that includes subsequences and RF cavities that in turn consist of RF gaps. The RF cavities themselves are not lattice elements. They are used to synchronize the phases of all RF gaps that belong to a particular RF cavity. Before using this type of lattice, it must be initialized by tracking a design particle to map its arrival time at each RF cavity. Only after that will changes to the cavity amplitudes or phases in the model reflect the changes in the real machine.

At present, a linac lattice can be built in two ways. First, it can be constructed right in a PyORBIT script by adding lattice elements one by one. Second, it can be built by using an input XML file and linac lattice parser. The parser assumes a certain structure of the input XML file. This structure will be standardized in the future when the list of necessary parameters is agreed upon among all users. At this moment, all classes in the linac packages are considered experimental, and they are kept in a specific SNS linac directory. All these classes are pure Python classes. They are lightweight and can be easily modified to accommodate different requests. It is also possible to implement a third type of abstract accelerator lattice if a more universal approach is required in the future.

There are several new C++ classes that have been created to simulate physics in linear accelerators. They include two types of space charge calculations and a simplified RF gap model. We plan to implement more sophisticated RF models in the near future.

\*shishlo@ornl.gov

# AN IMPLEMENTATION OF THE VIRTUAL ACCELERATOR IN THE TANGO CONTROL SYSTEM\*

P. Goryl<sup>#</sup>, A. I. Wawrzyniak, Solaris at the Jagiellonian University, Krakow, Poland  
 T. Szymocha, ACK Cyfronet AGH, Krakow, Poland  
 M. Sjöström, MAX IV laboratory, Lund, Sweden

## Abstract

Integrating physics codes into the control system gives a possibility to improve machine operation. Providing tools for making computations directly within the control system and letting exchange data between the control system and models is a way of simplifying the whole process of calculating and applying machine's operational parameters as well as keeping track of them. In addition, having a so-called on-line model could be useful for the system diagnostic and faults detection, especially when the objective approach is considered. The concept of the Virtual Accelerator as well as its implementation for the Tango control system will be presented as it is planned to be used for both facilities: the Solaris in Krakow, Poland and the MAX IV in Lund, Sweden. This includes the ModelServer tango device, the simplified C/C++ Tango API to be used with physics codes like Tracy 3 and the tango2elegant script providing an easy solution for integrating the eLegaNt tool with the Tango Control System.

## INTRODUCTION

The Virtual Accelerator is a concept of integrating and interfacing different simulation codes into the control system (CS). However, an implementation presented here could be used with any kind of computation codes. It has been successfully implemented at the SLS[1] using the CORBA protocol and at the Diamond Light Source for the EPICS control system[2].

The Virtual Accelerator implementation for the Tango CS presented in this paper has been developed with several goals:

- Standardize a way to starting and stopping computations from the control system
- Simplify data exchange between the control system and the simulation code
- Provide a standard interfaces to different kind of equipment (classes of devices in case of the Tango CS)
- Provide a central point for storing calculated machine parameters within the control system architecture thus making these directly available for all control system applications
- Provide a facility to debug control system scripts and high level applications before these will be run for a real machine. It is expected to make the machine commissioning more efficient.

## The Tango CS

The Tango control system implements an objective

approach to interface controlled devices. It provides an interface with attributes, representing process values (PVs) or state values and commands representing operations one can invoke on a particular device. Each device is in fact represented as an object of a certain class as it is in the Object Oriented Programming (OOP) [3].

The OOP introduce a mechanism called the polymorphism along with a mechanism of the classes inheritance. This provides a way to abstract from what is behind an interface. As an example, all power supplies integrated in a control system (CS) could expose the same interface to users regardless of a fieldbus the CS is using to communicate with a particular equipment. This also means that it is possible to use the same interface to a model of a controlled system as to the real one. With some assumptions actors interacting with the CS will not be able to distinguish if they work with a real or a modelled system. It does not mean that the same could not be achieved with a non-object oriented CS. Nonetheless, the OOP makes it natural.

Integrating physics codes with the CS takes advantage of the existing tools of the control system. The integration is expected to improve the system diagnostic as well as simplify applying to the machine calculated machine's parameters. The computation results could be logged with the Historical and the Temporary Databases (the HDB and the TDB). Computed settings could be remembered as a snapshot with the Tango SNAP tool. Making the model available through the control system could enable online comparison between the real machine and the virtual one. Distributing machine's parameters, simulation results and real machine's signals through the Tango control system will prevent from clutter caused by using different protocols for data exchange.

The Virtual Accelerator for the Tango Project provides the following components:

- The Model Server device. It is a device that standardizes and simplifies invoking of computation from the Tango CS.
- The Simple-Tango (STango) API. This is C/C++ library enabling access to a Tango CS in a 'one line code'. It hides some Tango complexity.
- The tango2elegant. This is a script interfacing the eLegaNt tool with the Tango CS.

## THE MODEL SERVER

The Model Server is a tool to run computations inside the Tango control system. It is implemented as a Tango device. Its class name is ModelServer. It is written in the Python language with the PyTango library. The Model-Server class inherits from the DynamicDS class[4].

\* Work supported by the European Regional Development Fund within the frame of the Innovative Economy Operational Program: POIG.02.01.00-12-213/09  
<sup>#</sup>piotr.goryl@uj.edu.pl

## SIMULATION OF ELECTRON CLOUD INSTABILITY

K. Ohmi, KEK, 1-1 Oho, Tsukuba, 305-0801, Japan

**Abstract**

We discuss coupled bunch and single bunch instabilities caused by electron cloud in positron circular accelerators. Unstable mode spectrum, which characterizes the instabilities, is focused.

**INTRODUCTION**

Electron cloud causes coupled bunch and single bunch instabilities. The coupled bunch instability caused by electron cloud has been observed at KEK-PF, since start of positron operation in 1988. The instability was confirmed at BEPC in IHEP, China. The instability has been observed in KEKB-Low Energy Ring, which is positron storage ring. Weak solenoid coils were wound along the whole ring to protect electrons near the beam. The unstable mode of the coupled bunch instability was affected by the solenoid status, ON or OFF. Corrective electron motion reflected to beam unstable mode. The coupled bunch instability has been observed at DAFNE in Frascati, Italy. DAFNE is a small e<sup>+</sup>e<sup>-</sup> collider ring with the circumference of 98m. Bending magnets and wiggler magnets are occupied in a large part of ring. It seemed that electrons in the bending field play important role. The unstable mode was characteristic for the electron motion in the bending field.

Single bunch instability has been observed in KEKB-LER. Generally fast head-tail instability is caused by merge between 0 and -1 synchrotron sideband modes in positron ring. In the single bunch instability, clear positive side band  $\nu_y + a\nu_s$  ( $1 < a < 2$ ) has been observed. The similar signal has been observed at PETRA-III, DESY, Germany. The instability has been observed in Csr-TA, Cornell, USA. The signal appears as negative side band,  $\nu_y - \nu_s$ .

Simulations have been performed to explain the both of single and coupled bunch instabilities. We present the simulation results with focusing unstable mode in this paper.

**COUPLED BUNCH INSTABILITY DUE TO ELECTRON CLOUD***Simulation of Electron Cloud Build Up and Coupled Bunch Instability*

Beam-electron cloud system in multi-bunch regime is described by following equations:

$$\frac{d^2 \mathbf{x}_p}{ds^2} + K(s) \mathbf{x}_p = \frac{2N_e r_e}{\gamma} \sum_{e=1}^{N_e} \mathbf{F}_G(\mathbf{x}_p - \mathbf{x}_e) \delta_P(s - s_e) \quad (1)$$

$$\frac{d^2 \mathbf{x}_e}{dt^2} = \frac{e}{m_e} \frac{d\mathbf{x}_e}{dt} \times \mathbf{B} - 2N_p r_e c \sum_{p=1}^{N_p} \mathbf{F}_G(\mathbf{x}_e - \mathbf{x}_p) \delta_P(t - t_p(s_e)) - r_e c^2 \frac{\partial \phi(\mathbf{x}_e)}{\partial \mathbf{x}_e} \quad (2)$$

where the electric potential of electron cloud is given by

$$\Delta \phi(\mathbf{x}) = \sum_{e=1}^{N_e} \delta(\mathbf{x} - \mathbf{x}_e) \quad (3)$$

Bunches, which are rigid Gaussian shape in transverse and are located equal spacing along s, are represented by their center of mass  $\mathbf{x}_p$ .  $\mathbf{F}_G$  is expressed by the Bassetti-Erskine formula.

The electron cloud build-up is simulated by integrating the second equation for the motion of macro-electrons  $\mathbf{x}_e$  under  $\mathbf{x}_p=0$ . The initial condition of electrons, where and when electrons are created, is sketched in Figure 1. When beam pass through the chamber cross-section, electrons are created with a energy distribution. When an electron hits the wall, secondary electrons are produced with a probability.

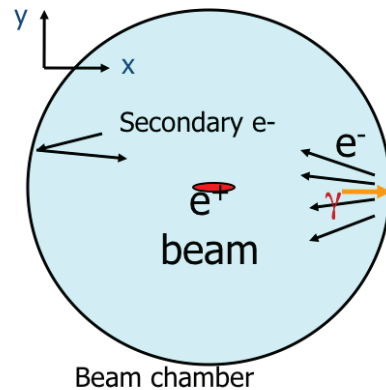


Figure 1: Electron cloud build-up model.

The coupled bunch instability is studied by solving the two coupled equations (1) and (2).

*Coupled Bunch Instability in KEK-PF*

Progress of electron cloud effects in these 17 years (since 1995) started from the interpretation of an instability observed in KEK-Photon Factory. Very strong coupled bunch instability had been observed since the positron storage had started. The threshold of the instability is very low 10-15mA. Either of positron or electron could be stored by changing the polarity of the magnets. The instability is observed only in positron storage. Figure 2 shows frequency spectrum for the instability published in [1]. The first electron cloud build-up code (PEI) is developed in 1995 [2], and the coupled bunch instability was interpreted as a wake effect of the electron cloud. The wake force was estimated by perturbation of the cloud due to a passage through of a shifted bunch [2]. Figure 3 shows the simulated wake force.

Growth rate for each mode is calculated by the wake force. Figure 4 shows unstable mode spectrum estimated by the simulated wake force. The growth rate is 0.3msec for m=250-300. The corresponding frequency is (h-m-

# TRACKING OF A PETRA III POSITRON BUNCH WITH A PRE-COMPUTED WAKE MATRIX DUE TO ELECTRON CLOUDS \*

A. Marković, U. van Rienen, University of Rostock, Germany

## Abstract

At the synchrotron radiation facility at DESY transversal tune spectra have been observed which are characteristic for an interaction of the positron beam with possible electron clouds in the ring. The filling patterns at which these incoherent tune shifts happen are favorable to the growth of the electron cloud density, i.e. long bunch trains with short intra-bunch distances. Eventually the vertical emittance growth with the originally designed equidistant filling (with 8 or 16 ns bunch spacing) has been avoided by fillings with short bunch trains and longer gaps between them and yet achieving the designed beam current of 100 mA. In this paper we examine the positron bunch stability of PETRA III for certain e-cloud densities and bunch parameters. A PIC simulation of the interaction of the bunch with an e-cloud yields the wake kick on the tail particles for an offset in the transverse centroid position of the head parts. With such a pre-computed wake matrix, we investigate the stability of a single bunch by tracking it through the linear optics of the ring while at each turn applying the kick from the e-cloud. The simulation results are in a good agreement with the measurements.

## INTRODUCTION

PETRA III at DESY is a synchrotron radiation facility running in a top up operation modus with positrons. The machine is characterized (Table 1) by an ultra low emittance and with an emittance ratio of 1% it features very flat bunches. The design beam current of 100 mA was planned to be achieved with fillings of 40 or 960 equally spaced bunches. However, for the filling scheme with 960 bunches with only 8 ns bunch-to-bunch distance a strong vertical emittance growth has been reported for currents about 50 mA [1]. The corresponding measurements of the tune spectra (Figure 1) show sidebands in the vertical tune which suggest incoherent effects. These effects are brought in connection with electron cloud effects on the bunch. Indeed the designed beam current of 100mA has been achieved by filling patterns where the e-cloud can not reach dangerous densities i. e. 60 trains of only 4 bunches with train to train distances of 80ns and bunch to bunch distance of 8ns. The e-cloud build up simulations with ELOUD 4.0 (reported in [1]) for a train with bunch to bunch spacing of 8 ns and bunch population of  $0.5 \cdot 10^{10}$  positrons (SEY  $\delta= 2.5$ ) show that after the first 4 bunches the e-cloud density is still below  $5 \cdot 10^{11} 1/m^3$  which is below the instability threshold computed as in [2]. In 2011 and 2012 further 100 mA runs were performed with trains

of 40, 60, 240 and 480 equidistantly spaced bunches with bunch to bunch distance of 192, 128, 32 and 16ns, respectively. Only during the run with 480 bunches a significant emittance growth has been measured. The measurements are very valuable since they give the opportunity to validate the simulations. Eventually the question the instability simulation should answer is at what e-cloud density the instability of a single bunch may occur.

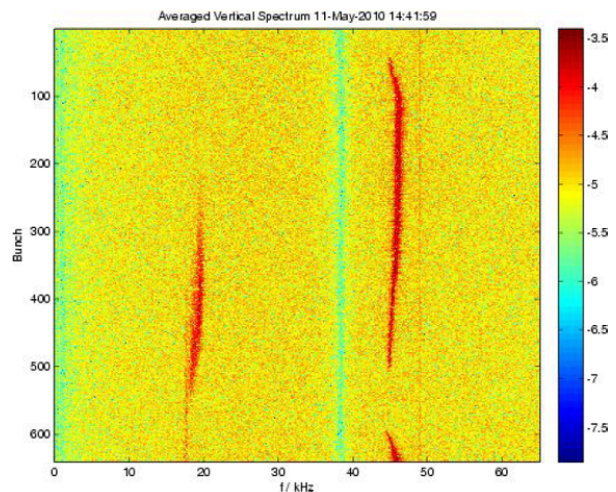


Figure 1: Vertical tune spectra of each of the 640 bunches with 8ns spacing, measured on May 11, 2010 [1]. The total beam current was 62 mA. The red color represents the sidebands and the vertical betatron frequency of 38kHz is green. (Courtesy of R. Wanzenberg.)

## SIMULATION

In order to simulate the stability of a single bunch, the bunch particles are tracked through the linear optics of the machine [3]. Thereby the action of the e-cloud on the bunch is approximated by a transverse wake kick which is applied on each turn. The idea of K. Ohmi to slice the 3D bunch and compute a wake function from every longitudinal slice of the bunch backwards, leads to a triangular wake matrix. In order to apply the computed wake matrix for the bunch tracking, properties of the wake field such as time invariance, superposition and linearity are supposed.

The program MOEVE PIC Tracking [4] simulates the interaction of a single bunch with an electron cloud. The cloud is modelled as a uniform distribution of electrons in a beam pipe and is assumed to be generated by the preceding bunches. Since the perturbation of the e-cloud in the transverse plane is due to the transverse displacement

\* Work supported by DFG under contract number RI 814/20-2.

# BEAM DYNAMICS STUDY CONCERNING SIS-100 PROTON OPERATION INCLUDING SPACE CHARGE EFFECTS

S. Sorge\*, GSI, Darmstadt, Germany

## Abstract

The projected SIS-100 synchrotron at GSI will be used for operation with intense proton and heavy ion beams. In order to avoid the crossing of the transition energy during proton operation a complicated optics scheme is proposed to provide a transition energy above the extraction energy of  $E = 29$  GeV. For the purpose of optimizing the lattice, and to find a suitable working point, regime simulation scans of the dynamic aperture are performed based on MAD-X tracking. In the next step working point candidates will be used for particle tracking simulations in order to estimate beam loss due to space charge induced resonance crossing. For these studies different codes and space charge models are considered.

## LATTICE PROPERTIES

Besides heavy ion operation, the SIS-100 synchrotron is also foreseen to deliver high intensity proton beams of  $2.0 \times 10^{13}$  protons in a short single bunch. The particles will be injected at  $E_{in} = 4$  GeV and fast extracted at  $E_{ex} = 29$  GeV. The working point is still under discussion. In this study,  $(Q_x, Q_y) = (21.8, 17.7)$  is used.

In order to stay below transition energy, linear optics were developed that provide a transition energy corresponding to  $\gamma_{tr} = 45.5$ . Applying three independent families of quadrupoles, the strongly oscillating dispersion function represented by the red curve in Fig. 1 will be created. In doing so the momentum compaction factor

$$\alpha_c = \frac{1}{\gamma_{tr}^2} = \frac{1}{C} \oint \frac{D_x(s) ds}{\rho(s)} \quad (1)$$

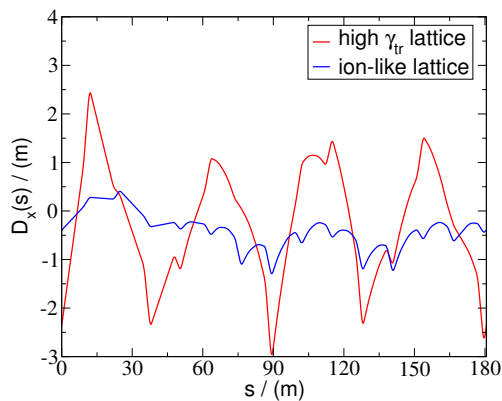


Figure 1: Dispersion function of the high  $\gamma_{tr}$  lattice in one of six SIS-100 sectors compared to that of an “ion-like” lattice of the same working point.

\*S.Sorge@gsi.de

Table 1: Maximum values of some lattice functions of high  $\gamma_{tr}$  lattice and ion-like lattice, both at the working point is  $(21.8, 17.7)$ .  $2\sigma$  emittances are  $(\epsilon_{x,2\sigma}, \epsilon_{y,2\sigma}) = (13 \times 4)$  mm mrad are assumed. The natural chromaticities in row 6 correspond to Eq. (2).

	high $\gamma_{tr}$	ion-like
quadrupole families	3	2
$\gamma_{tr}$	45.5	18.4
$D_{x,max}/(m)$	2.9	1.3
$(\beta_{x,max}, \beta_{y,max})/(m)$	(72, 29)	(19, 21)
max. $2\sigma$ beam widths at $\delta = 0$ , (h,v)/(mm)	(31, 11)	(16, 9)
$(\xi_{x,nat}, \xi_{y,nat})$	(-2.4, -1.4)	(-0.9, -1.1)

is minimised. The extrema of the high  $\gamma_{tr}$  dispersion function are much higher than those of the dispersion function generated with two quadrupole families used during heavy ion operation. In addition, the usage of the high  $\gamma_{tr}$  quadrupole settings increases other lattice variables, see Table 1. The chromaticities  $\xi_{x,nat}, \xi_{y,nat}$  shown in that table are defined by

$$\Delta Q = \delta \xi Q. \quad (2)$$

## MAGNET IMPERFECTIONS AND RESONANCES

Real magnets are with imperfections. In particular random gradient errors in the main quadrupoles lead to an increase of the maximum horizontal beta function. Assuming them to follow a Gaussian distribution truncated at  $2\sigma$  with the relative rms width of  $\sigma_{rel} \approx 0.003$  of the averaged focusing strength of all quadrupole families, the maximum horizontal beta function becomes increased from 72 m to about 100 m, the exact value depends on the actual sample of random errors. In addition, there are non-linear multipole errors in main dipoles and quadrupoles each consisting of a systematic and a random contribution. The systematic components depend on  $B\rho$  [1]. The random components are assumed to follow a Gaussian distribution truncated at  $2\sigma$  with  $\sigma$  be 30 % of the corresponding systematic component. In particular the random components drive non-linear resonances which restrict the choice of the working point. To make them visible and to find a suitable working point, the dynamic aperture was determined at  $100 \times 100$  working points in the range  $Q_x \in [21, 22], Q_y \in [17, 18]$ . The result is shown in Fig. 2. For  $Q_x < 21.5$  dynamic apertures could not be determined because the lattice properties are too difficult for MAD-X even to determine the lattice functions

# SIMULATION OF SPACE EFFECTS DURING MULTITURN INJECTION INTO THE GSI SIS18 SYNCHROTRON

S. Appel, GSI, Darmstadt, Germany

Oliver Boine-Frankenheim, TEMF, TU Darmstadt, Darmstadt, Germany

## Abstract

The optimization of the Multiturn Injection (MTI) from the UNILAC into the SIS18 is crucial in order to reach the FAIR beam intensities required for heavy ions. In order to achieve the design intensities, the efficiency of the multiturn injection from the UNILAC has to be optimized for high beam currents. We developed a simulation model for the MTI including the closed orbit bump, lattice errors, the parameters of the injected UNILAC beam, the position of the septum and other aperture limiting components, and finally the space charge force and other high-intensity effects. The model is also used to estimate the required proton and heavy-ion beam emittances from the UNILAC and from the projected p-linac. For the accurate prediction of the MTI efficiency a careful validation of the simulation model is necessary. We will present first results of the comparison between experiments and simulation for low and high uranium beam currents.

## INTRODUCTION

The GSI SIS18 synchrotron and the linac UNILAC are being upgraded in order to increase the beam intensity to the FAIR design parameter. For FAIR the SIS18 has to work as booster for the new SIS100 synchrotron. One crucial point in the upgrade program is the optimization of the Multiturn Injection (MTI) from the UNILAC into the SIS18. The beam loss during the MTI into the SIS18 must be minimized to avoid an intolerable increase of the dynamic vacuum pressure, which in turn leads to a reduced life-time of intermediate charge state heavy-ions [1]. The main beam loss is expected to occur on the injection septum. For FAIR intensities collective effects are expected to affect the MTI. The impact of space charge and image currents on the injection efficiency are therefore being investigated.

The aim of the present study is the development of a detailed simulation model for the MTI including the closed orbit bump and errors, the parameters of the injected UNILAC beam, the position of the septum and other aperture limiting components, and finally the space charge force and other high-intensity effects. The model can also be used to indicate the required proton and heavy-ion beam emittances from the UNILAC and from the projected p-linac. Before the model can be applied to predict and optimize the MTI for high currents a careful validation with MTI experiments is necessary.

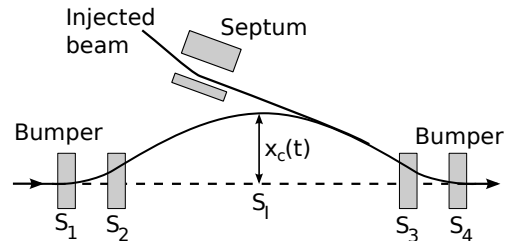


Figure 1: Layout of the multiturn injection.

## MULTITURN INJECTION

In the SIS18 the beam is stacked in the horizontal betatron phase space using a closed orbit bump to bring the stacked beam close to the injection septum (See Fig. 1). The incoming beam centre will have a linear  $x$  and an angular  $x'$  displacements with respect to the undeformed closed orbit. After injection the beam will undergo betatron oscillations. One turn later the beam will come again to the injection point. Due to the betatron oscillation around the closed orbit the beam will avoid the septum. Meanwhile a new beam will be injected. This beam will have a larger amplitude of the betatron oscillation as the orbit bump is reduced. The process goes on until the maximum number of injection is reached. The beam emittance after the injection process is considered as area of the smallest ellipse that contains all injected particles. The dilation during the injection is defined as [2]

$$D = \frac{\epsilon_f}{n_{MTI}\epsilon_i} \quad (1)$$

where  $\epsilon_i$  is the emittance of the injected beamlet,  $\epsilon_f$  the emittance of the final beam and  $n_{MTI}$  the number of injected beamlets. The final beam emittance must be smaller than the machine acceptance. This means, the best injection schemes have the smallest dilation and the lowest loss at the septum.

The injection bump is produced by four bumper magnets located in the injection region with positions

$$s_1 < s_2 < s_I < s_3 < s_4 \quad (2)$$

where  $s_I$  is the point of injection (See Fig. 1). If we require that the four bumper magnets produce no closed orbit distortion outside the injection region and the horizontal position and angle of the closed orbit  $x_c, x'_c$  at the injection position  $s_I$  are the degrees of freedom, then the angular kick produced by the bumper magnets are [3]

ISBN 978-3-95450-116-8

# LOW-ENERGY p-He AND mu-He SIMULATION IN GEANT4

Yu Bao

Paul Scherrer Institute, 5232 Villigen, PSI, Switzerland

## Abstract

The frictional cooling method is one of the most promising methods on cooling a muon beam. Several frictional cooling schemes have been simulated in Geant4 to be efficient to produce intense muon beams. Frictional cooling works at a low energy range, where the energy loss (momentum transfer) from elastic collision is not negligible. In this paper, the p-He collision process is implemented into Geant4 and the simulation results are compared to the literature data. The process is then scaled for mu-He interaction, which will provide more accurate Geant4 simulations at low energies.

## INTRODUCTION

Frictional cooling is one promising method to produce a “cold” beam. It balances the energy loss to a material with energy gain from an external electric field, so that the beam reaches an equilibrium energy and the energy dispersion is reduced. Several cooling schemes based on frictional cooling were outlined for various experiments [1–4]. In most of these schemes, low density helium gas is chosen as the retarding material for its high effective charge [5]. For accurately simulating the transport of the particles in the frictional cooling energy range in the helium gas, the low energy physics processes are needed.

Geant4 is a powerful toolkit for simulating the particle-material interactions. The energy loss of the particle is handled by the ionisation process according to the stopping power from the NIST table down to 1 keV. In the energy range between 10 eV and 1 keV the model of a free electron gas [6] is used, in which the energy loss is calculated proportional to the velocity of the particle. When the particle energy gets lower than 10 eV, it's treated as “stopped” and if there is no “AtRest” process the tracking of the particle will be terminated. The scattering of the particles are simulated in Geant4 by the multiple-scattering method, which has been proved to have the same accuracy as the single-scattering simulations, and the energy loss due to elastic scattering can be neglected at high energies.

At energies lower than 1 keV, the cross sections of the elastic processes are much larger than the inelastic ones. The energy loss due to the elastic scattering plays the dominant role in the particle transport. These processes were investigated in the plasma physics decades ago and were summarized by P. S. Krstic and D. R. Schultz in the reference [7].

In this work the elastic scattering process of the p-He interaction is implemented into Geant4 and is scaled for the  $\mu^+$ -He interaction. The multiple scattering and the ionisation processes in Geant4 are turned off at energies lower than 1 keV, and the elastic scattering process is used in the range between 1 keV and 0.1 eV. When the energy goes lower than 0.1 eV, the tracking is terminated.

## THEORY

The scattering is usually described by the differential cross section  $d\sigma(\theta, \phi)/d\Omega$ , defined as the ratio of the number of particles scattered per unit time into an element of solid angle  $d\Omega = \sin\theta d\theta d\phi$ , per unit solid angle, to the flux of incoming particles.

The total (elastic) scattering cross section is the flux of particles scattered in all directions, defined as:

$$\sigma_{el} = \int d\Omega \frac{d\sigma(\theta, \phi)}{d\Omega} = 2\pi \int_0^\pi \sin\theta |f(\theta)|^2 d\theta \quad (1)$$

and the momentum transfer cross section is defined as:

$$\begin{aligned} \sigma_{mt} &= \int d\Omega \frac{d\sigma(\theta, \phi)}{d\Omega} (1 - \cos\theta) \\ &= 2\pi \int_0^\pi \sin\theta |f(\theta)|^2 (1 - \cos\theta) d\theta \end{aligned} \quad (2)$$

in which  $f(\theta)$  is the amplitude of the scattered wave. The differential cross section is only a function of the scattering angle  $\theta$  for a certain particle velocity:

$$\sigma_d(\theta, v) = \frac{d\sigma(\theta, \phi)}{d\Omega} = |f(\theta)|^2 \quad (3)$$

$f(\theta)$  and all these cross sections are computed in the center-of-mass (CM) reference frame in Ref. [7] for ten points per energy decade at  $E_{CM} = 10^{0.1j-1} eV$ ,  $j = 0, 30$  (Data available for  $j \leq 50$  online<sup>1</sup>). Both the differential and the total cross sections are obtained from extensive quantum-mechanical calculations and can be regarded as having very high accuracy.

To see how the momentum transfer cross section relates to the particle transport, consider the elastic scattering of a particle labeled  $a$  from a material atom. In the CM frame the momentum of the particle is simply  $\mu v_a$ , where  $\mu$  is the reduced mass of the ion-atom pair and  $v_a$  is the drift velocity of particle  $a$ . Hence the momentum loss is  $\mu v_a (1 - \cos\theta_{CM})$  and  $\sigma_{mt}$  is the average momentum transfer in a

<sup>1</sup><http://www-cfadc.phy.ornl.gov/elastic/homeh.html>

# HIGH PRECISION CAVITY SIMULATIONS\*

W. Ackermann\*\*, T. Weiland, Technische Universität Darmstadt,  
 Institut für Theorie Elektromagnetischer Felder (TEMF),  
 Schlossgartenstraße 8, 64289 Darmstadt, Germany

## Abstract

The design of resonant radio frequency cavities used in particle accelerator machines to accelerate charged particles of various species is heavily based on proper computer simulations. While the determination of the resulting field distribution can be obtained by analytical means only for a limited number of cavity shapes it is essential to apply appropriate computer programs to find sufficiently accurate approximate solutions. The achievable quality first depends on the underlying mathematical model which then has to be solved accurately on a discrete level. The precise knowledge of the distribution of the electromagnetic fields both within the cavities as well as on the surface of the resonators is essential for appropriate cavity-shape optimizations and accurate beam dynamics studies.

## INTRODUCTION

In the context of highly resonating cavities a promising method to determine the electromagnetic field distribution inside the structures is given by the eigenmode analysis where a limited number of eigensolutions is used to characterize the devices within a specified frequency range. Selected eigenmodes can be determined with the help of suitable eigenmode solvers once the underlying continuous mathematical model is properly transformed into a convenient matrix formulation. Under actual operating conditions, the fields in the resonators have to be coupled to the fields in the external devices either to enable energy transfer from e.g. the sources to the beam or, conversely, to dump beam-driven parasitic modes to internal or external loads. Compared to lossless standing-wave structures where real-valued variables are sufficient to describe the entire field distribution this is no longer true in a dissipative environment where a resulting net energy transfer has to be supported. On the other hand, a complex-valued formulation completely enables to describe the physical space-dependent phase variation and additionally allows to characterize the oscillation by simultaneously extracting the corresponding quality factor next to the resonance frequency. Unfortunately, the solution of complex-valued eigenvalue systems is much more demanding compared to the widespread real-valued formulations and special care has to be put in the implementation of the computer programs to achieve good performances for large-scale applications.

\* Work partially supported by DESY, Hamburg

\*\*ackermann@temf.tu-darmstadt.de

## MATHEMATICAL MODELING

A proper mathematical model to describe the electromagnetic field distribution within highly resonating structures with an eigenmode analysis in mind is obviously based on Maxwell's equations in frequency domain. We use the differential notation

$$\text{curl } \vec{H} = \vec{J} + j\omega\vec{D} \quad (1a)$$

$$\text{curl } \vec{E} = -j\omega\vec{B} \quad (1b)$$

$$\text{div } \vec{B} = 0 \quad (1c)$$

$$\text{div } \vec{D} = \rho \quad (1d)$$

to point out the interdependence of the applied electromagnetic field components. In this context,  $\vec{E}$  and  $\vec{H}$  represent the phasors of the electric and magnetic field strength while  $\vec{D}$  and  $\vec{B}$  specify the electric and magnetic flux densities, respectively. The symbol  $\omega$  represents the angular frequency while  $\vec{J}$  and  $\rho$  describe the sources of the electromagnetic fields. In the following we concentrate on linear isotropic materials which may be inhomogeneous if required. This limitation simplifies the material relations to  $\vec{D} = \epsilon\vec{E}$  and  $\vec{B} = \mu\vec{H}$  with space-depending scalar proportionality factors. Finally, the electric conductivity  $\sigma$  give rise to the electric current density  $\vec{J} = \sigma\vec{E}$  which is responsible for the specific bulk-related losses.

### Discretization

To transform the continuous formulation into a suitable matrix equation we discretize (1) with the help of the finite element method (FEM) [1]. Eliminating either the electric or the magnetic field combines the two first-order differential equations into one second-order equation. This procedure simplifies the overall solution process because only one type of field either with tangential or normal continuity conditions has to be properly represented on the discrete level. In the end, the initially eliminated field can be reconstructed in a postprocessing step if one of the curl relations in (1) is applied to the selected quantity.

With the well-known Nédélec elements in mind we set the focus of the formulation on the electric field only and combine (1a) and (1b) to the double-curl equation

$$\text{curl} \left( \frac{1}{\mu} \text{curl } \vec{E} \right) + j\omega\vec{J} - \omega^2\epsilon\vec{E} = 0 \quad (2)$$

which finally will be discretized following Galerkin's approach. The electric field strength  $\vec{E} = \sum_i x_i \vec{\omega}_i^{3D}$  is expanded in terms of locally defined real-valued vector basis

# IMPLEMENTATIONAL ASPECTS OF EIGENMODE COMPUTATION BASED ON PERTURBATION THEORY\*

K. Brackebusch<sup>†</sup>, U. van Rienen, Institute of General Electrical Engineering,  
University of Rostock, Germany

## Abstract

Geometry perturbations affect the eigenmodes of a resonant cavity and thereby can improve but also impair the performance characteristics of the cavity. To investigate the effects of both, intentional and inevitable geometry variations parameter studies are to be undertaken. Using common eigenmode solvers involves to perform a full eigenmode computation for each variation step, even if the geometry is only slightly altered. Therefore, such investigations tend to be computationally extensive and inefficient. Yet, the computational effort for parameter studies may be significantly reduced by using perturbative computation methods. Knowing a set of initial eigenmodes of the unperturbed geometry these allow for the expansion of the eigenmodes of the perturbed geometry in terms of the unperturbed modes. In this paper, we study the complexity of a numerical implementation of perturbative methods. An essential aspect is the computation and analysis of the unperturbed modes since the number and order of these modes determine the accuracy of the results.

## INTRODUCTION

Aiming to design a cavity with best possible performance it is necessary to optimize miscellaneous of its characteristics that all depend on the cavity's eigenmodes. The cavity shape mainly influences these characteristics and has to be changed numerous times during the optimization process. Any geometry modification entails a full recomputation of the eigenmodes causing an immense total computational effort. Perturbative methods allow for avoiding this repetitive procedure. The methods (discussed here) base on the approach of computing the eigenmodes (denoted as unperturbed) of exclusively one initial geometry using a common computation method and deriving the eigenmodes (denoted as perturbed) of a modified geometry directly from the unperturbed eigenmodes with substantially less effort.

To do so, the interaction of each unperturbed mode  $i$  with every other unperturbed mode  $k$  has to be determined by forming an expression that includes their resonant frequencies  $f$  and a volume integration over the scalar product of their electric / magnetic fields  $\mathbf{E}(\mathbf{r})$ ,  $\mathbf{H}(\mathbf{r})$

$$IT_{E(i,k)} = \iiint_{\Delta V} \mathbf{E}_i(\mathbf{r}) \cdot \mathbf{E}_k(\mathbf{r}) dV \quad (1)$$

\* Work supported by Federal Ministry for Research and Education BMBF under contracts 05H09HR5 and 05K10HRC

<sup>†</sup> korinna.brackebusch@uni-rostock.de

$$IT_{H(i,k)} = \iiint_{\Delta V} \mathbf{H}_i(\mathbf{r}) \cdot \mathbf{H}_k(\mathbf{r}) dV \quad (2)$$

Here  $\Delta V$  is the volume that is removed by the modification from the unperturbed volume  $V$ . Applying further arithmetic operations to the resulting interaction term (IT) matrix finally yields the perturbed resonant frequencies and weighting factors that allow for expanding each perturbed electromagnetic field as a series of the unperturbed fields. In [1] and [2] two perturbative methods differing in the composition of their ITs and arithmetic operations are described in detail.

In [2] and [3] their applicability was proved by means of analytically evaluable cavity geometries providing very accurate results. Using analytically computed unperturbed eigenmodes all operations can be implemented with very high precision and very low effort. However, for most cavity structures the unperturbed modes have to be numerically computed. This is not only more complex and affected by additional numerical errors but also involves some difficulties that are discussed in the following. The numerical implementation was investigated using the example of a cylindrical cavity subject to one-dimensional perturbations to compare its outcomes with the analytically computed ones.

## NUMERICAL IMPLEMENTATION

The computation of the unperturbed eigenmodes is the first and most expensive operation but has to be done only once for a certain cavity structure. It is required for the ITs and the series expansion and therefore particularly important for the accuracy of the results. The simulations are done with CST MWS Eigenmode Solver [4]. The integrals  $IT_E$  and  $IT_H$  solely depend on the fields in the boundary region (where the perturbation occurs). Besides an appropriate mesh density, hence a precise discretization of the boundary is significant. Since a discrepancy between discretized and actual boundary leads to an abrupt transition of the fields to zero (Fig. 1) an insufficient discretization may seriously impair the accuracy of the  $IT_E$  and  $IT_H$ . The Finite Element Method (FEM) combined with a tetrahedral mesh and curved elements proved to reproduce the boundary much more precisely than the hexahedral dual grid of the Finite Integration Theory (FIT). Therefore, here, FEM should be used for the eigenmode computation of cavities with a curved shape.

For the further processing the computed fields have to be exported from CST MWS as discrete field points. But despite the achieved precise boundary discretization using FEM some of these field values are still affected by the de-

# AN APPLICATION OF THE NON-CONFORMING CROUZEIX-RAVIART FINITE ELEMENT METHOD TO SPACE CHARGE CALCULATIONS

C. Bahls\*, U. van Rienen, University of Rostock, Rostock, Germany

## Abstract

The calculation of space charge effects in linear accelerators is an important prerequisite to understand the interaction between charged particles and the surrounding environment. These calculations should be as efficient as possible. In this work we explore the suitability of the Crouzeix-Raviart Finite Element Method for the computation of the self-field of an electron bunch.

## INTRODUCTION

Current and future accelerator design requires efficient 3D space charge calculations. One possible approach to Space Charge Calculations is the Particle-in-Cell (PIC) method, especially the Particle-Mesh method which calculates the potential in the rest-frame of the bunch.

This computation usually is done by solving Poisson's equation on the domain  $\Omega$ , using a charge weighting  $f(x)$ :

$$-\Delta u(x) = f(x), \quad \forall x \in \Omega.$$

This equation is subject to some boundary conditions:

$$\begin{aligned} u(x) &= g_D(x), & \forall x \in \partial\Omega_D, \\ \text{grad } u(x) \cdot n(x) &= g_N(x), & \forall x \in \partial\Omega_N. \end{aligned}$$

These computations should be as efficient as possible.

## SPACE CHARGE CALCULATIONS

We are aiming at computing the self-field of the bunch. Denoting with  $\mathbf{D}$  the dielectric flux and with  $\rho$  the charge density we are estimating a solution to Gauss' law:

$$\text{div } \mathbf{D} = \rho.$$

Usually there are infinitely many solutions to that equation, as in fact a very large subspace of all vectorial functions on the domain fulfils the equation. One can add any divergence-free field (for example a rotational field) to a known solution without changing the divergence, therefore recovering additional solutions to the field equation.

For the moment we are only interested in curl-free solutions of Gauss' law, so we will only try to estimate fields  $\Psi(x)$  which are gradients of a scalar potential  $u(x)$ , as:  $\Psi(x) = -\text{grad } u(x)$ , so our equations become:

$$\begin{aligned} \text{grad } u(x) + \Psi(x) &= \mathbf{0} & \forall x \in \Omega, \\ -\text{div } \varepsilon(x) \Psi(x) &= \rho(x) & \forall x \in \Omega. \end{aligned}$$

\*christian.bahls@gmx.de

Removing the auxiliary vector function  $\Psi(x)$  this usually gets shortened to the following equation:

$$-\text{div } \varepsilon(x) \text{ grad } u(x) = \rho(x) \quad \forall x \in \Omega.$$

If the permittivity tensor  $\varepsilon(x)$  isotropic and can be replaced by a divergence free scalar function  $\varepsilon(x)$  this becomes:

$$-\Delta u(x) = \varepsilon(x)^{-1} \rho(x) \quad \forall x \in \Omega.$$

Our currently used numerical scheme [5] - solving Poisson's equation  $-\Delta u(x) = \rho(x)/\varepsilon_0$  in vacuum using a finite difference scheme - seems to be less than optimal for estimating the electric field.

We are losing one order of convergence ( $O(h^2) \rightarrow O(h^1)$ ) by the numerical computation of the electric field from the potential  $u$  (even if using the exact derivative on the underlying function space).

The discretized solution  $u_h$  on an equidistant structured mesh approximates the solution  $u$  with an order  $O(h^2)$ :

$$u_h(x) = u(x) + O(h^2).$$

The gradient  $\Psi$  (which corresponds to our accelerating field) will then be approximated with an order of  $O(h^1)$ :

$$\Psi_h(x) = \Psi(x) + O(h^1).$$

As we are mainly interested in the electric field we would like to approximate it with the same order of accuracy as the potential.

So we want to discretize and solve for the vector field  $\Psi$  directly. The discretization used has to be curl-free and should somehow allow for a reasonable definition of the divergence of the field (e.g. be conformal).

## Raviart-Thomas Mixed Finite Elements

One suitable ansatz-space is the lowest order Raviart-Thomas space  $\mathbf{RT}_0$  whose linear vector functions have following element-wise linear expression:

$$\Psi_h(\mathbf{x}) = \mathbf{a}_k + b_k \mathbf{x},$$

where  $\mathbf{x}$  is in the element  $T_k$  of the triangulation  $\mathbf{T}$  of  $\Omega$ .

For the discretisation to be conformal the normal components of the field have to be continuous at every interface (edges in 2D or faces in 3D).

# ANALYZING MULTIPACTING PROBLEMS IN ACCELERATORS USING ACE3P ON HIGH PERFORMANCE COMPUTERS\*

Lixin Ge<sup>1</sup>, Kwok Ko, Kihwan Lee, Zenghai Li, Cho Ng, Liling Xiao  
SLAC National Accelerator Laboratory, Menlo Park, CA 94025, USA

## Abstract

Track3P is the particle tracking module of ACE3P, a 3D parallel finite element electromagnetic code suite developed at SLAC which has been implemented on the US DOE supercomputers at NERSC to simulate large-scale complex accelerator designs [1-3]. Using the higher-order cavity fields [4] generated by ACE3P codes, Track3P has been used for analysing multipacting (MP) in accelerator cavities [5]. The prediction of the MP barriers in the ICHIRO cavity at KEK was the first Track3P benchmark against measurements. Using a large number of processors, Track3P can scan through the field gradient and cavity surface efficiently, and its comprehensive post-processing tool allows the identifications of both the hard and soft MP barriers and the locations of MP activities. Results from applications of this high performance simulation capability to accelerators such as the Half Wave Resonator (HWR) [6], Quarter Wave Resonator (QWR) for FRIB [7], 704 MHz SRF gun cavity for BNL ERL [8] and the Muon cooling cavity for Muon Collider [9] will be presented.

## INTRODUCTION

Multipacting (MP) is an undesired, resonant built-up of electrons inside RF structures. It can cause wall heating and high power RF components like couplers, windows, etc. breakdown. There are also other bad effects, such as significant power loss, low achievable field gradient and thermal breakdown in superconducting structures.

Due to the critical role of multipacting effects on accelerator design, much work has been done on multipacting studies to identify potential MP activities and their locations and to mitigate MP effects using different methods such as modifying geometry to eliminate MP barriers, changing surface conditions to reduce secondary emission yield (SEY) and imposing external DC biasing field.

In recent years, with more computing power, first 2D, then also full 3D simulation tools have been developed to investigate potential multipacting activities in RF-structures [10]. There are several requirements for realistic multipacting simulation, namely, high resolution EM field, correct representation of particle emission from curved surface, realistic SEY curve for surface material and comprehensive post-processing of particle data to identify MP events.

\* The work was supported by the U.S. DOE contract DE-AC02-76SF00515 and used the resources of NERSC at LBNL under US DOE Contract No. DE-AC03-76SF00098.

<sup>1</sup>lge@slac.stanford.edu

## ACE3P CODE SUITE

For more than a decade, SLAC has been developing the conformal, higher-order, C++/MPI based parallel finite element suite of electromagnetic codes [1-3]. ACE3P consists of the following modules: Omega3P for calculating cavity modes and damping, and S3P for transmission in open structures in frequency domain; T3P for calculating wakefields and transients in time domain; Track3P for multipacting and dark current studies using particle tracking; Pic3P for RF gun design with particle-in-cell (PIC) method; and TEM3P for multi-physics analysis including EM, thermal and mechanical effects.

There are several strengths of the parallel finite-element method used in ACE3P. First, high-fidelity geometry modelling can be achieved using curved quadratic tetrahedral elements. Second, higher-order field interpolation functions ( $p = 1-6$ ) improve field accuracy as shown in Fig. 2 when using linear, quadratic and cubic basis functions for solving the eigenmode of the cavity shown in Fig. 1. Third, parallel processing speeds up the computation by taking advantages of the code scalability. The calculation took less than 1 minute to obtain the mode frequency within 0.001% using a mesh with 67k quadratic elements on 16 CPUs with 6GB memory. All these factors are important for multipacting simulation as will be seen later in this paper.

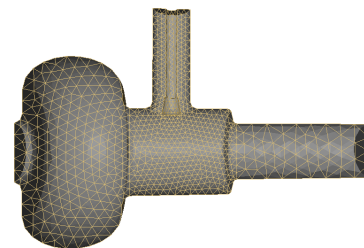


Figure 1: End cell cavity with input coupler.

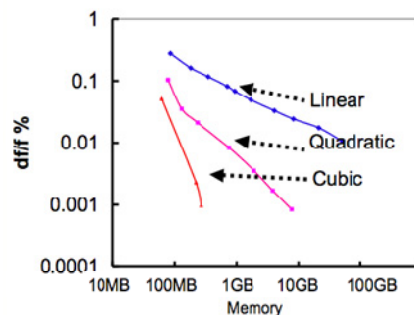


Figure 2: Convergence study for using linear, quadratic and cubic basis functions.

# GPGPU IMPLEMENTATION OF MATRIX FORMALISM FOR BEAM DYNAMICS SIMULATION

N. Kulabukhova\*, Saint-Petersburg State University, Russia

## Abstract

Matrix formalism is a map integration method for ODE solving. It allows to present solution of the system as sums and multiplications of 2-indexes numeric matrix. This approach can be easy implement in parallel codes. As the most natural for matrix operation GPU architecture has been chosen. The set of the methods for beam dynamics has been implemented. Particles and envelope dynamics are supported. The computing facilities are located in St. Petersburg State University and presented by the NVIDIA Tesla-based clusters.

## INTRODUCTION

The performance available on graphics processing units (GPUs) has led to interest in using GPUs for general-purpose programming [1]. It is difficult, however, for most programmers to program GPUs for general-purpose uses.

The raw computational power of a GPU dwarfs that of the most powerful CPU, and the gap is steadily widening. Furthermore, GPUs have moved away from the traditional fixed-function 3D graphics pipeline toward a flexible general-purpose computational engine. Today, GPUs can implement many parallel algorithms directly using graphics hardware. Well-suited algorithms that leverage all the underlying computational horsepower often achieve tremendous speedups[2]. Truly, the GPU is the first widely deployed commodity desktop parallel computer.

Here, we provide a comparison of different sort of parallel technologies of the classic graphics pipeline; our goal is to highlight those aspects of the real-time rendering calculation that allow graphics application developers to exploit modern GPUs as general-purpose parallel computation engines.

## COMPARISON OF GPU AND CPU

The highly parallel workload of real-time computer graphics demands extremely high arithmetic throughput and streaming memory bandwidth but tolerates considerable latency in an individual computation since final images are only displayed every 16 milliseconds. These workload characteristics have shaped the underlying GPU architecture: Whereas CPUs are optimized for low latency, GPUs are optimized for high throughput. The GPUs specialized architecture is not well suited to every algorithm. Many applications are inherently serial and are characterized by incoherent and unpredictable memory access. Nonetheless, many important problems require significant

computational resources, mapping well to the GPUs many-core arithmetic intensity, or they require streaming through large quantities of data, mapping well to the GPUs streaming memory subsystem. Porting a judiciously chosen algorithm to the GPU often produces speedups of five to 20 times over mature, optimized CPU codes running on state-of-the-art CPUs, and speedups of more than 100 times have been reported for some algorithms that map especially well. Some successful examples of using GPUs are described in [2].

In contrast, most CPU programs use a sequential programming model and are not benefiting from the continued increase in transistors due to Moores law. They will need to be rewritten or modified substantially to obtain increased performance from new CPUs with multiple cores on a chip. Furthermore, CPU clock speeds have plateaued due to power concerns. On the other hand, GPU architectures have a number of disadvantages for parallel programming. First, GPUs have a SIMD programming model. GPUs are moving toward a SPMD model, although use of loops and control-flow instructions in GPU pixel shaders may currently degrade performance, not improve it. Second, the actual architectures of GPUs are hidden behind device drivers that support APIs that implement virtual machines. This abstraction and lack of detail can hamper obtaining the most performance out of a graphics processor. For example, the virtual machines have no model of caches and no easy way for programmers to indicate how to traverse memory to facilitate memory reuse. This can make it difficult to write parallel programs where memory locality is crucial to performance. In addition, we must target APIs designed to support graphics that introduce extra complexity and overhead. Third, the programmable parts of GPUs have had limited support for primitive types typically found on CPUs.

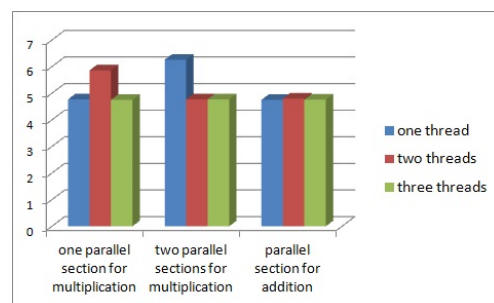


Figure 1: Diagram of comparative performance.

\*kulabukhova.nv@gmail.com

# A MASSIVELY PARALLEL GENERAL PURPOSE MULTI-OBJECTIVE OPTIMIZATION FRAMEWORK, APPLIED TO BEAM DYNAMIC STUDIES

Y. Ineichen, A. Adelman\*, PSI, Villigen, Switzerland

C. Bekas, A. Curioni, IBM Research – Zurich, Switzerland

P. Arbenz, Department of Computer Science, ETH Zurich, Switzerland

## Abstract

Particle accelerators are invaluable tools for research in the basic and applied sciences, in fields such as materials science, chemistry, the biosciences, particle physics, nuclear physics and medicine. The design, commissioning, and operation of accelerator facilities is a non-trivial task, due to the large number of control parameters and the complex interplay of several conflicting design goals.

We propose to tackle this problem by means of multi-objective optimization algorithms which also facilitate massively parallel deployment. In order to compute solutions in a meaningful time frame, that can even admit on-line optimization, we require a fast and scalable software framework.

In this paper, we present an implementation of such a framework and report first results of multi-objective optimization problems in the domain of beam dynamics.

## INTRODUCTION

In contemporary scientific research, particle accelerators play a significant role. Fields, such as material science, chemistry, the biosciences, particle physics, nuclear physics and medicine rely on reliable and effective particle accelerators as research tools. Achieving the required performance is a complex and multifaceted problem in the design, commissioning, and operation of accelerator facilities. Today, tuning machine parameters, e.g., bunch charge, emission time and various parameters of beamline elements, is most commonly done manually by running simulation codes to scan the parameter space. This approach is tedious, time consuming and can be error prone. In order to be able to reliably identify optimal configurations of accelerators we propose to solve large multi-objective design optimization problems to automate the investigation for an optimal set of tuning parameters. Observe that multiple and conflicting optimality criteria call for a multi-objective approach.

We developed a modular multi-objective software framework (see Fig. 1) where the core functionality is decoupled from the “forward solver” and optimizer (master/slave). This allows to easily interchange optimizer algorithms, forward solvers and optimization problems. A “pilot” coordinates all efforts between the optimization algorithm and the forward solver. This forms a robust and general framework

\* andreas.adelmann@psi.ch

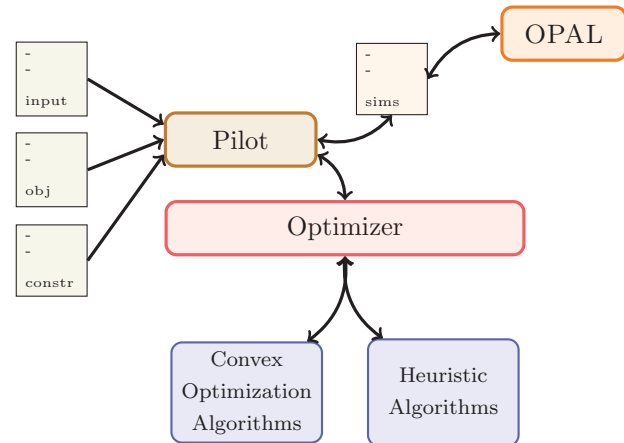


Figure 1: Multi-objective framework: the pilot (master) solves the optimization problem specified in the input file by coordinating optimizer algorithm and workers running forward solves.

for massively parallel multi-objective optimization. Currently the framework offers one concrete optimization algorithm, an evolutionary algorithm employing a NSGAI selector [1]. Normally simulation based approaches are plagued by the trade-off between level of detail and time to solution. We address this problem by using forward solvers with different time and detail complexity.

The first section covers a brief introduction to multi-objective optimization theory and describes the available optimizer. Next we discuss the implementation of the framework and present a proof of concept application of a beam dynamics problem.

## MULTI-OBJECTIVE OPTIMIZATION

Optimization problems deal with finding one or more feasible solutions corresponding to extreme values of objectives. If more than one objective is present in the optimization problem we call this a multi-objective optimization problems (MOOP). A MOOP is defined as

$$\min f_m(\mathbf{x}), \quad m = 1 \dots M \quad (1)$$

$$\text{s.t. } g_j(\mathbf{x}) \geq 0, \quad j = 0 \dots J \quad (2)$$

$$x_i^L \leq \mathbf{x} = x_i \leq x_i^U, \quad i = 0 \dots n, \quad (3)$$

where we denote  $f$  as the objectives (1),  $g$  the constraints (2) and  $x$  the design variables (3).

# THE TRIUMF OPTIMIZATION PLATFORM AND APPLICATION TO THE E-LINAC INJECTOR\*

C. Gong and Y.C. Chao  
 TRIUMF, 4004 Wesbrook Mall, Vancouver V6T 2A3, Canada

## Abstract

Multi-objective genetic algorithms (MOGA) have demonstrated their usefulness for the global optimization of accelerator design using Elegant [1] and Astra [2]. A MOGA platform developed at TRIUMF seeks to expand the capabilities of such tools by allowing multiple simulation engines to be used. The TRIUMF optimization software platform was applied to the transport design of an injection line leading from a cryomodule to the beam dump. The optimization involves two simulation engines, Astra and MAD-X, and demonstrates the ability for the platform to handle multi-engine optimization for a realistic problem. Results of the optimization are shown.

## INTRODUCTION

A software platform for global optimization was created at TRIUMF [3]. The platform uses Multi-Objective Genetic Algorithms (MOGA) [4] as a wrapper around simulation engines. MOGA creates an initial population, with each member of the population some combination of randomly chosen variables. For each of a fixed number of iterations, the members are assigned a density, based on how well they satisfy the optimization constraints and objectives. Members are then randomly chosen, with a bias based on the density function, to 'breed' new members (by mutation, crossing variables, etc). Such algorithms are suitable for global optimization because they ignore the geometry of the search space, and given a large enough population and long enough running time, will always find the global optimum. In accelerator design, MOGA codes are wrappers for simulation engines such as Astra [5]. Each member of the population is an individual Astra run with different input variables such as magnet strengths and RF phase. Constraints and objectives are set on the Astra outputs, such as emittance and bunch length.

Previous single-engine MOGA codes [1, 2] have demonstrated their usefulness for accelerator design. However, since different engines are more useful in different situations, as listed in Table 2, modern accelerators require multi-engine simulations to encompass the wide range of design parameters. This motivates the TRIUMF code platform (Fig. 1), designed to handle multi-engine problems with arbitrary topology descriptions. The code was tested and performed satisfactorily in trial problems in a parallel-capable Linux environment [3].

The ARIEL/e-linac [6] project currently underway at

\*Work supported by Natural Sciences and Engineering Research Council of Canada and National Research Council of Canada

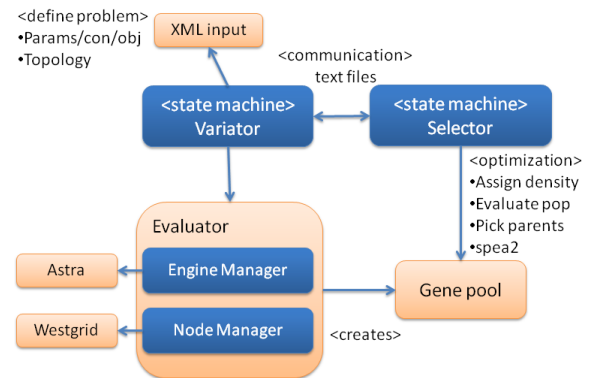


Figure 1: The architecture is based on A Platform and Programming Language Independent Interface for Search Algorithms [7]. The main components of the design are Variator, Selector, and Evaluator. Variator is a state machine which reads from the input file and defines the optimization problem. Evaluator handles the direct evaluation of all individuals in the population, including assigning and managing jobs to network nodes [8], and running the engine executables. Selector is a state machine which calculates the density, i.e. fitness, of the individuals and selects those for reproduction. The benefits of such a framework is decoupling between the algorithm, the problem definition, and the wrapper.

TRIUMF sees the possibility of operating a machine in dual rare isotope (RIB) and light source operation (FEL) (Fig. 2). The assortment of problems present in such a machine and the coupling between parameters, especially the machine settings shared by the low intensity RIB and high intensity FEL beams, means it would be difficult to separate the simulation into individual modules. The pre-mentioned problems leads to a design requiring the use of multi-engine simulations. The optimization platform was created in preparation as a wrapper for such simulations. A sample of anticipated problems is listed in Table 1.

## TRIUMF E-LINAC: INJECTOR CRYOMODULE TO DUMP

We demonstrate the platform capabilities in a realistic and practical problem for TRIUMF's e-linac project [6]. The injector consists of 300 keV beam from a thermionic gun going through a buncher and accelerated to 10 MeV through the injection cryomodule (ICM), which houses a 9-cell superconducting cavity. For the current stage test plan, the beam after the ICM terminates on a beam dump. Three

# GLOBAL OPTIMIZATION OF THE ANKA LATTICE USING MULTIOBJECTIVE GENETIC ALGORITHMS (MOGA)\*

M. Streichert<sup>†</sup>, N. Hiller, E. Huttel, V. Judin, B. Kehrer, M. Klein<sup>‡</sup>,  
S. Marsching, C. Meuter, M.J. Nasse, A.-S. Müller, M. Schuh, N.J. Smale  
Karlsruhe Institute of Technology (KIT), Karlsruhe, Germany

## Abstract

The optimization of a storage ring lattice is a multiobjective problem, since the parameter space of possible solutions can be very large and a high number of constraints have to be taken into account during the optimization process. In this paper we used Genetic Algorithms (GA) and MultiObjective Genetic Algorithms (MOGA), which can solve such problems very efficiently and rapidly, to find the optimized settings for the ANKA storage ring lattice.

## INTRODUCTION

ANKA is the synchrotron light source of the Karlsruhe Institute of Technology (KIT)[1]. It consists of 4 super periods with two double bend achromats (DBA) structures each. Each DBA structure contains 2 bending magnets, 5 quadrupole families and two chromatic sextupole families to control the vertical and horizontal chromaticity. We implemented a Global Scan of All Stable Settings (GLASS)[2], based on linear optics to find all possible quadrupole settings of the ANKA lattice. However, the GLASS technique requires a lot of computational power. To decrease the computation time, we considered a symmetric super period by reducing the number of quadrupole families from 5 to 3. Furthermore, we implemented a parallel code to make use of multicore computers. However, the whole scan took up to 28 hours. For optimizations with all five quadrupole families, the GLASS technique is no longer an effective approach. Hence we employed much faster genetic algorithms to find optimal quadrupole settings. We used the GLASS scan to benchmark GA and MOGA for the three quadrupole families and performed global optimizations with GA for all five quadrupole families.

## GENETIC ALGORITHMS

GA optimization is a promising technique to find the optimal solution in a multi-dimensional, non-continuous parameter space. This technique can easily be implemented with the existing simulation models for ANKA and does not require knowledge or gradient information of the response function. We compared the GA results with the GLASS results to benchmark and to explore the optimum settings for the GA, for instance the population size, the maximum number of generations etc. We performed

GA optimization to find the optimal low-emittance optics. Since not all settings of quadrupole strengths lead to stable or feasible solutions, we implemented the following constraints in GA:

- $|\text{tr}(M_{x,y})| < 2$ ,  $\beta_{x,y} < 40$  m,
- $|\eta_x| < 2$  m,  $J_x, J_s > 0$ ,
- no tune resonance up to the 2<sup>nd</sup> order,

where  $M_{x,y}$  is the transversal one turn transfer matrix,  $\beta_{x,y}$  transversal beta function,  $|\eta_x|$  the horizontal dispersion function and  $J_x, J_s$  are the damping partition numbers. Beam energy dependent fringe field integrals and quadrupole components in the ANKA bending magnets[3] were taken into account in our optimizations to get a realistic model for the ANKA lattice at the beam energy of 2.5 GeV. The optimization was performed in the range of  $-2.4$  to  $2.4$  m<sup>-2</sup>, corresponding to the maximum possible current for the ANKA quadrupole magnets. For a fair comparison of both techniques, we discretized the parameter space for the GA optimization with the same grid spacing ( $0.02$  m<sup>-2</sup>) as for the GLASS scan, reduced the number of quadrupole families from 5 down to 3, and turned off the sextupole magnets.

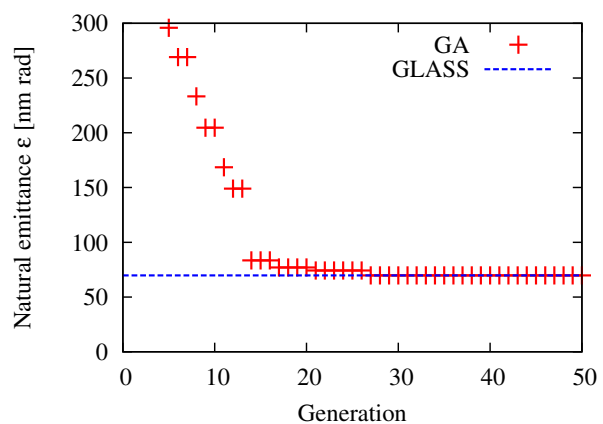


Figure 1: Comparison of the GA with the GLASS results. Minimization of the emittance at 2.5 GeV with minimal chromaticity values of  $-10$  as additional constraint.

After 50 generations the GA converged to the same value of  $69.8$  nm rad, which we found by using the GLASS (see Fig. 1). However, for the whole GLASS scan, 28 hours

\* This work has been supported by the Initiative and Networking Fund of the Helmholtz Association under contract number VH-NG-320.

<sup>†</sup> max.streichert@student.kit.edu

<sup>‡</sup> now at SOLEIL, Gif-sur-Yvette, France

# MULTI-OBJECTIVE GENETIC OPTIMIZATION OF LINAC BEAM PARAMETERS FOR A SEEDED FEL

Marco Apollonio\*, Riccardo Bartolini, Ian Martin,  
Diamond Light Source, Oxfordshire, OX11 0DE, United Kingdom

## Abstract

The optimization of the beam dynamics in a Linac for free electron lasers (FELs) can be a very time consuming process, in which several parameters of the acceleration and compression sections need to be varied simultaneously. The optimization procedure is required to tackle different and often opposing goals at a time, depending on the adopted FEL scheme. As such, multi-objective genetic algorithms are an interesting choice, given their ability to target several, often conflicting objectives. We have studied an optimization strategy based on a combination of multi-objective optimization with a fast parallel computation of the FEL performance and, for the specific case of the proposed UKs New Light Source (NLS), we illustrate the benefits of this method for the optimization of the average gain length and its variation along the beam pulse. The method can be extended to other sets of objectives, such as power and bandwidth of the FEL.

## INTRODUCTION

X-ray free electron lasers are the natural evolution of 3<sup>rd</sup> generation light sources towards brighter, shorter and fully coherent photon pulses. The presently operating machines (see *e.g.* [1]) represent not only a proof of principle but established tools for new science. A typical structure adopted in these projects consists of a high brightness electron gun, a linear accelerator used to reach the final energy, and are equipped with few compression stages to increase the bunch peak current. A properly optimized linac section should maintain a high brightness throughout. The required linac tuning depends on the kind of lasing we want to achieve. In the simplest scheme, the self-amplified spontaneous emission (SASE), a large peak current, small energy spread and small normalized emittance are key elements. Any portion of the bunch with a length equal to the FEL cooperation length and with the aforementioned beam qualities, will contribute to an independent SASE pulse with its saturation length and limited time coherence. In order to improve the performance of a SASE scheme a seeding laser can be used. In the seeded mode of operation, the temporal coherence can in principle be extended to the length of the seed pulse. However this mode demands a higher beam quality control over a wider region of the pulse length. Proposed schemes like high gain harmonic generation (HG), cascaded HG or ECHO enabled harmonic generation (EEHG) all require a careful control over the energy spread. Beam uniformity beyond the full seed length both in terms of current and emittance is also

an important asset. In general the length of the uniform portion of the beam should be larger than the seed laser pulse, in order to take into account the unavoidable arrival time jitter between the electron bunch and the laser pulse. In this way one makes sure that the laser seed is always overlapping a uniform region of the electron bunch.

In order to reach this, beam dynamics needs to be optimized by means of start-to-end simulations, taking into account collective effects like coherent synchrotron radiation (CSR), longitudinal space charge (LSC) and transverse and longitudinal wakefields present in the accelerating stages. Usually a large number of often correlated machine parameters need to be varied while the resulting objective functions can be mutually conflicting (*e.g.* high peak current and current uniformity in a bunch). Multi-objective genetic algorithms (MOGA) represent an interesting approach to this class of optimization problems, and as such have been already used to characterize accelerators in many different cases (see *e.g.* [2]).

In this paper the stress is on the use of a MOGA for the tuning of a seeded FEL linac. Even though focused on the specific design for the New Light Source, the strategy adopted here can be easily ported to another machine.

## OPTIMIZATION FOR THE NLS LINAC

The NLS was a project for a 4<sup>th</sup> generation light source comprising three seeded FELs driven by a single 2.25 GeV superconducting linac [3]. The baseline set-up diagram is shown on Fig. 1 together with the most relevant parameters of the machine. More details can be found in [4]. Downstream of the main linac a collimation section and a spreader section are used to remove the beam halo and off-momentum electrons respectively and to bring the beam to the three FELs.

### Objectives and Optimization Procedure

The universal figure of merit describing the exponential amplification in a high gain FEL is the non-dimensional Pierce parameter  $\rho$  [5]. Another important figure related to  $\rho$  is the gain length, which describes the power growth in the undulator section and can be expressed in the 1-D model, by:

$$L_g = \frac{\lambda_u}{4\pi\sqrt{3}\rho} \quad (1)$$

where  $\lambda_u$  is the undulator period. A more realistic expression for the gain length, which takes into account the average size, emittance and energy spread of the beam is given by the Xie parametrization [6]. Both SASE and seeded modes require good electron bunch quality to deliver the shortest possible gain length. In the seeded case

\* marco.apollonio@diamond.ac.uk

# LOW NOISE PARTICLE-IN-CELL SIMULATIONS OF LASER PLASMA ACCELERATOR 10 GeV STAGES\*

E. Cormier-Michel<sup>†</sup>, D. L. Bruhwiler<sup>‡</sup>, J. R. Cary, B. M. Cowan, E. J. Hallman,  
Tech-X Corporation, Boulder, CO 80303, USA  
E. Esarey, C. G. R. Geddes, W. P. Leemans, C. B. Schroeder, J.-L. Vay,  
LBNL, Berkeley, CA 94720, USA

## Abstract

Because of their ultra-high accelerating gradient, laser plasma based accelerators (LPA) are contemplated for the next generation of high-energy colliders and light sources. The upcoming BELLA project will explore acceleration of electron bunches to 10 GeV in a 1 meter long plasma, where a wakefield is driven by a PW-class laser. Particle-in-cell (PIC) simulations are used to design LPA stages relevant to the upcoming experiments. Simulations in a Lorentz boosted frame are used to gain significant speed up and to simulate the 10 GeV stages at full scale parameters, which are otherwise impractical. As criteria on energy spread and beam emittance become more stringent, PIC simulations become more challenging as high frequency noise artificially increases those quantities. To reduce numerical noise, we consider using a Poisson solve to calculate the beam self-fields. This method allows correct cancellation of the beam transverse self-forces and prevents artificial emittance growth.

## INTRODUCTION

Laser-plasma accelerators (LPA) can reach accelerating gradients several orders of magnitude larger than conventional accelerating structures [1], opening the path to more compact light sources and particle colliders. Recently, mono-energetic electron beams have been accelerated to 100 MeV in a 3 mm long plasma [2, 3, 4] and 1 GeV in a 1 cm plasma [5, 6], using 10 and 40 TW lasers respectively. Energy gain is increased by using higher laser power and lower density for longer acceleration length. The BELLA project at LBNL will explore increasing the energy gain to 10 GeV, using a 1 meter long plasma and a PW-class laser [7]. A succession of this type of stages can be used efficiently to build a TeV linear collider [8].

Particle-in-Cell (PIC) simulations are an essential tool to understand the physics inherent to laser-plasma acceleration and to design future devices. As longer stages are used to reach higher energy, simulations become more computationally intensive, since grid size and time step are lim-

ited by the laser wavelength, typically of the order of 1 micron. To make simulations more affordable, reduced models are used such as the Ponderomotive Guiding Center method [9, 10, 11, 12, 13], or envelope model, where the laser wavelength is no longer resolved and the smallest scale length is the plasma wavelength which scales with the stage length and energy gain. The latter method allows order of magnitude speed-up but is limited because it can not model the laser all the way into depletion. Simulations in a Lorentz boosted frame reduce the number of time steps needed for the simulations while still resolving the laser wavelength [14, 15]. This method has proven successful in simulating 10 GeV LPA stages with orders of magnitude speedup [16].

Accurate representation of the accelerated beam is limited by numerical noise in PIC simulations. This becomes more of an issue as the condition on beam energy spread and emittance becomes more stringent. Introduction of higher order particle shapes has allowed significant reduction of numerical noise in LPA simulations with PIC [17], representing beam properties within a few % of what is obtained in experiments, in contrast to results using linear interpolation which differ by an order of magnitude [18]. To more accurately represent beam evolution with % level energy spread and a fraction of mm mrad emittance, as required by applications, we explore using a method commonly used in tracking codes [19, 20, 21] but that has never been used in the context of LPA, in which the beam self-fields are calculated using a Poisson solve in the beam rest frame. This method provides correct relativistic cancellation of the beam transverse self-forces and prevents high frequency numerical noise responsible for artificial emittance growth of the beam.

## SIMULATIONS IN A BOOSTED FRAME

Methods presented by J.-L. Vay and collaborators [16] are used in the Vorpil framework [22] to perform simulations in a relativistic boosted frame of 10 GeV LPA stages, relevant to the BELLA project, with parameters similar to those presented in [23]. The boosted frame technique allows the simulation to be performed at full scale, i.e., 1 m long stage at the nominal plasma density  $n_0 = 10^{17} \text{ cm}^{-3}$ . An externally injected 2 pC beam is used, with normalized emittance  $\epsilon_n = 0.5 \text{ mm mrad}$  and initial energy  $E = 1 \text{ GeV}$ . The evolution of the beam properties is consistent for different values of the simulation frame relativis-

\* Work supported by the US DOE office of science, office of High-Energy Physics under grants numbers DE-FC02-07ER41499 (SciDAC-2; ComPASS Project), DE-SC0004441 (SBIR), and DE-AC02-05CH11231 (LBNL). This research used resources of the National Energy Research Scientific Computing Center, which is supported by US DOE Office of Science under Contract No. DE-AC02-05CH11231.

<sup>†</sup> ecormier@txcorp.com

<sup>‡</sup> Current address: 1348 Redwood Ave., Boulder CO 80304

# NUMERICAL MODELING OF COLLECTIVE EFFECTS IN FREE ELECTRON LASER

Igor Zagorodnov, DESY, Hamburg, Germany

## Abstract

In order to have a free electron laser (FEL) of high performance we need to design and optimize it taking into account the dynamics of electrons and their interactions with each other and with their surroundings. An accurate self-consistent simulation of collective effects in the charged beams remains a challenging problem for numerical analysis. In this paper we consider only the modeling of FEL process in an undulator section. We give a short overview of the numerical methods adopted in different FEL codes. Advantages and drawbacks of these methods will be discussed. Some approaches to improve the accuracy and efficiency of the codes will be presented and the remaining challenges in FEL modeling will be highlighted.

## INTRODUCTION

An accurate self consistent simulation of collective effects in the charged beams remains a challenging problem for numerical analysis. During the last decades several numerical codes have been developed to model the non-linear process in a self-amplified spontaneous emission (SASE) free electron lasers (FEL). In this paper we review the mathematical FEL model used in these codes [1-4]. To illustrate the numerical methods we use those implemented in code ALICE [5].

Modelling of the FEL is challenging due to different scales of the process [6]. The disparity of scales up to 12 orders of magnitude imposes several limitations on the size of the systems that can be modelled on the basis of classical Maxwell-Vlasov set of equations.

In order to be able to study the FEL process two main approximations are used: wiggler-period averaging of the equations of motion and slowly-varying envelope approximation of the Maxwell equations.

## FEL MATHEMATICAL MODEL

We consider the case of helical undulator with the magnetic field on the axis given by

$$\vec{B}_\perp^w = (\nabla \times \vec{A}_\perp^w)_\perp = \frac{\partial}{\partial z} \begin{pmatrix} -A_y^w \\ A_x^w \end{pmatrix} = \frac{mc}{e} K k_w \begin{pmatrix} \cos(k_w z) \\ -\sin(k_w z) \end{pmatrix}.$$

Following the approach of [1] the equations of motion for helical undulator can be derived from Hamiltonian

$$h(\vec{r}_\perp, ct; \vec{P}_\perp, P_t; z) = -\gamma \left[ 1 - \frac{1 + |\vec{P}_\perp|^2 + |\vec{a}_\perp|^2 + 2(\vec{P}_\perp, \vec{a}_\perp)}{\gamma^2} \right]^{0.5} + a_z.$$

In order to avoid the necessity to resolve the fast "slalom" motion we carry out *wiggler-period averaging* of the Hamiltonian. The scalar product disappears and we obtain the averaged Hamiltonian

$$h(\vec{r}_\perp, ct; \vec{P}_\perp, P_t; z) = -\gamma \left[ 1 - \frac{1 + |\vec{P}_\perp|^2 + |\vec{a}_\perp|^2}{\gamma^2} \right]^{0.5} + a_z.$$

The squared module of the transverse part of the vector potential  $\vec{a} = e\vec{A}/(mc)$  can be approximated as

$$|\vec{a}_\perp|^2 = K^2 + 2a_s K \sin(\psi + \varphi_s).$$

Here  $\psi = (k + k_w)z - \omega t$  is a particle phase,  $K$  is an undulator parameter,  $a_s \exp(i\varphi_s)$  is a normalized complex amplitude of the amplified wave

$$A_x + iA_y = -imc e^{-1} a_s e^{i(kz - \omega t + \varphi_s)},$$

$$\vec{E}_\perp = -\frac{\partial}{\partial t} \vec{A}.$$

The canonical moments are defined by relations

$$\vec{P}_\perp = \gamma \frac{d\vec{r}_\perp}{dz} \beta_z - \vec{a}_\perp, \quad P_t = -\gamma + \frac{e}{mc^2} \varphi.$$

The equations of motion derived from the averaged Hamiltonian read

$$\frac{d\psi}{dz} = k_w - k(2\gamma^2)^{-1} \left( 1 + |\vec{P}_\perp|^2 + K^2 \right),$$

$$\frac{d\gamma}{dz} = \frac{eK}{mc^2 \gamma^2} \Re(\tilde{E} e^{i\psi}) - \frac{e}{mc^2} E_z,$$

$$\frac{d\vec{r}_\perp}{dz} = \frac{\vec{P}_\perp}{\gamma \beta_z},$$

$$\frac{dP_x}{dz} = -\left( \frac{K^2 k_x^2}{\gamma \beta_z} + \frac{eg}{mc} \right) x, \quad \frac{dP_y}{dz} = -\left( \frac{K^2 k_y^2}{\gamma \beta_z} - \frac{eg}{mc} \right) y,$$

where  $g = \partial_y B_x$  describes the gradients of the focusing quadrupole lattice and we have used the following representations of the undulator parameter and the transverse EM field

$$K(x, y, z) = K_0(x, y, z) \left( 1 + \frac{k_x^2}{2} x^2 + \frac{k_y^2}{2} y^2 \right),$$

$$E_\perp = E_x + iE_y = \tilde{E}(\vec{r}, t) e^{i(kz - \omega t)} + c.c.$$

We split the electromagnetic field in the transverse and the longitudinal components. The longitudinal electrostatic field comes from the bunching and can be suggested to be a nearly periodic one. Then the Fourier components of the longitudinal field can be found from the equation [1]

$$\left( \nabla_\perp^2 - \frac{n^2(k + k_w)^2}{\gamma_z^2} \right) E_z^{(n)} = \frac{in(k + k_w)}{\epsilon_0 \gamma_z^2} \rho^{(n)},$$

$$\rho^{(n)}(\vec{r}_\perp) = \frac{1}{2\pi} \int_0^{2\pi} \rho(\vec{r}_\perp, \psi) e^{-in\psi} d\psi = -\frac{I}{Nv_z} \sum_{i=1}^N e^{-in\psi_i} \delta(\vec{r}_\perp - \vec{r}_{i\perp}).$$

# WAVE - A COMPUTER CODE FOR THE TRACKING OF ELECTRONS THROUGH MAGNETIC FIELDS AND THE CALCULATION OF SPONTANEOUS SYNCHROTRON RADIATION

M. Scheer\*, Helmholtz-Zentrum Berlin für Materialien und Energie, Berlin, Germany

## Abstract

WAVE is developed at BESSY - now Helmholtz-Zentrum Berlin (HZB) - since 1990 to calculate spontaneous synchrotron radiation for arbitrary magnetic fields. A variety of field models for dipoles, wavelength shifters, and undulators is available. Field maps can be read and written. Many routines to handle magnetic fields are implemented, including simulations of field error e.g. due to misalignment. Coherent radiation of electrons in a bunch and energy losses due to radiation are taken into account. Phase-space distributions of the beam electrons are taken into account by various algorithms. Generating functions and linear transfer matrices for particle tracking purposes can be calculated. Subroutines to calculate the effects of insertion devices on the storage ring are included. The program runs in batch mode, controlled by input files, but a simple GUI is also provided. The results are given as ASCII data or binary formats of the programs PAW, ROOT, and HDF5. Parallel runs of WAVE on a cluster are supported. WAVE has been checked and validated with the synchrotron radiation code of the German National Bureau of Standards (PTB) based on Schwinger's formula.

## INTRODUCTION

The development of WAVE started in 1990 within the framework of a study for the PTB. Subject of this study was the question, whether a superconducting wave-length shifter (WLS) can be used at the planned storage ring BESSY II for radiometry in the X-ray regime. The code was developed as a tool to calculate the synchrotron radiation of a WLS with very high precision and also to investigate the impact of the WLS on the storage ring with respect to emittance change, beam polarization and dynamical aperture. This study has become the starting point for the PhD thesis of the author [1], where more details are given. From 1994 the calculation of undulator radiation became more important and many routines to model and handle magnetic fields of undulators has been implemented. WAVE is written in FORTRAN 90 and can be compiled and used on a variety of platforms and operating systems. However, nowadays it is developed mainly for Linux.

\*Michael.Scheer@Helmholtz-Berlin.de

## MAGNETIC FIELDS

The periodic magnetic fields of undulators can be approximately described by analytical formulas. Although these formulas are available in WAVE, many problems, e.g. the calculations of effects of field errors or endpole configurations, require more sophisticated methods. Complex setups like helical undulators coupled by a modulator build of rotatable, cylindrical magnets [2] are treated in WAVE as an arrangement of permanent magnets. Undulator parameters as gap, shift, dimensions and magnetization of the magnets as well as taper, misalignments, and field errors can be set by the user. The magnets can be read from an external file or defined as complete devices in the input file of WAVE. The fields of the individual magnets are calculated using the current sheet method. Another very powerful method is to model the fields by a Fourier series of analytical 3D functions [1, 3]. This includes algorithms to expand the vertical field given on the longitudinal axis of an insertion device to a Maxwell conform 2D or 3D field. However, sometimes the usage of field maps is more flexible or necessary. WAVE can handle 3D field maps with different interpolation schemes. Another group of features include symmetry operations and options to make fields periodic along the longitudinal device axis. For applications not covered by WAVE, the user can also provide his own magnetic field routine.

## TRACKING

The tracking algorithm of WAVE considers the magnetic field as constant for each time step. Thus, the trajectory consists of pieces of circles with orientation and bending radii according to the local field. An option allows to calculate the energy loss due to the synchrotron radiation for each tracking step and to adapt the energy of the electron accordingly. This can be done continuously or by a Monte-Carlo technique which generates discrete photons in order to take quantum fluctuations into account. For special purposes, the user may provide an own routine called for each tracking step.

## SYNCHROTRON RADIATION

The spectrum calculation is mainly a numerical integration of well-known formulas given e.g. in [4]. WAVE uses a modified version:

# A FAST INTEGRATED GREEN FUNCTION METHOD FOR COMPUTING 1D CSR WAKEFIELDS INCLUDING UPSTREAM TRANSIENTS

C.E. Mitchell, Ji Qiang, and R.D. Ryne, Lawrence Berkeley National Laboratory, USA

## Abstract

An efficient numerical method for computing wakefields due to coherent synchrotron radiation (CSR) has been implemented using a one-dimensional integrated Green function approach. The contribution from CSR that is generated upstream and propagates across one or more lattice elements before interacting with the bunch is included. This method does not require computing the derivative of the longitudinal charge density, and accurately includes the short-range behavior of the CSR interaction. As an application of this method, we examine the importance of upstream transient wakefields within several bending elements of a proposed Next Generation Light Source.

## BACKGROUND

The accurate modeling of coherent synchrotron radiation is a numerical challenge of key importance to the development of future light sources [1]. Recent 3D simulations of the CSR generated by Gaussian bunches of various shapes [2] confirm that a 1D model of the longitudinal CSR wakefield is accurate provided that the transverse rms beam size  $\sigma_{\perp}$  satisfies  $\sigma_{\perp} \ll R(\sigma_z/R)^{2/3}$ , where  $R$  is the bending radius and  $\sigma_z$  is the longitudinal rms beam size. A number of such 1D models appear in the literature [3]–[7], many of which have been implemented in existing beam dynamics codes.

In these models, the energy loss per unit length at a longitudinal location  $z$  within the bunch is given by:

$$W(z) = \int_{-\infty}^z \lambda(z') K_{CSR}(z, z') dz', \quad (1)$$

where  $\lambda$  is the longitudinal number density of the bunch, and  $K_{CSR}$  is related to the longitudinal component of the Liénard-Wiechert field  $\mathbf{E}^{LW}$  of a single particle [6]. The integration kernel  $K_{CSR}$  varies rapidly near  $z \approx z'$  on the scale  $R/\gamma^3 \ll \sigma_z$ , and the integral (1) is therefore difficult to resolve numerically. This problem is typically avoided by computing the equivalent integral

$$W(z) = \int_{-\infty}^z \frac{d\lambda(z')}{dz'} I_{CSR}(z, z') dz', \quad (2)$$

where

$$I_{CSR}(z, z') = - \int_{-\infty}^{z'} K_{CSR}(z, z'') dz''. \quad (3)$$

The kernel  $I_{CSR}$  exhibits less singular behavior than  $K_{CSR}$  near  $z \approx z'$ . However, this method requires that one evaluate the numerical derivative of the longitudinal charge density, which in general contains significant numerical noise. It is also typical to approximate  $I_{CSR}$  by an

asymptotic form. (See, for example, equation (19) of [4].)

In the following section, we describe an efficient method for evaluating (1) that makes use of the longitudinal charge density  $\lambda$  directly. The short-range behavior of the CSR kernel is treated analytically, so that only longitudinal variations in the charge density need to be resolved [8, 9]. In addition, this method can be used to treat the case of entry and exit transient fields [4], as well as the case of transient fields in a general lattice due to upstream elements [6].

## INTEGRATED GREEN FUNCTION METHODS

Let  $\lambda_j = \lambda(z_j)$ ,  $j = 1, \dots, N$  denote the values of the longitudinal number density of the bunch at a set of equidistant sample points  $z_j$ ,  $j = 1, \dots, N$ , and let  $\{P_j : j = 1, \dots, N\}$  denote a basis of piecewise polynomials of given degree. This basis can always be chosen such that  $P_j(z_k) = \delta_{j,k}$ . We can then write the interpolated longitudinal density  $\lambda_{approx} \approx \lambda$  in the form

$$\lambda_{approx} = \sum_{j=1}^N \lambda_j P_j(z). \quad (4)$$

Using (4) in (1) gives an approximate longitudinal wakefield  $W_{approx} \approx W$  of the form

$$W_{approx}(z_k) = \sum_{k'=1}^N \lambda_{k'} w_{k,k'}, \quad \text{where} \quad (5)$$

$$w_{k,k'} = \int_{-\infty}^{z_k} P_{k'}(z') K_{CSR}(z_k, z') dz'.$$

For the models described in [3]–[6], the weights  $w_{k,k'}$  may be determined analytically in terms of rational functions, log, arctan, and polynomial roots. In particular, the quantities  $w_{k,k'}$  have been determined explicitly for the 1D models described in [4, 6] in the cases of both piecewise constant and piecewise linear basis functions.

For example, a set of piecewise-constant basis functions is given, for stepsize  $h$ , by:

$$P_{k'}(z) = \begin{cases} 1, & z_{k'} - h/2 \leq z \leq z_{k'} + h/2, \\ 0, & \text{else} \end{cases} \quad (6)$$

when  $1 < k' < k$ , with similar expressions for  $P_1$  and  $P_k$ .

We then have for  $1 \leq k \leq N$ :

$$w_{k,k'} = I_{CSR} \left( z_k, z_{k'} - \frac{h}{2} \right) - I_{CSR} \left( z_k, z_{k'} + \frac{h}{2} \right), \quad (7)$$

# THE CONVERGENCE AND ACCURACY OF THE MATRIX FORMALISM APPROXIMATION\*

S. Andrianov<sup>†</sup>, SPbSU, St. Petersburg, Russia

## Abstract

To the present time there has been developed a large number of different codes for the particles beam dynamics modeling. However, their precision, accuracy and reliability of the numerical results are not sufficiently guaranteed in the case of long-term evolution of particle beams in circular accelerators. Here we discuss convergence estimates of the matrix presentation for Lie series. We also consider some problems of the matrix formalism accuracy for constructing the evolution operator of the particle beam. In this article there is paid a special attention to problems of symplecticity and energy conservation for long time evolution of particles beams.

## INTRODUCTION

The well known Lie methods for nonlinear dynamics allow us to constructive evaluate the corresponding maps and use them for accelerator physics [1]. But it should be note that evaluation procedures of corresponding Lie maps is enough time-consuming process. Besides, it is very difficult to evaluate corresponding procedures and estimate the required accuracy of the corresponding evaluations. This procedure is necessary for correct calculation for different problems of accelerator physics, particularly for long time beam evolution. Unfortunately the most popular methods have not enough practical instruments for accuracy estimates. The trend of accelerator physics leads us to necessity to have a tool to assess not only the accuracy of computational procedures, but also to preserve certain qualitative properties of the computational procedures (such as symplecticity, energy conservation and so on). Usually these problems are solved only in numerical mode up to some order of integration steps  $\mathcal{O}(h^n)$ . In the present paper we demonstrate some analytical estimates for the corresponding solutions using the matrix formalism for Lie approach [2, 3]. We also consider some problems of the matrix formalism accuracy for constructing the evolution operator of the particle beam.

## THE ACCURATE EVALUATION OF TRUNCATED LIE MAPS

### Matrix Series Presentations for Lie Maps

In some previous papers we presented the matrix formalism for Lie maps generated by ordinary differential equa-

tions, which can be written in the the following form

$$\frac{d\mathbf{X}}{dt} = \mathbf{F}(\mathbf{X}, t) = \sum_{k=1}^{\infty} \mathbb{P}_k(t) \mathbf{X}^{[k]}, \quad \mathbf{X}_0 = \mathbf{X}(t_0), \quad (1)$$

where  $\mathbf{F} = \{F_1, \dots, F_{2n}\}^T$  and  $\mathbf{X}^{[k]}$  is a vector of all phase moments for the phase vector  $\mathbf{X}$  ( $\dim \mathbf{X} = 2n$ ), for example,  $\mathbf{X} = \{x, p_x, y, p_y\}^T$  and  $\mathbb{P}^{1k}$  (with matrix size  $\dim \mathbb{P}^{1k} = \binom{2n+k-1}{k}$ ) are matrices containing partial derivatives

$$\{\mathbb{P}^{1k}(t)\}_{ij} = \frac{1}{k_1! \dots k_{2n}!} \left. \frac{\partial^k F_i(x_j, t)}{\partial x_1^{k_1} \dots \partial x_{2n}^{k_{2n}}} \right|_{x_1 = \dots = x_{2n} = 0}.$$

The eq.(1) generates the Lie operator [1] in according the following equality

$$\mathcal{L}_{\mathbf{F}} = \mathbf{F}^*(\mathbf{X}, t) \frac{\partial}{\partial \mathbf{X}} = \sum_{k=1}^{\infty} (\mathbf{X}^{[k]})^T \mathbb{P}_{1k}^T \frac{\partial}{\partial \mathbf{X}} = \sum_{k=1}^{\infty} \mathcal{L}_{\mathbf{F}_k}.$$

So, for corresponding Lie map [1] we can write

$$\begin{aligned} \mathcal{M}(t|t_0; \mathcal{L}_{\mathbf{F}}) &= \text{T exp} \int_{t_0}^t \mathcal{L}_{\mathbf{F}}(\mathbf{X}, \tau) d\tau = \\ &= \text{T exp} \sum_{k=1}^{\infty} \int_{t_0}^t \mathcal{L}_{\mathbf{F}_k} d\tau = \mathcal{M} \left( t|t_0; \sum_{t_0}^t \mathcal{L}_{\mathbf{F}_k} \right) = \\ &= \prod_{k=1}^{\infty} \mathcal{M} \left( t|t_0; \sum_{t_0}^t \mathcal{L}_{\mathbf{G}_k} \right), \quad (2) \end{aligned}$$

where the symbol "T" denotes the so called chronological ordering exponent Lie operator [3] (or the Dyson operator). Here  $k$  indicates the order of corresponding homogeneous polynomials. Evaluation of (2) can be realized in the frame of two following approaches:

1. The Magnus representation for chronological exponent operators [3, 4].
2. The Zassenhaus formula for homogeneous polynomials  $\mathbf{G}_k$ ,  $k \geq 1$  calculation). Using these approaches we can write some symbolic formulas for Lie map  $\mathcal{M}$  evaluation. For example, if we introduce the following notations [3]

$$\mathbb{P}_m^{k1} = \prod_{j=1}^k \mathbb{G}_m^{\oplus((j-1)(m-1)+1)} \quad (\text{here } \oplus \text{ denotes the Kronecker sum}),$$

then we have the following equality

$$\exp(\mathcal{L}_{\mathbf{G}_m}) \circ \mathbf{X} = \mathbf{X} + \sum_{k=1}^{\infty} \frac{\mathbb{P}_m^{k1}}{k!} \mathbf{X}^{[k(m-1)+1]}.$$

\*Work supported by Federal Targeted Program "Scientific and Scientific-Pedagogical Personnel of the Innovative Russia in 2009-2013" (Governmental Contract no. p 793)

<sup>†</sup> sandrianov@yandex.ru

# UNDULATOR RADIATION INSIDE A DIELECTRIC WAVEGUIDE

A.S. Kotanjyan, Department of Physics, Yerevan State University, Armenia

A.A. Saharian, Departamento de Fisica-CCEN, Universidade Federal da Paraíba, Brazil, and  
Department of Physics, Yerevan State University, Armenia

## Abstract

We investigate the radiation from a charge moving along a helix around a dielectric cylinder immersed in a homogeneous medium. The radiation intensity in the exterior medium at large distances from the cylinder has been considered previously and here we are mainly concerned with the radiation propagating inside the cylinder. Numerical examples are given for a dielectric cylinder in the vacuum. It is shown that the presence of the cylinder can lead to the considerable increase of the radiation intensity. The insertion of a dielectric waveguide provides an additional mechanism for tuning the characteristics of the undulator radiation by choosing the parameters of the waveguide. The radiated energy inside the cylinder is redistributed among the cylinder modes and, as a result, the corresponding spectrum differs significantly from the homogeneous medium or free-space results. This change is of special interest in the low-frequency range where the distribution of the radiation energy among small number of modes leads to the enhancement of the spectral density for the radiation intensity. The radiation emitted on the waveguide modes propagates inside the cylinder and the waveguide serves as a natural collector for the radiation.

## INTRODUCTION

The motion of charged particle along a helical orbit is used in helical undulators for generating electromagnetic radiation in a narrow spectral interval at frequencies ranging from radio or millimeter waves to X-rays. The unique characteristics, such as high intensity and high collimation, have resulted in extensive applications of this radiation in a wide variety of experiments and in many disciplines (see, for instance, [1] and references given therein). These applications motivate the importance of investigations for various mechanisms of controlling the radiation parameters. From this point of view, it is of interest to consider the influence of a medium on the spectral and angular distributions of the radiation.

In [2, 3] we have investigated the radiation generated by a charge moving along a helical orbit around/inside a dielectric cylinder enclosed by a homogeneous medium. It has been shown that under certain conditions strong narrow peaks appear in the angular distribution of the radiation intensity in the exterior medium. At these peaks the radiated energy exceeds the corresponding quantity in the case of a homogeneous medium by several orders of magnitude. In these investigations we have considered the radiation at large distances from the cylinder. In the present paper we consider the radiation intensity inside a dielectric cylinder emitted by a charge moving along a helical trajectory around the cylinder (for the radiation

from a charged particle rotating inside a dielectric cylinder see [4]).

## RADIATION INSIDE A DIELECTRIC WAVEGUIDE

Consider a point charge  $q$  moving along the helical trajectory of radius  $\rho_0$  outside a dielectric cylinder with radius  $\rho_1$  and with permittivity  $\varepsilon_0$ . We will assume that this system is immersed in a homogeneous medium with dielectric permittivity  $\varepsilon_1$  (magnetic permeability will be taken to be unit). We denote with  $\omega_0 = 2\pi/T = v_{\perp}/\rho_0$  the angular velocity of the charge,  $v_{\parallel}$  and  $v_{\perp}$  are the particle velocities along the axis of the cylinder and in the perpendicular plane, respectively.

Electromagnetic fields inside the cylinder can be presented in the form of the Fourier expansion

$$F_l(r, t) = 2 \operatorname{Re} \sum_{m=0}^{\infty} e^{im(\phi - \omega_0 t)} \int_{-\infty}^{\infty} dk_z e^{ik_z(z - v_{\parallel} t)} F_{ml}(k_z, \rho), \quad (1)$$

where  $F = E$  and  $F = H$  for electric and magnetic fields respectively. The radiation parts in the field are determined by the singular points of the integrand. The only poles of the Fourier components  $F_{ml}(k_z, \rho)$  are the zeros of the function

$$U_m(k_z) = V_m \left( \varepsilon_0 |\lambda_1| \rho_1 \frac{J'_m}{J_m} + \varepsilon_1 \lambda_0 \rho_1 \frac{K'_m}{K_m} \right) - m^2 \frac{\lambda_0^2 + |\lambda_1|^2}{\lambda_0^2 |\lambda_1|^2} \left( \varepsilon_0 |\lambda_1|^2 + \varepsilon_1 \lambda_0^2 \right), \quad (2)$$

where  $J_m = J_m(\lambda_0 \rho_1)$  and  $K_m = K_m(|\lambda_1| \rho_1)$  are the Bessel and Macdonald functions and the prime means the differentiation with respect to the argument of the function,

$$\lambda_j^2 = \omega_m^2(k_z) \varepsilon_j / c^2 - k_z^2, \quad \omega_m(k_z) = m\omega_0 + k_z v_{\parallel},$$

and

$$V_m = |\lambda_1| \rho_1 \frac{J'_m}{J_m} + \lambda_0 \rho_1 \frac{K'_m}{K_m}.$$

The corresponding modes are exponentially damped in the region outside the cylinder. These modes are the eigenmodes of the dielectric cylinder and propagate inside the cylinder.

We denote by  $\lambda_0 \rho_1 = \lambda_{m,s}$ ,  $s = 1, 2, \dots$ , the solutions to equation  $U_m = 0$  with respect to  $\lambda_0 \rho_1$  for the modes with  $m \neq 0$ . The corresponding modes  $k_z = k_{m,s}^{(\pm)}$  are related to these solutions by the formula

# STORAGE RING EDM SIMULATION: METHODS AND RESULTS

Yu. Senichev<sup>†</sup>, A. Lehrach, R. Maier, D. Zyuzin, Forschungszentrum Jülich, Germany  
 M. Berz, K. Makino, Michigan State University, USA,  
 S. Andrianov, A. Ivanov, Saint Petersburg State University, Russia  
 on behalf of the JEDI collaboration

## Abstract

The idea of an electric dipole moment (EDM) search using the electrostatic storage ring with polarized beam is based on an accumulation of additional tiny spin rotations, about one billionth of a radian per second, which only occur in the presence of EDM. This method can be realized under conditions of long-time spin coherence  $\sim 1000$  seconds. During this time, each particle performs about  $10^9$  turns in the ring moving on different trajectories. Under such conditions, the spin-rotation aberrations associated with various types of space- and time-dependent nonlinearities start playing a crucial role. Computer simulation is necessary to design such a ring, taking into account all the factors affecting the spin. We used COSY Infinity and an integrating program with symplectic Runge-Kutta methods in conjunction with analytical methods and T-BMT differential equation solving. We developed a new lattice based on the alternating spin rotation. As a result, we can achieve a spin coherence time (SCT) of  $\sim 5000$  seconds. The difficulties of these studies are that aberration growth is observed on the scale of  $10^9$  turns and a few million particles. For this simulation, we used a supercomputer with a parallel computing process.

## METHODS OF SIMULATION

At Forschungszentrum Jülich, two approaches are currently being considered for the EDM search in a storage ring: a method using a resonant RF spin flipper technique in the COSY ring [1] and frozen spin in the “magic” ring specially projected for the EDM search [2,3,4]. The resonance method has the character of preliminary studies of SCT and measuring techniques of spin decoherence arising for various reasons. In this paper, all results were obtained by the second method based on the “magic” ring conception.

The main difficulty in solving the problem of spin-orbital motion simulation together with the EDM signal lies in the fact that the signal expected directly from the EDM is extremely small. In particular, from sufficiently reliable estimations made in [2], it follows that due to EDM the spin in the “magic” ring rotates with the angular velocity of  $10^{-9}$  radians per second. Taking into account the fact that the ring structure contains several hundred elements, and each particle performs about  $10^6$  revolutions per second, this means that EDM rotates the spin through an angle of approximately  $\sim 10^{-18}$  radians per element on average. Accordingly, the EDM signal is expected to change the value of the spin projections on the same tiny scale. Thus, in the EDM search we meet a

<sup>†</sup>y.senichev@fz-juelich.de

problem that has not previously been encountered in accelerator physics: the arithmetic coprocessor has a mantissa length of 52 bits and can make a mistake in calculating spin projections after each element. This is a very serious limitation for using programs with the standard mantissa, and must be taken into account. Therefore using a powerful program we take a different approach, where the EDM signal is not implemented, and only the induced error signal is studied. This approach allows us to define the possible low level of the EDM signal and solve the problem from the opposite side.

In our studies, we use the following mathematical tools:

- COSY Infinity program [5], based on map generation using differential algebra and the subsequent calculation of the spin-orbital motion for an arbitrary particle;
- integrating program to study the effects that do not require a long numerical time;
- numerical integration of T-BMT differential equations for a spin in optics with smoothly approximated parameters of orbital motion;
- analytical approach.

Each of these methods is an integral part of our research.

## COSY Infinity

COSY Infinity is known as a very powerful instrument for particle tracking in electromagnetic fields. COSY Infinity is a program for the simulation, analysis and design of particle optical systems, based on differential algebraic methods. Full spin-orbital tracking simulations of the entire experiment are absolutely crucial for systematically exploring the feasibility of the planned experiments. In the EDM search, it is the only program which allows the spin-orbit motion of millions of particles to be simulated over a real time scale experiment during  $n \times 1000$  seconds. At present, we use the MPI (Message Passing Interface) version of the COSY Infinity program installed on a supercomputer with  $3 \cdot 10^5$  processors. It is planned to use the COSY Infinity program and to include higher-order nonlinearities, normal form analysis, symplectic tracking and especially spin tracking upon the incorporation of RF-E and RF-B flippers into the program. In order to study subtle effects and simulate the particle and especially spin dynamics during accumulation and build-up of the EDM signal, custom-tailored fast trackers are needed capable of following up to 10–100 billions turns for samples of up to  $10^4$ – $10^6$  particles.

At the initial stage of EDM research, we use COSY Infinity to study the behaviour of the spin aberrations for a large number of particles and a long-time calculation.

# IMPLEMENTING NEW BEAM LINE ELEMENTS INTO A MOMENT METHOD BEAM DYNAMICS CODE\*

T. Roggen<sup>†</sup>, H. De Gersem, B. Masschaele  
KU Leuven Kulak,

Wave Propagation and Signal Processing Research Group, Kortrijk, Belgium

W. Ackermann, S. Franke, T. Weiland

TU Darmstadt, Theorie Elektromagnetischer Felder (TEMF), Darmstadt, Germany

## Abstract

Developing beam dynamics simulation tools using the moment method has advantages in terms of precision and efficiency when interests lie in average or rms dimensions of the beam, projected emittances or total energy. The moment method implemented in the V-Code solves the Vlasov equation by time integration, from an initial particle distribution represented by a discrete set of characteristic moments, accounting for all acting internal and external forces along the particle's path. The moment method delivers highly accurate beam dynamics results within a very small CPU time. This article proposes, illustrates and validates a new beam line element (BLE) for a radio frequency quadrupole (RFQ) for insertion in the V-Code. The focus will be on the RFQ cell structure, the electric field distribution and the insertion of the field distribution in the moment code.

## INTRODUCTION

New particle accelerator projects rely heavily upon numerical simulations ranging from proof of concept to optimisation and fine tuning of the accelerator's individual components. Beam dynamics simulations are of vast importance to guarantee compatibility between all individual accelerator components in the optimisation cascade. Moment based algorithms have a major calculation time window advantage over full particle in cell (PIC) codes, while their accuracy is superior to macro-particle tracking algorithms. The V-Code is a sixth order moment Vlasov solver which takes into account space charge effects [1, 2]. An initial particle bunch is represented in a six dimensional phase space with longitudinal and transverse dynamics. For improved accuracy not only the average bunch coordinates and momenta, but also higher order correlation parameters (up to the sixth order) are accounted for in a phase distribution function  $f(\tau, \vec{r}, \vec{p})$ ,  $\tau = ct$  being the equivalent time,  $c$  the speed of light,  $t$  the time,  $\vec{r}$  the space coordinates and  $\vec{p}$  the normalized momentum ( $\vec{p} = \vec{P}/mc$ ). V-Code allows an accelerator component's electromagnetic field distribution (exerting a force  $\vec{F}$  on the particles) to be represented by a multipole expansion of the field data from finite element (FE) or finite difference time domain (FDTD) simu-

lation results. Eventually, for  $\gamma = E/mc^2$  the normalized energy, with energy  $E$  and mass  $m$ , all parameters of the Vlasov equation (Eq.1) are known, enabling to use time integration to find a solution.

$$\frac{\partial f}{\partial \tau} + \frac{\partial f}{\partial \vec{r}} \vec{p} + \frac{\partial f}{\partial \vec{p}} \frac{\vec{F}}{mc^2} = 0 \quad (1)$$

This contribution proposes, illustrates and validates a new BLE for a radio frequency quadrupole (RFQ) for insertion in the V-Code. The focus will be on the RFQ cell structure, the electric field distribution and the insertion of the field distribution in the moment code.

## FIELD DATA FILES

The required BLE field component to reconstruct the electromagnetic fields in V-Code is calculated using 3D field information from the BLE model in CST Studio Suite 2012. BLE-specific data extraction and post-processing guarantee smooth field transitions at borders and inside a BLE. The field component is then stored in a \*.dat field data file and read by V-Code to reconstruct a 3D field distribution using multipole expansion techniques.

## RADIO FREQUENCY QUADRUPOLE

A radio frequency quadrupole (RFQ) is a low-velocity, high-current accelerator component that can accelerate hadrons from protons to uranium to energies of about  $2q/A$  [MeV/n] ( $q$  being the ion charge and  $A$  the ion mass in amu). It allows for velocity independent electric focussing and adiabatic bunching, resulting in compact bunches and nearly 100 % capture and transmission efficiency. RFQs come in two flavours: four vane structures and four rod structures (Figure 1), with differences in required space, RF mode sensitivity and manufacturing techniques. The operating principle is analogue though.

The four electrodes in quadrupole configuration produce RF induced electric fields for focussing of the ion beam. With a longitudinal sinusoidal modulation of the electrodes, the vertical pair shifted out of phase by  $\pi$ , an accelerating longitudinal field component is introduced. Since the electric field between the rods finds its origin in the potential difference between the rods, and not in the RF electric field, a quasistatic approach is valid as long as the electrode gap is small compared to the RF wavelength [3]. The scalar potential function  $U(r, \theta, z, t)$ , as proposed in [4], is given in (2).  $r, \theta, z$  are the polar coordinates, time  $t$ ,

\* This research is funded by grant "KUL 3E100118" "Electromagnetic Field Simulation for Future Particle Accelerators", project FP7-Euratom No. 269565 and the Belgian Nuclear Research Centre (SCK-CEN).

<sup>†</sup> toon.roggen@kuleuven-kulak.be

# MODELING OF COHERENT SYNCHROTRON RADIATION USING A DIRECT NUMERICAL SOLUTION OF MAXWELL'S EQUATIONS\*

A. Novokhatski<sup>#</sup>, SLAC National Accelerator Laboratory,  
Menlo Park, CA 94025, USA

## Abstract

We present and discuss the properties of coherent electromagnetic fields of a very short, ultra-relativistic bunch, which travels in a rectangular vacuum chamber under the influence of a bending force of a magnet. The analysis is based on the results of a direct numerical solution of Maxwell's equations together with Newton's equations. We use a new dispersion-free time-domain algorithm which employs a more efficient use of finite element mesh techniques and hence produces self-consistent and stable solutions for very short bunches. We investigate the fine structure of the CSR fields. We also discuss coherent edge radiation. We present a clear picture of the field using the electric field lines constructed from the numerical solutions. This approach should be useful in the study of existing and future concepts of particle accelerators and ultrafast coherent light sources, where high peak currents and very short bunches are envisioned.

## INTRODUCTION

The coherent synchrotron radiation (CSR) fields have a strong action on the beam dynamics of very short bunches, which are moving in the bends of all kinds of magnetic elements. They are responsible for additional energy loss and energy spread; micro bunching and beam emittance growth. These fields may bound the efficiency of damping rings, electron-positron colliders and ultrafast coherent light sources, where high peak currents and very short bunches are envisioned. This is relevant to most high-brightness beam applications. On the other hand, these fields together with transition radiation fields can be used for beam diagnostics or even as a powerful source of THz radiation.

A history of the study of CSR and a good collection of references can be found in [1]. Electromagnetic theory suggests several methods on how to numerically calculate CSR fields. The most popular method is to use Lienard-Wiechert potentials. Another approach is to numerically solve the approximate equations, which are a Schrodinger type equation. Some numerical algorithms and codes are described in [2]. We suggest that a direct solution of Maxwell's equations together with Newton's equations can describe the detailed structure of the CSR fields [3].

Modeling ultrafast phenomena requires a special algorithm for solving the electromagnetic equations. This algorithm must be free of frequency dispersion which means that all propagating waves must have their natural

phase velocity, completely independent of the simulation parameters like mesh size or time step. We suggest an implicit algorithm which does not have stability issues and employs a more efficient use of finite element mesh techniques. This method can produce self-consistent stable solutions for very short bunches. We have already used this same approach long ago for wake field calculations. An implicit, dispersion-free time-domain algorithm was used in the computer code designed in 1976 for wake field dynamics studies at the Novosibirsk Electron-Positron Linear Collider VLEPP [4]. The algorithm details can be found in [5].

## ELECTROMAGNETIC CSR SIMULATION

We may suggest that a direct solution of Maxwell's equations together with Newton's equations can describe the detailed structure of the CSR fields, the fields generated by an ultra-relativistic bunch of charged particles moving in a metal vacuum chamber inside a bending magnet. Electromagnetic components  $\mathbf{E}$ ,  $\mathbf{B}$  must satisfy the equations

$$\frac{1}{c} \frac{\partial}{\partial t} \mathbf{E} = \nabla \times \mathbf{B} - \frac{4\pi}{c} \mathbf{j}_b \quad \nabla \cdot \mathbf{E} = 4\pi\rho_b \quad \mathbf{E}_{\text{wall}} \times \mathbf{n} = 0$$

$$\frac{1}{c} \frac{\partial}{\partial t} \mathbf{B} = -\nabla \times \mathbf{E} \quad \nabla \cdot \mathbf{B} = 0 \quad \mathbf{B}_{\text{wall}} \cdot \mathbf{n} = 0$$

A charge density and a charge current must satisfy a continuity equation

$$\rho_b = \sum_k \rho_k(\mathbf{x}) \quad \mathbf{j}_b = \sum_k \rho_k(\mathbf{x}) \mathbf{v}_k \quad \nabla \cdot \mathbf{j}_b + \frac{1}{c} \frac{d}{dt} \rho_b = 0$$

A Newton force includes electromagnetic components and a bending magnetic field

$$\frac{d}{dt} \mathbf{p}_k = e\mathbf{E} + \frac{\mathbf{v}_k}{c} \times e(\mathbf{B} + \mathbf{B}_{\text{bend}}) \quad \mathbf{p}_k = m\mathbf{v}_k / \sqrt{1 - \frac{v_k^2}{c^2}}$$

There are a lot of finite-difference schemes, which numerically solve Maxwell's equations since the first one was published in 1966 [6]. Most of them are so-called "explicit" schemes, which means that the value of the field at the new time step is calculated only by the field values from the previous time step. Stability conditions for these schemes do not allow a time step to be greater than or equal to a space (mesh) step. This limitation brings an additional troublesome effect for wavelengths that are comparable to a mesh step. We state that this effect works like a frequency dispersion media, which is "hidden" in the finite-difference equation.

\*Work supported by Department of Energy contract DE-AC03-76SF00515.

<sup>#</sup>novo@slac.stanford.edu

# RAPID INTEGRATION OVER HISTORY IN SELF-CONSISTENT 2D CSR MODELING\*

Klaus Heinemann, David Bizzozero, James A. Ellison, Stephen R. Lau  
Mathematics and Statistics, University of New Mexico, Albuquerque, NM, USA  
Gabriele Bassi, Brookhaven National Laboratory, Upton, NY, USA

## VLASOV-MAXWELL APPROACH TO BUNCH COMPRESSORS

This paper discusses three strategies in our work on the Vlasov-Maxwell (VM) system for a bunch compressor: the current paradigm, a modified paradigm, and a future paradigm. Each strategy only requires knowledge of the fields in the bunch. In the current paradigm we reduce the field calculation to a 2D integral over the 2D charge and current densities of the bunch and their time history. The current paradigm is implemented in our code VM3@A (Vlasov-Maxwell Monte-Carlo Method at Albuquerque) using a time stepping algorithm. Here a major expense is in the integration over history at each time step. The modified paradigm relies on spatial Fourier transformations to reduce the 2D integral to 1D convolutions (one convolution per mode) over history, where we approximate the convolution kernel by a sum of exponentials. As a result the history dependence is effectively localized in time, and each time step then relies only on field information at the present and previous time steps. We present a toy model for the modified paradigm and results are encouraging. We then briefly discuss a future paradigm which involves a 3D Maxwell simulation, using a domain  $\mathcal{D}$  which snugly surrounds the bunch. Such a simulation will require radiation boundary conditions set on  $\partial\mathcal{D}$ .

The exact problem we deal with in all three strategies is the IVP for the coupled system consisting of the 6D Vlasov equation for the phase space density  $f$  and the Maxwell equations for the self field  $\mathbf{E}, \mathbf{B}$  with boundary conditions on two perfectly conducting shielding plates. The initial self field is zero for the current paradigm and its modification. Details of the VM approach and the current paradigm are found in [1, 2, 3].

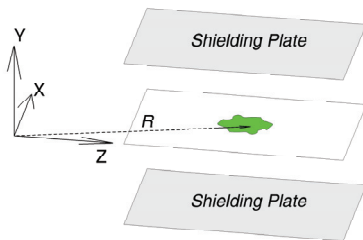


Figure 1: Geometry of sheet bunch model

\*Work supported by US DOE grant DE-FG02-99ER41104

## CURRENT PARADIGM

The current paradigm and its modification are based on a special case of the VM system, the *sheet bunch model*, where the bunch is confined to the mid-plane between the two shielding plates; whence

$$\begin{aligned} f(\mathbf{R}, Y, \mathbf{P}, P_Y; u) &= \delta(Y)\delta(P_Y)f_{sheet}(\mathbf{R}, \mathbf{P}; u) \\ \rho_f(\mathbf{R}, Y; u) &= \delta(Y)\rho_{sheet}(\mathbf{R}; u) \\ \mathbf{j}_f(\mathbf{R}, Y; u) &= \delta(Y)\mathbf{j}_{sheet}(\mathbf{R}; u), \end{aligned}$$

where  $u = ct$ ,  $\mathbf{R} = (Z, X)$ ,  $\mathbf{P} = (P_Z, P_X)$ , and  $\rho_f, \mathbf{j}_f$  are the charge and current densities associated with  $f$ . Our setup is shown in Fig. 1.

For the sheet bunch model  $\mathbf{E}, \mathbf{B}$  are only needed in the part of the  $Y = 0$  plane occupied by the bunch. Moreover,  $E_Y, B_X, B_Z$  vanish in the  $Y = 0$  plane, and so we only need  $E_Z, E_X, B_Y$ . We define

$$\mathbf{F}(\mathbf{R}; u) := (E_Z(\mathbf{R}, 0; u), E_X(\mathbf{R}, 0; u), B_Y(\mathbf{R}, 0; u)),$$

and the exact solution in the  $Y = 0$  plane is

$$\begin{aligned} \mathbf{F} &= \mathbf{F}_0 + \sum_{m=1}^{\infty} \mathbf{F}_m, \quad \text{where} \quad (1) \\ \mathbf{F}_0(\mathbf{R}; u) &= \frac{-1}{4\pi} \int_0^u \int_{-\pi}^{\pi} dv d\theta \mathbf{S}(\mathbf{R} + \mathbf{e}(\theta)(u-v), v) \quad (2) \end{aligned}$$

is the nonshielding term and the  $\mathbf{F}_m$  are image charge contributions needed to satisfy the boundary conditions. Here,  $\mathbf{e}(\theta) = (\cos \theta, \sin \theta)$  and the source  $\mathbf{S}$  is determined by  $\rho_{sheet}, \mathbf{j}_{sheet}$ . The nonshielding term alone is sufficient for some applications.

For the  $v$ -integration we use an adaptive Gauss-Kronrod integrator. The  $\theta$ -integration is done with the trapezoidal rule. The domain of  $\theta$ -integration is small for most  $v$ -values, as shown in Fig. 2 of [1]a.

The evolution of the source is governed by the Vlasov equation. We approximate this by a Monte Carlo particle method in accelerator coordinates [1]. At time  $u$  we know the particle phase space positions for  $0 \leq v \leq u$ .  $\mathbf{F}(\mathbf{R}, u)$  is then computed as an integral over history and used to evolve the particles phase space positions to  $u + \Delta$ , where  $\Delta$  is small enough so the fields are constant to good approximation. The new source at  $u + \Delta$  is then determined using a density estimation procedure (e.g. kernel density estimation with a product of Epanechnikov kernels [3]) and the process is repeated.

# BRINGING LARGE-SCALE ANALYTICS TO ACCELERATORS\*

N. Malitsky<sup>#</sup>, BNL, Upton, NY 11973, USA

## Abstract

The report presents a new approach for storing and processing both the accelerator control data and the experimental results. It is based on the analysis and consolidation of several modern technologies, such as the EPICS control infrastructure, the SciDB array-oriented data management and analytics platform, the HDF5 file format, and others.

## INTRODUCTION

The efficient data management and processing systems are essential tools in the commissioning and operation of the accelerator facilities and large scientific experiments. For example, analysis of historical data is heavily involved in the troubleshooting process, detection and study of the composite behaviour patterns, comparison and design of the different operational scenarios, and many other operational tasks. The data acquisition system (DAQ) is responsible for collecting the detector measurements which are the primary results of the dedicated experiments.

Building these systems however represents a serious challenge for control developers that have to acquire and store heterogeneous data streams coming at different rates from tens of thousands of distributed devices. The conventional technologies, such as relational database management systems, were not designed for such requirements. As a result, many of the control teams had to build new proprietary tools from scratch or try to accommodate the existing technologies with some ad hoc extensions. For example, the Experimental Physics and Industrial Control System (EPICS [1]) collaboration maintains more than four archiver systems. Constrained by the associated technologies and available resources, each of these solutions cannot address all requirements and present some trade-off among different objectives: performance, reliability, extensibility, and others.

The scale, data rate, and complexity of the new light source facilities introduce the next challenge and demands for new approaches. Particularly, the BNL National Synchrotron Light Source II (NSLS II) and SLAC Linac Coherent Light Source II (LCLS II) projects shift the frontiers of control systems towards millions of control process variables and streaming rates of up to one million events per second. Similar requirements are introduced by other accelerator projects. Furthermore, recent progress in the development of light source detectors is leading to dramatic changes in the amount and complexity of available experimental data. These quantitative changes in requirements trigger two principal topics: demand for an

efficient analytics-oriented database technology and consolidation of the control and experimental data management systems aiming to foster scientific discoveries.

Highly scalable data management and processing are two emerging topics in both industry and academics. Triggered by Google's web technologies, this domain represents an active factory of the new types of the analytics-oriented data storages, such as Casandra, CouchDB, Hbase, and MongoDB. Most of them are designed after Google's I/O stack: Google File System, Bigtable distributed storage system, and MapReduce processing framework.

Despite success in numerous projects, the web-oriented environment however cannot be directly applied to scientific applications. First, a Bigtable is a sparse, distributed multi-dimensional sorted map indexed by row key, column key, and a timestamp. It treats data as uninterpreted strings allowing flexible representations of structured and semi-structured formats. Unlike the web-oriented projects, scientific applications commonly relied on the multi-dimensional array-oriented data model. The map-based approach however is inefficient or incapable of addressing array-oriented queries. Second, the original MapReduce processing framework does not support complex iterative algorithms required by machine learning and scientific applications. This limitation prompted the new wave of hybrid data-intensive techniques merging or extending different data models and parallel paradigms: SciDB, GraphLab, SciHadoop, HadoopDB, MapReduce-MPI, and others.

To address the data challenges of the new modern light source facilities and the variety of technical solutions, we proposed an integrated configurable environment for connecting the different types of accelerator data with the modern large-scale analytics engines. The following sections subsequently overview the EPICS-based accelerator and beamline control system, the HDF5 file format [2] for storing experimental data of the modern light source facilities, two important representatives of the analytics approaches, the SciDB array-oriented parallel database [3] and the GraphLab distributed framework for processing complex algorithms on graphs [4], and finally the proposed large-scale integrated data management and analytics environment for accelerator and beamline experiments.

## EPICS ACCLERATOR AND BEAMLIN CONTROL SYSTEM

EPICS is the Experimental Physics and Industrial Control System that has been started in 1989 at Los Alamos National Laboratory and in use today at a significant proportion of the particle physics laboratories

\*Work supported by DOE contract DE-AC02-98CH10886

<sup>#</sup>malitsky@bnl.gov

# SIMULATION OF BASEBAND BTFs USING A PARTICLE-IN-CELL CODE

P. Görge<sup>\*</sup>, O. Boine-Frankenheim, TEMF, TU-Darmstadt, Darmstadt, Germany

W. Fischer, S. White, Brookhaven National Laboratory, Upton, NY, U.S.A.

## Abstract

A simulation model for transverse bunched beam transfer functions (BTFs) at the base harmonic is presented. It is based on a code including different machine effects, most notably transverse space charge using a two-dimensional (2D) Poisson solver. A simplified model for the simulation of the strong-strong beam-beam effect was implemented using either 2D field data or analytic expressions under the assumption of Gaussian beams for the beam-beam interaction. The validity of the BTF model is verified based on the comparison of BTF and Schottky spectra features with analytic expectations from literature. The simulation model is then applied to the RHIC proton lattice. A linear transfer map is used between interaction points. BTFs including the beam-beam effect are simulated. Measurements are compared to simulation results at machine conditions.

## MOTIVATION

Transverse BTFs of coasting beams were shown to give great diagnostic opportunities [1], for example enabling the direct measurement of the incoherent space charge tune shift. Our aim is to investigate the diagnostic opportunities of the transverse BTFs of bunched beams. We decided to start the investigation with the baseband beam transfer functions of bunched beams experiencing the beam-beam effect. The choice of baseband BTFs was made because both at Brookhaven National Laboratory (BNL) as well as GSI a high sensitivity BTF system based on the direct diode detection method developed at CERN [2] is in use. The choice of the beam-beam effect was made because it is localized and reduces overall simulation time.

## THE BTF MODEL

In the measurement of BTFs, the beam is transversely excited using a kicker operating at a certain frequency. The response of the beam center of charge oscillation is measured using a pickup. The process is repeated over a range of frequencies and the relative complex response amplitude as a function of excitation frequency gives the beam transfer function. In our simulation model we started from an existing code [3] to implement a simplified baseband beam transfer function: The codebase provides particle tracking based on the 6D transfer maps computed by MADX [4] with the addition of different effects such as chromaticity, self-consistent space charge and others. The BTF simulation consists of a combination of two modifications:

1. In one cell of the tracking lattice, a transverse periodic excitation is added to the momenta of all particles.

<sup>\*</sup> goergen@temf.tu-darmstadt.de

For the RHIC case where bunch lengths are far below 1/100 of the machine circumference we consider it safe to expect that all particles in one bunch get the same kick amplitude from an excitation signal at a frequency below the revolution frequency.

2. In the cell of the kick we also compute the offset of the center of charge  $\langle x \rangle$  from the reference trajectory and store it together with the excitation amplitude and frequency.
3. The particle distribution is initialized and tracked for a few thousand turns to equilibrate possible matching errors due to the beam-beam effect. The equilibrated particle distribution is stored.
4. The simulation is run for a range of frequencies, simulating excitation for 3500 turns. The same number of samples is taken in the real-life BTF measurements. After each run, the equilibrated particle distribution is reloaded in order to save the time needed to simulate until the excited oscillation dies down.
5. In offline analysis, we compute the complex response amplitude and excitation amplitude exactly at the excitation frequency using the discrete time Fourier transform (DTFT). The division of the complex response amplitude by the excitation amplitude gives the BTF.

## Testing of the BTF Model

In order to verify our implementation we compare our simulation with analytically accessible scenarios found for example in [5]. A popular example concerns a particle distribution with a Gaussian frequency spread. The analytic result [5] is given in units of the normalized frequency deviation  $u$  defined as a function of the mean particle betatron frequency  $\bar{\omega}$ , the driving frequency  $\Omega$  and the frequency width of the distribution  $\Delta\omega$  via the equation:

$$u = \frac{\bar{\omega} - \Omega}{\Delta\omega}. \quad (1)$$

For a Gaussian frequency distribution the analytic BTF  $R(u) = f(u) + ig(u)$  is given by:

$$f(u) = \sqrt{\frac{2}{\pi}} e^{-u^2/2} \int_0^\infty \frac{dy}{y} e^{-y^2/2} \sinh(uy) \quad (2)$$

$$g(u) = \sqrt{\frac{\pi}{2}} e^{-u^2/2} \quad (3)$$

We replicated the situation of a Gaussian frequency spread in the transverse direction for the PIC simulation of a longitudinally frozen bunch: We made use of Gaussian momentum distribution that acted via chromaticity as a Gaussian tune

# DYNAMICS OF FERRITE CAVITIES AND THEIR EFFECT ON LONGITUDINAL DIPOLE OSCILLATIONS\*

C. Spies<sup>†</sup>, U. Hartel, M. Glesner, TU Darmstadt, Darmstadt, Germany  
H.-G. König, H. Klingbeil, GSI, Darmstadt, Germany

## Abstract

In this paper, we consider ferrite cavities of the type that is currently used in the SIS18 at GSI and will be used in the future SIS100 which is being built in the frame of the FAIR project. We analyze the dynamics of the cavities in conjunction with their local control loops. An emphasis is put on the cavities' reaction to changes in the desired amplitude or resonant frequency. Using simulations, we show that the cavities' dynamics hardly influence longitudinal dipole oscillations, and conclude that a low-order model for the RF cavities is sufficient.

## FERRITE CAVITIES

In a heavy-ion synchrotron, the frequency of the RF accelerating fields is typically relatively low ( $< 10$  MHz) and highly variable [1]; for instance, in the planned SIS100 synchrotron at the GSI Helmholtz Centre for Heavy-Ion Research,  $^{238}\text{U}^{28+}$  ions will be injected at about  $0.56 \cdot c_0$  and accelerated to about  $0.92 \cdot c_0$ . Ferrite cavities for low RF frequencies are significantly smaller than, e. g. a  $\frac{\lambda}{2}$  resonator cavity, and their resonance frequency can be tuned.

In a ferrite cavity, the metal beam pipe is interrupted by a short ceramic "gap" and surrounded by ferrite rings. Bias and excitation loops are wound around the ferrite rings (see Fig. 1). The RF current excites an RF magnetic field in the ferrite rings, which in turn induces an RF electric field along the beam pipe. This field enters the ceramic gap and accelerates the charged particles. The RF field also effects a reactive current in the metal beam pipe and casing.

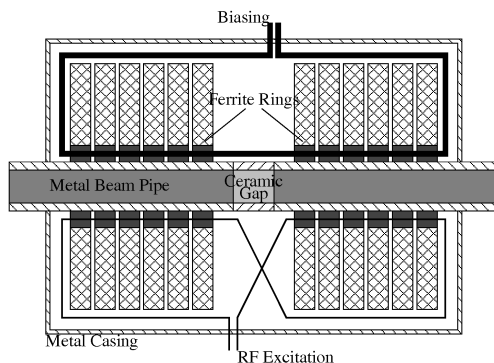


Figure 1: Schematic diagram of a ferrite cavity.

The cavity's behavior is equivalent to an RLC parallel oscillator (see Fig. 2) whose input is the RF excitation current [1]. The voltage across the RLC circuit is the voltage

across the ceramic gap. The capacitance is primarily that of the ceramic gap and is constant. The inductance depends on the differential magnetic permeability of the ferrite material and can be tuned by the bias current. The resistance represents both Ohmic and magnetic losses and may be frequency and/or voltage dependent.

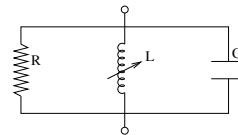


Figure 2: Equivalent circuit.

## Resonance Frequency Control

From the equivalent circuit in Fig. 2, it is obvious that the accelerating voltage is maximized when the cavity is operated at its resonant frequency. In that case, the voltage is in phase with the excitation current. Therefore, each cavity is equipped with a local controller that measures the phase difference between excitation current and gap voltage. It outputs a low-level voltage that controls a solid-state amplifier which in turn generates the bias current.

The controller is an analog circuit based on operational amplifiers (OpAmps) and has a linear *PI* characteristic, i. e. its step response is the sum of that of a proportional (*P*) and that of an integral (*I*) controller. Additionally, there is a pilot control path that nonlinearly maps the setpoint frequency to an approximation of the required bias current.

## Amplitude Control

Each cavity is also equipped with a local amplitude controller that measures the gap voltage (using a voltage divider) and compares it to the voltage setpoint. It outputs a low-level voltage that is used to modulate a low-level RF input signal, which is in turn fed into an amplifier chain that generates the excitation current.

The controller is an analog OpAmp circuit and has a linear *PPT*<sub>1</sub> characteristic, i. e. its step response is the sum of that of a *P* element and that of another *P* element with first-order lag (*PT*<sub>1</sub>). Additionally, there is a constant-gain pilot control path.

## Cavity Synchronization

Since the resonance frequency control described in section cannot detect phase shifts in the modulator-amplifier chain, another local controller measures the phase difference between the gap voltage and a reference signal and

\* Work supported by the German Ministry of Education and Research, Grant No. 06DA9028I

<sup>†</sup> christopher.spies@mes.tu-darmstadt.de

# DESIGN OF A COMPUTER BASED RESONATOR-SIMULATOR FOR TESTS OF RF CONTROL SYSTEMS\*

T. Bahlo, C. Burandt, R. Eichhorn<sup>†</sup>, J. Enders, M. Konrad, P. Nonn  
 Institut für Kernphysik, TU Darmstadt, Germany

## Abstract

In order to test RF control systems for accelerator cavities without being dependent on available prototypes, a resonator-simulator has been developed. The Simulator is based on a Xilinx VIRTEX-4 FPGA module and has been configured using MATLAB Simulink with a special Xilinx blockset. The underlying model for this configuration is a parallel RLC circuit that has been parameterised with common RF quantities like the resonance frequency, driving frequency, bandwidth and quality factor. This approach allows the behaviour of normal conducting cavities with quality factors up to  $10^4$  as well as superconducting cavities with quality factors up to  $10^9$  to be simulated. Besides, it can be operated in continuous-wave mode as well as in pulsed mode. We report on the mathematical model, its digital representation and on the benchmarking against realistic cavity behaviour.

## INTRODUCTION

For experiments with intense antiproton beams, a dedicated proton LINAC is foreseen as an injector for the future Facility for Antiproton and Ion Research (FAIR). The proposed scheme with normal conducting crossed-bar H-mode cavities operated in a pulsed mode is planned to feed directly into the heavy-ion synchrotron SIS18 of the present GSI Helmholtz center for heavy-ion research [1]. The corresponding digital radio frequency control system for a test-bench setup is currently being developed at TU Darmstadt [2]. Due to the fact that there are no cavity prototypes available, a cavity simulator has been developed. This device is able to simulate normal conducting as well as superconducting cavities with common physical effects like beam loading, amplifier saturation and Lorentz-force detuning (LFD). In consequence of its ability to simulate superconducting cavities it also can be used to improve the digital control system [3] of the Darmstadt electron LINAC S-DALINAC [4] without being dependent on an available superconducting resonator or RF periphery.

## THE RESONATOR MODEL

The simulator is based on a resonator model consisting of a parallel circuit of a resistor  $R$ , an impedance  $L$  and a capacity  $C$  that is driven by a generator current  $I_{\text{gen}}$  as shown in Fig. 1. The corresponding differential equation describing the voltage reads:

$$\ddot{U} + \frac{1}{RC} \dot{U} + \frac{1}{LC} U = \frac{1}{C} \dot{I}_{\text{gen}} \quad (1)$$

\* Work supported by the BMBF contract 06DA9024I

<sup>†</sup> now at: CLASSE, Cornell University, Ithaca, NY 14853, U.S.A.

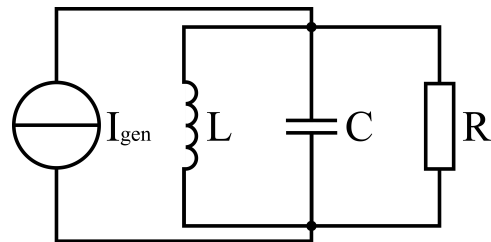


Figure 1: The equivalent circuit representing the cavity

It is convenient to rewrite this equation with more common RF parameters like the resonance frequency  $\omega_r$ , the quality factor  $Q$  and the half width at half maximum  $\Delta\omega_{1/2}$ . With these the equation reads:

$$\ddot{U} + \frac{\omega_r}{Q} \dot{U} + \omega_r^2 U = \frac{\omega_r}{Q} \dot{U}_{\text{gen}} \quad (2)$$

To solve Eq. (2) one can use Eq. (3) as an ansatz which is motivated by the in-phase and quadrature procedure commonly used with RF control systems. The in-phase signal is denoted by  $V$ , while  $W$  represents the quadrature component.

$$U(t) = (V + iW) \cdot e^{i\omega t} \quad (3)$$

Time discretisation and the introduction of several approximations (details described, e.g., in [5]) lead to:

$$\begin{aligned} V(t+\Delta t) &= V(t) + [\omega_{1/2}(V_{\text{gen}} - V(t)) - \Delta\omega W] \Delta t \\ W(t+\Delta t) &= W(t) + [\omega_{1/2}(W_{\text{gen}} - W(t)) + \Delta\omega V] \Delta t \end{aligned}$$

## HARDWARE

The simulator has been implemented on an Lyrtech VHS-ADAC board providing 8 DAC and 8 ADC channels with a resolution of 14 bit and a Xilinx VIRTEX-4 FPGA-module. The latter has been configured using the “Xilinx System Generator for DSP” [6] library for MATLAB/Simulink. This software package allows the designer to generate high-performance HDL code directly from the Simulink interface using pre-optimized algorithms for the Xilinx hardware. Using this tool greatly simplifies the configuration of the FPGA.

## COMPARISON TO A REAL RESONATOR

A pulsed control system has to be able to tune the cavity’s electrical field magnitude and phase to the wanted value as fast as possible. During this process it reacts on fast changes of these quantities. So for the simulator it is very crucial to reproduce the transient response of a real cavity with high precision.

# SPACE CHARGE AND ELECTRON CLOUD SIMULATIONS

G. Franchetti\*, GSI, Darmstadt, Germany  
F. Zimmermann, CERN, Geneva, Switzerland

## Abstract

Tracking of high intensity effects for few turns of a circular accelerator is at reach of present computational capabilities. The situation is very different when the prediction of beam behavior is extended to hundred of thousands of turns, where special approaches for the control of computer artifact are necessary sometimes to the expense of a complete physical modeling. The identification of the key physical ingredients helps to the development of computer algorithms capable of treating the long term tracking.

Here we present the latest status of long-term tracking simulations of high intensity bunches for SIS100, and also discuss a more realistic modeling of the incoherent effect of an electron cloud for the LHC.

## INTRODUCTION

The motivation of these studies has started with the approval of the FAIR project at GSI. In the SIS100 synchrotron of the FAIR project [1] bunches of  $U^{28+}$  ions are stored for about one second and then accelerated: During this cycle beam loss cannot exceed 10% [2, 3, 4].

The simultaneous presence of space charge and the lattice induced nonlinear dynamics may create a diffusional regime leading to beam loss [5, 6]. The modeling of this unusual beam operation has been subject of studies in the past decade and relies on analytic models [7], which allow the suppression of a characteristic noise of PIC codes [8]. This approach neglects the coherent effects created by the Coulomb force as, for instance, the excitation of unstable modes of the beam [9]. On the other hand in the PIC self-consistent studies in Ref. [10] it is also shown that coherent nonlinear resonances are not of relevance for Gaussian beam distributions. Therefore in all studies for SIS100 it was adopted a modeling of “frozen” type and a quest to understand the dynamics was undertaken.

Over the years a systematic approach has been taken which had a two-fold purpose:

1) Understand the basics of the mechanism (lattice resonance affected by space charge created by a bunched beam) in order to more effectively improve SIS100 performances and to devise possible cure for too high beam loss level [7]. Up to now the studies to understand the mechanisms of periodic resonance crossing have been confined to “frozen” algorithms.

2) Benchmarking the code prediction against experiments performed on a real machine. These studies started with an experimental campaign at the CERN-PS in the years 2002-2003 [11]. Few years later a new campaign was

made at GSI in the SIS18 [6]. The results of these campaigns have shown that the simulation do not predict correctly the beam loss. The experiments always yield more beam loss of what is predicted with a computer code. The reason for this discrepancy is not fully understood as to the imperfection of the modeling implemented in computers also one has to account an imperfect knowledge of the real machine used for the benchmarking.

In the year 2004-2005 it was suspected that a similar diffusional mechanism could be created by the electron cloud during the electron pinch process driven by the passage of a proton bunch. Studies presented in Ref. [12] have shown that the effect of a resonance crossing is indeed at the base of a slow incoherent emittance growth. The issue of the modeling of the electron pinch is very central for the emittance growth prediction. The complexity of the dynamics of the electrons during the pinch process makes hard to use an analytic modeling. Attempts to investigate the emittance growth with analytic modeling of the electron pinch are reported in Ref. [5]. Differently from the space charge, the benchmarking with a beam experiment is here much more difficult because the knowledge of all electron cloud parameters is very difficult.

It is worth mentioning that the synergy between electron cloud and space charge studies allowed the development of a new theoretical framework which redefines the concept of fixed points for non adiabatic resonance crossing [13].

In these proceedings we report the state of the simulations for the SIS100 and we address recent development in the modeling of electron-cloud incoherent effects for the LHC.

## SPACE CHARGE SIMULATION

As result of the studies on the periodic resonance crossing and all the considerations on nonlinear and high intensity effects the working point of the SIS100 was chosen as  $Q_{x/y} = 18.84/18.73$ . The studies presented in Ref. [5, 6] estimated the SIS100 beam loss, however without clear evidence that periodic resonance crossing is the issue. In recent studies we have found that this is the case.

### *Modeling of the Dynamics at Injection*

**Random errors, reference beam, and reference error seed.** In SIS100 the nonlinearities are given by standard multipoles in sc dipoles [14, 15] now optimized with respect to those in Ref. [5, 6], and by the multipoles for sc quadrupoles [16]. Chromatic correction sextupoles are ignored. The systematic multipoles yield a short term dynamic aperture ( $10^3$  turns) of  $5.3\sigma$  for a reference beam of 8.75 mm-mrad rms emittance with the beam magnetic

\* g.franchetti@gsi.de

# SIMULATING THE WIRE COMPENSATION OF LHC LONG-RANGE BEAM-BEAM EFFECTS

T.L. Rijoff, F. Zimmermann, CERN, Geneva, Switzerland

## Abstract

The performance of the Large Hadron Collider (LHC) and its minimum crossing angle are limited by long-range beam-beam collisions. Wire compensators can mitigate part of the long-range effects. We perform simulations to explore the efficiency of the compensation at possible wire locations by examining the tune footprint and the dynamic aperture. Starting from the weak-strong simulation code BBTrack we developed a new Lyapunov calculation tool, which seems to better diagnose regular or chaotic particle behavior. We also developed faster ways to execute the simulation and the post-processing. These modifications have allowed us to study different wire positions (longitudinal and transverse), varying wire currents, several wire shapes, and a range of beam-beam crossing angles, in view of a prototype wire installation in the LHC foreseen for 2014/15. Our simulations demonstrate that the wire can provide a good compensation, including for reduced crossing angle. Among the benefits of an LHC wire compensator are a better overlap of colliding bunches, as well as the possibility of smaller  $\beta^*$  or higher beam current.

## INTRODUCTION

To reach high energy and high luminosity it is important to compensate the negative effects due to the electromagnetic interactions between the two beams before and after the collision points, the so called beam-beam effects [1]. This possible limitation of the collider performance can be partially mitigated with a DC wire compensator [2]. A very good compensation should be obtained when the wire has a distance from the beam equal to the average long range distance (for nominal crossing angle this means  $9.5 \sigma$ ), and with a wire current that depends on the number of long range interactions  $n_{LR}$  according to the formula  $I_{opt} = n_{LR} c e N_b / L_w$  ( $c$  speed of light and  $e$  elementary charge). If we consider 32 LR interactions ( $n_{LR}$ ) in total at one Interaction Point (IP), with  $1.15 \times 10^{11}$  particles per opposite bunch ( $N_b$ ), and a wire length ( $L_w$ ) of 1 m, we obtain  $I_{opt} = 176.8$  A.

From the longitudinal point of view, the best compensation is obtained when the  $\beta_x + \beta_y$  at the wire and when the betatron phase advance between the LR collision points and the wire is as small as possible. For the nominal LHC optics an optimal location has been found at 104.9 m from the IP [3], in the MAD optics this location carries the label “BBC” (Beam Beam Compensator).

For technical reasons we need to explore solutions different from the one indicated above: so (1) we analysed what happens moving the wire into the shadow of the collimator (for nominal crossing angle this means to  $11 \sigma$ ), (2) we checked what happens if we use the same electric

current as at  $9.5 \sigma$  ( $I=176.8$  A) as when scaling the current quadratically ( $I = 237$  A) (3) we tried different longitudinal wire locations: (4) we tested a modified optics [4].

We analyzed the following scenarios: Head On (HO): 2 head-on collisions at IPs1 and 5, Head On Long Range (HOLR): 2 HO collisions plus 16 LR collisions at each side of the IP1 and IP5, Beam Beam Compensator (BBC): HOLR plus a wire at 105 m after IP1 and IP5, Tertiary Collimator Target (TCT): HOLR plus a wire at 147 m before IP1 and IP5, TCT opt  $\beta$ : HOLR plus a wire at 150 m after IP1 and 147 m before IP5, TCT opt  $\beta$ : 2 HOLR plus a wire at 147 m before IP1 and 150 m after IP5 and Quadrupole 5 (Q5): HOLR plus a wire at 199 m after IP1 and IP5

We find that BBC offers the best compensation, but the simulated performance is promising also for TCT if we use the modified optics, which could be studied experimentally in the LHC from about 2015 onward, and for TCT opt  $\beta$  with nominal LHC optics.

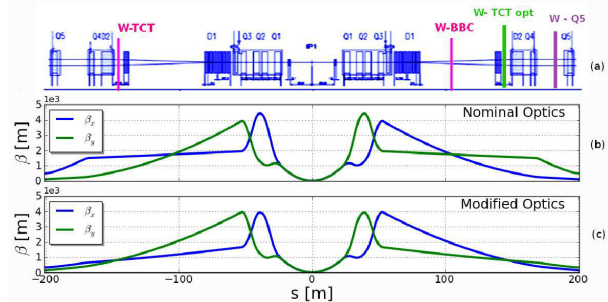


Figure 1: IP1: possible wire positions (row 1),  $\beta$  functions for LHC nominal optics (row 2) and modified optics (row 3)

For the most interesting cases we varied the crossing angle in the range  $[12, 6.3] \sigma$ , and found that suitably placed LHC wire compensators should allow for a reduction of the crossing angle by the equivalent of at least 1-2  $\sigma$  while maintaining the same stable region in phase space as for the larger crossing angle without compensator.

## SIMULATION TOOLS

We used the weak-strong code BBTrack [5] to track the particles, and we developed new postprocessing tools to analyse tune footprints and particle stability [6].

### Stability Analysis

We tracked each particle, together with a twin particle launched with a small transverse offset of  $10^{-8}$  m, for at least 300,000 turns. To determine the stability of a particle trajectory, on each turn ( $j$ ) a Lyapunov indicator,  $\lambda[j]$ , is computed from the time evolution of the normalized distance  $d$  in phase space between the two twin particles.

# ELECTRON CLOUD SIMULATIONS WITH PyECLOUD

G. Iadarola\*, Università di Napoli Federico II, Napoli, Italy and CERN, Geneva, Switzerland  
G. Rumolo, CERN, Geneva, Switzerland

## Abstract

PyECLOUD is a newly developed code for the simulation of the electron cloud (EC) build-up in particle accelerators. Almost entirely written in Python, it is mostly based on the physical models already used in the E-CLOUD code but, thanks to the implementation of new optimized algorithms, it exhibits a significantly improved performance in accuracy, speed, reliability and flexibility. PyECLOUD simulations have been already broadly employed for benchmarking the EC observations in the Large Hadron Collider (LHC). Thanks to the new feature of running EC simulations with bunch-by-bunch length and intensity data from machine measurements, the scrubbing process of the LHC beam pipes could be reconstructed from heat load measurements in the cryogenic dipoles. In addition, PyECLOUD simulations also provide the estimation of the bunch-by-bunch energy loss, which can be compared with the measurements of the stable phase shift.

## INTRODUCTION

The Electron Cloud (EC) has been recognized as a possible limitation to the performances of the Large Hadron Collider (LHC). [1] In 2011, a one week scrubbing run was enough to lower the Secondary Electron Yield (SEY) of the LHC beam screens to values which allow an almost EC free operation with 50ns bunch spacing.

On the other hand Machine Development (MD) sessions with 25ns beams showed that a severe EC is still developing with this bunch spacing, the main observables being the heat load on the cryo-magnets, the dynamic pressure rise as well as detrimental effects on the beam, namely fast EC induced instabilities, which could be avoided with high chromaticity settings, and slower incoherent effects as particle losses, emittance growth and energy losses, especially on the last bunches of the injected trains.[2]

Analysis and predictions on the EC formation rely most entirely on numerical simulations. CERN has a long experience in the EC build-up simulation, mostly carried out with the E-CLOUD code, developed and maintained at CERN since 1997. [3]

Unfortunately this code, written in FORTRAN 77, resulted not very suitable to be adapted to the length and the irregular structure of the beams employed in the MD sessions.

Therefore we have decided to write a fully reorganized code, in a newer and more powerful language, considering that the initial effort would be compensated by a significantly increased efficiency in future developments and

\* giovanni.iadarola@cern.ch

debugging.

The new code has been called PyECLOUD, since it is almost entirely written in Python and is largely based on the physical models of the E-CLOUD code. On the other hand, several features have been modified, and in some cases completely redesigned, with respect to E-CLOUD, with substantial improvements in terms of reliability, accuracy, speed and usage flexibility. [4]

## PyECLOUD

As E-CLOUD, PyECLOUD is a 2D macroparticle (MP) code, where the electrons are grouped in MPs in order to reduce the computational burden.

The dynamics of the MP system is simulated following the stages sketched in Fig. 1.

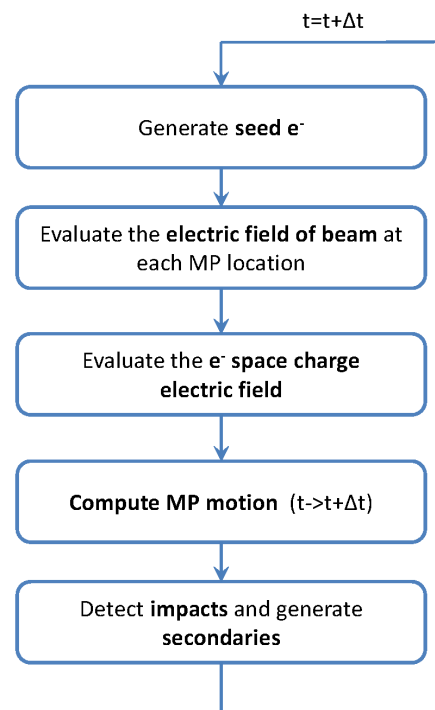


Figure 1: Flowchart representing PyECLOUD main loop.

At each time step  $\Delta t$ , *seed* electrons, due to residual gas ionization and/or to synchrotron radiation induced photoemission from the walls, are generated with the same time evolution of the beam and with transverse position and momentum determined by theoretical or empirical models.

Then the electric field acting on each MP is evaluated: the field of the beam is precomputed on a suitable rectangular grid, loaded from file and obtained at each MP location by a linear (4 points) interpolation; the *space charge*

## SIMULATIONS FOR ION CLEARING IN AN ERL \*

G. Pöplau<sup>†</sup>, A. Markovík, U. van Rienen, University of Rostock, Rostock, Germany  
A. Meseck, HZB, Berlin, Germany

*Abstract*

Light sources of the next generation such as ERLs (Energy Recovering Linacs) require very high quality bunches in order to achieve the research objectives they are designed for. It is essential to avoid sources of instabilities such as ionized residual gas. In order to enable detailed numerical studies the tracking code MOEVE PIC tracking developed by the research group at the University of Rostock was expanded to simulations of the behavior of an ion cloud in the environment of electromagnetic fields. In this paper we take further steps to study possible designs of clearing electrodes - a common countermeasure for the clearing of ions. We present simulations with different compositions of the residual gas. The numerical results taking into account the design of the ERL *BERLinPro* show how the clearing time depends on the percentage of heavy ions in the ion cloud.

## INTRODUCTION

Energy Recovery Linacs (ERLs) being the most promising candidates for next-generation light sources put very high demands on preservation of beam brightness and reduction of beam losses. Thus, it is mandatory to avoid the impact of ionized residual gas considered as a source for instabilities in accelerators [1].

Recently, we have presented simulations for the clearing of ionized residual gas with electrodes performed with an upgraded version of software package MOEVE PIC Tracking. It has been currently further developed to model the interaction of the ions with the electron beam in presence of external electromagnetic potentials such as the field of clearing electrodes [2, 3]. The tracking code allows for studies on clearing times for electrodes with different voltage as well as detailed studies of the behavior of the ions in the environment of the electrodes.

In this paper, we especially consider the influence of different compositions of the residual gas on the clearing times. For our numerical studies, we have chosen two different compositions of ion species in the residual gas due to [1] and [4], respectively. The numerical results indicate that the essential influence on the clearing time for the special composition is caused by the varying percentage of ions much heavier than  $H_2^+$ . Furthermore, the parameters for the bunch are taken from the design of *BERLinPro* due to [5].

\* Work supported by BMBF under contract number 05K10HRC

<sup>†</sup> gisela.poeplau@uni-rostock.de

## MOEVE PIC TRACKING FOR THE SIMULATION OF ION CLOUDS

The new version of the software package MOEVE PIC Tracking presented in [3] allows for the computation of the interaction of the ion cloud with the bunch and includes the field generated by the clearing electrodes. All simulations take into account the 3D space charge fields of both bunch and ion cloud. Hence, this approach allows for very detailed numerical studies of the dynamics of ion clouds beyond established theoretical results [6, 7]. For a more detailed description of the upgrade of MOEVE PIC Tracking we refer to [3] and references therein.

Further, the clearing times for different voltages of the electrodes are studied in [3]. The simulations with parameters of *BERLinPro* confirmed the consideration of the peak current of the bunch rather than the average current in order to assign the voltage of the electrodes. We restricted the ion species in the cloud to  $H_2^+$  ions.

In this paper we present simulations for ion clouds with different compositions of ion species. For the first test case (mixture 1) the residual gas consists of  $H_2^+$  ions (98%),  $CH_4^+$  (1%) and  $CO^+$  ions (1%) due to the studies for the Cornell X-ray ERL [1]. Mixture 2 was taken with  $H_2^+$  ions (48%),  $CH_4^+$  (16%),  $CO_2^+$  (18%),  $CO^+$  (14%) and  $CO_2^+$  (17%) ions due to measurements at SPEAR3 [4]. The main difference of these two compositions lies in the percentage of the ions much heavier than  $H_2^+$ : for mixture 1 it is 2% and in mixture 2 it is 52%. The data of these residual gas compositions are summarized in Table 2. Beam pipe and electrodes are modelled as in [3], i. e. we set a circular beam pipe with a radius of 2 cm and button-like electrodes with a diameter of 16 mm. The electrodes are located on opposite sides of the beam pipe and the voltage of each is set to the same value of  $-2700$  V due to the observations in [3].

The ion clouds are modelled with a total number of 1 million ions with the mixtures specified in Table 2. The ions are distributed over the whole pipe's cross-section

Table 1: Main Parameters of *BERLinPro*

maximum beam energy	50 MeV
maximum beam current $I$	100 mA
nominal beam charge $Q$	77 pC
maximum repetition rate	1.3 GHz
normalized emittance	$10^{-6}$ m
bunch length $\sigma_t$	2 ps

# NUMERICAL STUDIES ON THE INFLUENCE OF FILL PATTERNS ON ION CLOUDS\*

A. Meseck, HZB, Berlin, Germany

G. Pöplau<sup>†</sup>, U. van Rienen, University of Rostock, Rostock, Germany

## Abstract

Energy Recovery Linacs (ERLs) are the most promising candidates for next-generation light sources now under active development. An optimal performance of these machines requires the preservation of the high beam brightness generated in the injector. For this, the impact of the ionized residual gas on the beam has to be avoided as it causes instabilities and emittance growth. Obviously, the vacuum chamber has to be cleared out of ions but as the potential of the electron beam attracts the ions, it is not enough to install vacuum pumps.

One measure for ion clearing is the generation of gaps in the bunch train. In this paper, we present numerical studies of the behavior of an ion cloud that interacts with bunch trains taking into account the effects of the clearing gaps. In the studies different longitudinal distributions for the particles in the bunch and different “fill patterns” i.e. different spacings of the clearing gaps are investigated. The simulations are performed with the software package MOEVE PIC Tracking developed at Rostock University where recently new features for the simulation of ion effects have been implemented. The presented numerical investigations take into account the parameters of the ERL *BERLinPro* with the objective to deduce appropriate measures for the design and operation of *BERLinPro*.

## INTRODUCTION

The expected extraordinary performances of the next generation light sources, such as ERLs, require intense high brightness electron beams. Therefore, the ion-caused instabilities and emittance growth degrading the beam quality are serious threats to these sources and have to be avoided.

In an electron accelerator, several effects like collision with the electron beam, synchrotron radiation and field emission can lead to ionization of the rest gas in the beam pipe. The negative potential of the electron beam can trap the positive ions which in turn leads to an increase of the beam halo, to emittance blowup and to transverse and longitudinal instabilities by interacting resonantly with the beam. There are several measures of avoiding the ion-trapping such as utilizing clearing electrodes or using short or long clearing-gaps. A long gap between two trains of high-repetition rate bunches allows for ions to drift out of the beam potential and thus to reach the wall of the vac-

Table 1: Main Parameters of *BERLinPro*

maximum beam energy	50 MeV
maximum beam current $I$	100 mA
nominal beam charge $Q$	77 pC
maximum repetition rate	1.3 GHz
normalized emittance	$10^{-6}$ m
bunch length $\sigma_t$	2 ps
vacuum pressure	$10^{-10}$ mbar

uum chamber, while a short clearing-gap causes large oscillations of ions around the beam which in turn clears the vicinity of the bunches from the ions.

However, the applicability of the long-gap approach in ERLs suffers from two effects. The first effect is the transient effect of the RF systems which requires very long ion-clearing-gaps [1]. The second effect is the fast beam-ion instability. This is because a long gap does not preclude ions from accumulating in a single bunch train and interacting resonantly with the beam [1, 2]. Therefore, short clearing-gaps seem to be favorable, in particular as experimental and numerical studies indicate that multibunch trains with short gaps are very effective in suppressing the ion trapping process [3]. Please note that in an ERL, also for a short clearing-gap the transient RF effects have to be avoided by ensuring that the clearing-gap in the accelerating and in the decelerating beam coincide.

Although short bunch gaps in the ERL-beam allow for suppression of the ion accumulation in the vicinity of the beam, they are not totally welcome because they change the cw characteristics of the radiation delivered by the ERL. Therefore, to keep the time characteristic as cw-like as possible, frequent but extremely short bunch gaps are favorable. In the presented paper we study whether a bunch gap as short as one accelerating bucket occurring very frequently can excite oscillations large enough to clear the vicinity of the beam. For this, we use the software package MOEVE PIC Tracking [4, 5] to investigate numerically the behavior of an ion cloud that interacts with bunch trains with short gaps betwixt. For the simulations the parameter settings planned for *BERLinPro* [6] have been used. The parameters that are relevant for the simulations in this paper are given in the Table 1.

## SIMULATION TOOL MOEVE

For the presented study, the behavior of an ion cloud that interacts with bunch trains and clearing-gaps has been sim-

\* Work supported by BMBF under contract number 05K10HRC

<sup>†</sup> gisela.poeplau@uni-rostock.de

# PARTICLE TRACKING IN ELECTROSTATIC FIELDS WITH ENERGY CONSERVATION

A. Ivanov\*, Saint-Petersburg State University, Russia

## Abstract

The key idea of the research is to consider spin dynamics in electrostatic fields. Due to the fact, that spin rotation frequency explicitly depends on velocity of the particle and its kinetic energy is changed in electrostatic fields it is important to use some technique that provides both conservation energy and simplicity condition. An appropriate mathematical model is described and the results of numerical calculation are shown. In conclusion, fringe fields influence is examined and compared with case of ideal fields.

## INTRODUCTION

In the article particle dynamics is considered in 8-dimensional space. A state of dynamic system is described as  $(x, x', y, y', S_x, S_y, S_s, t)$  vector, where  $x, x'$  and  $y, y'$  are transverse and vertical displacement and velocity respectively;  $S_x, S_y, S_s$  are components of spin vector in curvilinear coordinate system (see Fig. 1);  $t$  is time variable. Note, that a state vector depends on arc length  $s$ , which is chosen as an independent variable.

The article consist of three parts. Firstly, mathematical models of the particle and spin dynamics are discussed. In the second part the numerical step-by-step integration approach is presented. And the last part is numerical experiment of fringe fields modeling, where the energy conservation is especially important condition.

## MODEL DESCRIPTION

This section is devoted to the mathematical models of particle motion and spin dynamics. Both trajectory and spin equations are presented in generalized form along the design orbit. In case of straight orbit equations are similar to description in Cartesian coordinates. Equations along the arc of a circle are presented without derivation.

Particle dynamics in electrostatic fields is described by the Newton-Lorenz equation

$$\frac{dp}{dt} = qE, \tag{1}$$

where  $p$  is the momentum,  $q$  is the charged of the particle,  $E$  is the electric field.

For spin description BMT equation is used [1]

$$\begin{aligned} \frac{dS}{dt} &= \omega \times S, \gamma = \frac{1}{\sqrt{1 - v^2/c^2}}, \\ \omega &= \frac{Q}{m_0^2 c^2} \frac{1}{\gamma} \left( G + \frac{1}{1 + \gamma} \right) p \times E, \end{aligned} \tag{2}$$

where  $G = (g - 2)/2$ ,  $g$  is the anomalous spin factor,  $\gamma$  is the Lorentz factor.

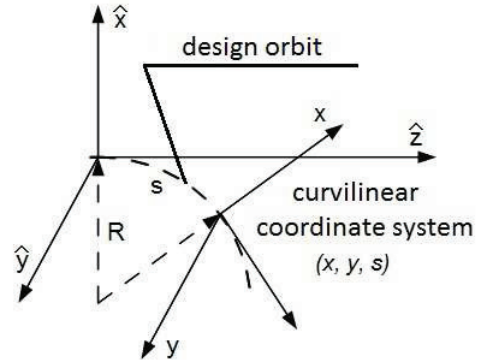


Figure 1: Curvilinear coordinate system.

## Trajectory Equations

Derivation of the trajectory equations that describe the orbital motion uses generalized coordinates. The design orbit is chosen in accordance to symmetry of field distribution. For example, in quadrupole lenses it is a straight line, in cylindrical or spherical deflectors it is arc of a circle. Along the arc length the equations are following

$$\begin{aligned} x'' + \left(1 - \frac{v^2}{c^2}\right)^{1/2} \frac{HG}{v} x' - \left(1 + \frac{x}{R}\right) \frac{1}{R} &= \frac{QH}{m_0 v} \left(1 - \frac{v^2}{c^2}\right)^{1/2} H E_x / v, \\ y'' + \left(1 - \frac{v^2}{c^2}\right)^{1/2} \frac{HG}{v} y' &= \frac{QH}{m_0 v} \left(1 - \frac{v^2}{c^2}\right)^{1/2} H E_y / v, \end{aligned} \tag{3}$$

where  $H, G$  is functions of variable  $x, x', y, y', R$ ,  $R$  is a radius of curvature of the design orbit.

## Spin Dynamics

The BMT equation in case of arc design orbit is presented as

$$\begin{aligned} S'_x &= S_s / R + \frac{Q}{m_0 c^2} \left( G + \frac{1}{1 + \gamma} \right) ((h_s E_x - x' E_s) S_s - \\ &\quad - (x' E_y - y' E_x) S_y), \\ S'_y &= \frac{Q}{m_0 c^2} \left( G + \frac{1}{1 + \gamma} \right) ((x' E_y - y' E_x) S_x - \\ &\quad - (y' E_s - h_s E_y) S_s), \end{aligned} \tag{4}$$

\*05x.andrey@gmail.com

# TRAVELING POLES ELIMINATION SCHEME AND CALCULATIONS OF EXTERNAL QUALITY FACTORS OF HOMS IN SC CAVITIES\*

T. Galek<sup>†</sup>, T. Flisgen and U. van Rienen, Rostock University, Rostock, Germany

B. Riemann, Technical University Dortmund, Dortmund, Germany

A. Neumann, Helmholtz-Zentrum Berlin, Berlin, Germany

## Abstract

The main scope of this work is the automation of the extraction procedure of the external quality factors  $Q_{ext}$  of Higher Order Modes (HOMs) in Superconducting (SC) radio frequency (RF) cavities. The HOMs are generated by charged particle beams traveling through a SC cavity at the speed of light ( $\beta \approx 1$ ). The HOMs decay very slowly, depending on localization inside the structure and cell-to-cell coupling, and may influence succeeding charged particle bunches. Thus it is important, at the SC cavity design optimization stage, to calculate the  $Q_{ext}$  of HOMs. Traveling Poles Elimination (TPE) scheme was used to automatically extract  $Q_{ext}$  from the transmission spectra and careful eigenmode analysis of the SC cavity was performed to confirm TPE results. The eigenmode analysis also delivers important information about band structure, cell-to-cell coupling and allows rapid identification of modes that could interact with the charged particle bunches.

## INTRODUCTION

The SC RF cavity presented in this article is a 1.3 GHz 7-cell Cornell design modified TESLA cavity with JLab HOM waveguide couplers as shown in figure 1. The discussed SC RF cavity will be used in the Berlin Energy Recovery Linac Project (BERLinPro), which is currently under development for a CW LINAC technology and expertise required to drive next-generation Energy Recovery Linacs (ERLs) [1]. The main priority on the current stage of the cavity design requires strongly damped HOMs in order to obtain high performance of the linac.

Using a modern simulation software one can efficiently calculate all the necessary quantities during the optimization steps. Simulations used to obtain results presented in this article can be divided into two main categories: eigenmode simulations and frequency domain simulations. The eigenmode simulations give us important information about all the modes that can exist in the model structure in the given frequency range. Important quantities can be calculated as a post processing step, e.g.  $R/Q$  which is a measure of a mode interaction with the charged particle beam,  $E_{peak}/E_{acc}$  and  $H_{peak}/E_{acc}$  which are relevant to suppression of field emission and thermal break down. The frequency domain simulations are used to obtain S-

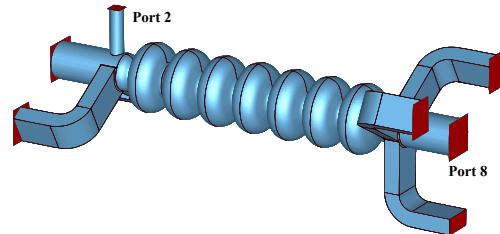


Figure 1: 7-cell TESLA cavity with coaxial input and HOM waveguide couplers

parameter spectra from which  $Q_{ext}$  factors of HOMs can be extracted. For this purpose we present an automated procedure that is using vector fitting with rational functions to express the S-parameter transmission spectra with a set of poles. The Traveling Poles Elimination (TPE) scheme is a simple iterative procedure which main purpose is to detect static poles and calculate external quality factors. All the simulations were performed using CST Microwave Studio 2012 (CST MWS) [2].

## POLE FITTING

### Rational Fitting of S-Parameter Spectra

For the extraction of the external quality factors  $Q_{ext}$  from S-parameter spectrum the fast implementation of the Vector Fitting (VF) algorithm was used [3]. The vector fitting is an iterative procedure of pole relocation by solving a linear least squares problem until the convergence criterion is met. The VF employs a method to ensure stable poles by flipping unstable poles into the left half complex plane. To achieve a faster convergence the algorithm uses, during the pole identification step, a relaxed non-triviality constraint and utilizes the matrix structure [4, 5, 6].

The S-parameter spectra are assumed to follow the complex rational function approximation

$$S(f) = \sum_{k=1}^N \frac{a_k}{2\pi i f - p_k} + R_k, \quad (1)$$

where  $i^2 = -1$  is the imaginary unit,  $a_k$  the residues,  $p_k$  complex conjugate pairs of poles and  $R_k$  a frequency-independent residual summarizing all other contributions. The complex pole  $p_k = \alpha_k + i\omega_k$  contains a resonance frequency  $\omega_k = 2\pi f_k$  and an attenuation constant  $\alpha_k$ . The quality factor  $Q_k$  for a given pole can be obtained using

\*Work funded by EU FP7 Research Infrastructure Grant No. 227579 and by German Federal Ministry of Research and Education, Project: 05K10HRC.

<sup>†</sup> tomasz.galek@uni-rostock.de

# COMPARISONS OF DIFFERENT ELECTROMAGNETIC SOLVERS FOR ACCELERATOR SIMULATIONS\*

J. Xu<sup>†</sup>, X. Zhufu, R. Zhao, Institute of Software, Beijing, 100190, China  
 C. Li, X. Qi, L. Yang, Institute of Modern Physics, Lanzhou, 730000, China  
 M. Min, Argonne National Laboratory, Argonne, IL 60439, USA

## Abstract

Electromagnetic simulations are fundamental for accelerator modeling. In this paper two high-order numerical methods will be studied. These include continuous Galerkin (CG) method with vector bases, and discontinuous Galerkin (DG) method with nodal bases. Both methods apply domain decomposition method for the parallelization. Due to the difference in the numerical methods, these methods have different performance in speed and accuracy. DG method on unstructured grid has the advantages of easy parallelization, good scalability, and strong capability to handle complex geometries. Benchmarks of these methods will be shown on simple geometries in detail first. Then they will be applied for simulation in accelerator devices, and the results will be compared and discussed.

## INTRODUCTION

Time dependent electromagnetic simulations are bases for many accelerator simulations. It is an important area in computational electromagnetics. Many numerical methods have been developed till now, such as finite difference (FDM), finite volume (FVM) and finite element methods (FEM). FEM has the advantage of handling complex geometries, therefore many efforts have been made with FEM. For FEM methods, there are two types of methods have been proved successful, they are CG with vector base and DG with Nodal base. In this paper we will study the performance of these two methods.

The paper is organized in the following way: the numerical method is explained and algorithms are compared in section 2, validation is shown in section 3, then benchmarks results are shown in section 4, and a comparison on wakefield simulations is given in section 5. At last, the conclusion is drawn in section 6.

## NUMERICAL METHOD

### Maxwell's Equation

In 3D domain  $\Omega$ , time dependent Maxwell's equations can be written as:

$$\frac{\partial \mathbf{B}}{\partial t} = -\nabla \times \mathbf{E}, \quad \frac{\partial \mathbf{D}}{\partial t} = \nabla \times \mathbf{H} + \mathbf{J} \quad (1)$$

$$\nabla \cdot \mathbf{D} = \rho, \quad \nabla \cdot \mathbf{B} = 0, \quad \mathbf{x} \in \Omega, \quad (2)$$

$$\hat{\mathbf{n}} \times \mathbf{E} = 0, \quad \hat{\mathbf{n}} \cdot \mathbf{H} = 0 \quad \mathbf{x} \in \partial\Omega, \quad (3)$$

where, the electric field  $\mathbf{E}$ , electric flux density  $\mathbf{D}$ , as well as the magnetic field  $\mathbf{H}$  and the magnetic flux density  $\mathbf{B}$  are related through the constitutive relations  $\mathbf{D} = \epsilon\mathbf{E}$ ,  $\mathbf{B} = \mu\mathbf{H}$ .

### CG Formulation

Maxwell's Equation (1) can be written in following inhomogeneous wave equation

$$\nabla \times \frac{1}{\mu_r} \nabla \times \mathbf{E} + \frac{\epsilon_r}{c_0^2} \frac{\partial^2 \mathbf{E}}{\partial t^2} = -\mu_0 \frac{\partial \mathbf{J}}{\partial t} \quad (4)$$

which times edge bases and apply electric (PEC) boundary condition to arrive at

$$\mathbf{M} \frac{1}{c_0^2} \frac{d^2 \mathbf{e}}{dt^2} + \mathbf{S} \mathbf{e} = -\bar{\mathbf{f}} \quad (5)$$

where  $\mathbf{M}$  and  $\mathbf{S}$  are mass and stiffness matrices in the following

$$\mathbf{M}_{ij} = \int_{\Omega} \epsilon_r \vec{W}_i \cdot \vec{W}_j d\Omega \quad (6)$$

$$\mathbf{S}_{ij} = \int_{\Omega} \frac{1}{\mu_r} \nabla \times \vec{W}_i \cdot \nabla \times \vec{W}_j d\Omega \quad (7)$$

$$f_i = \int_{\Omega} \mu_0 \vec{W}_i \cdot \frac{\partial \vec{J}}{\partial t} d\Omega \quad (8)$$

Based on the Newmark-Beta formulation [1, 2], Equation (5) can be solved to obtain  $e^{n+1}$  with

$$e^{n+1} = (M + \beta(c_0\delta t)^2 S)^{-1} \cdot \{ (2M - (1 - 2\beta)(c_0\delta t)^2 S)e^n - (M + \beta(c_0\delta t)^2 S)e^{n-1} + (c_0\delta t)^2 (\beta f^{n+1} + (1 - 2\beta)f^n + \beta f^{n-1}) \} \quad (9)$$

More detailed information can be found in [1, 2, 3]. The CG method is based on Nédélec edge bases, which is explained in detail in [4], and we omit it due to the constraint of page limit.

### DG Formulation

The discrete form of DG is:

$$\frac{d\mathbf{E}_N}{dt} = \mathbf{M}^{-1} \mathbf{S} \times \mathbf{H}_N + \mathbf{S}^E$$

\* Work supported by Funding from Chinese Academy of Sciences

<sup>†</sup> xu\_jin@iscas.ac.cn

# STOCHASTIC RESPONSE SURFACE METHOD FOR STUDYING MICROPHONING AND LORENTZ DETUNING OF ACCELERATOR CAVITIES\*

J. Deryckere, T. Roggen<sup>†</sup>, B. Masschaele, H. De Gerssem, KU Leuven - Kulak, Kortrijk, Belgium

## Abstract

The dependence of the resonant frequency of an RF cavity on its geometry is represented by a stochastic response surface model, which is constructed on the basis of a few eigenmode solutions extended with sensitivity information. The response surface model is used for statistic analysis and for calculating the effect of Lorentz detuning.

## INTRODUCTION

High energy cavities are used within a very small frequency range. Any mechanical deformation, albeit small, may lead to an unacceptable shift of the frequency of the applied eigenmode [1]. To achieve a design that is robust against microphoning and Lorentz detuning [2–5], the simulation tool should deal with small changes in geometry in a consistent way and should be able to calculate the resonance frequencies with a relative accuracy of  $10^{-5}$ . The simple and straightforward procedure which changes and remeshes the geometry and repeats the eigenmode solving, turns out to be inefficient because the introduced discretisation errors will mask the small changes in eigenfrequency, unless an prohibitively fine mesh is used [6]. This paper introduces two techniques to overcome this problem: (a) the eigenmode solver also delivers the sensitivities of the eigenfrequency and thereby increases the amount of information obtained for a single set of geometric parameters; (b) the eigenfrequency is modelled by a stochastic response surface method which allows reliable interpolation and uses the concept of uncertainty to deal with errors introduced by remeshing.

## CAVITY EIGENMODE SOLVERS

The eigenmodes of the cavity are calculated by solving one of

$$\nabla \times \left( \frac{1}{\mu} \nabla \times \vec{E} \right) = \omega^2 \varepsilon \vec{E} \quad (1)$$

$$\nabla \times \left( \frac{1}{\varepsilon} \nabla \times \vec{H} \right) = \omega^2 \mu \vec{H} \quad (2)$$

with  $\vec{E}$  and  $\vec{H}$  the electric and magnetic field strengths,  $\omega$  the angular frequency,  $\varepsilon$  the permittivity and  $\mu$  the permeability [7, 8]. Only the eigenmodes with the lowest eigenfrequencies are relevant. When discretised by the finite-element (FE) method or the finite-integration technique

\*Work supported by the grant KUL\_3E100118, grant KUL\_3E080005, project FP7-Euratom No. 269565 and the Belgian Nuclear Research Centre (SCK-CEN).

<sup>†</sup>toon.roggen@kuleuven-kulak.be

(FIT), (1) and (2) become

$$\mathbf{K}_{\frac{1}{\mu}} \widehat{\mathbf{e}} = \omega^2 \mathbf{M}_{\varepsilon} \widehat{\mathbf{e}} \quad (3)$$

$$\mathbf{K}_{\frac{1}{\varepsilon}} \widehat{\mathbf{h}} = \omega^2 \mathbf{M}_{\mu} \widehat{\mathbf{h}} \quad (4)$$

and will further be expressed generically by  $\mathbf{K}_{\alpha} \mathbf{u} = \omega^2 \mathbf{M}_{\beta} \mathbf{u}$  where  $(\alpha, \beta, \mathbf{u})$  either stands for  $(\frac{1}{\mu}, \varepsilon, \widehat{\mathbf{e}})$  or  $(\frac{1}{\varepsilon}, \mu, \widehat{\mathbf{h}})$  and  $\widehat{\mathbf{e}}_j$  and  $\widehat{\mathbf{h}}_j$  are the degrees of freedom for the electric and magnetic field strengths respectively. The matrix coefficients are

$$\mathbf{K}_{\alpha, i, j} = \int_V \alpha (\nabla \times \vec{w}_i) \cdot (\nabla \times \vec{w}_j) dV \quad (5)$$

$$\mathbf{M}_{\beta, i, j} = \int_V \beta \vec{w}_i \cdot \vec{w}_j dV \quad (6)$$

with  $\vec{w}_i(x, y, z)$  FE or FIT shape functions and  $V$  the computational domain.

In many situations, the cavity has a cylindrical symmetry and only modes with  $\vec{E} = (E_r, 0, E_z)$  and  $\vec{H} = (0, H_{\theta}, 0)$  are relevant. Then, a substantial saving of computation cost is achieved by only triangulating the  $rz$ -cross-section of the cavity and discretising (2) by the shape functions

$$\vec{w}_j = \frac{N_j(r, z)}{2\pi r} \vec{e}_{\theta} \quad (7)$$

$$N_j^{(k)}(r, z) = \frac{a_j^{(k)} + b_j^{(k)} r^2 + c_j^{(k)} z}{2S^{(k)}} \quad (8)$$

where  $\vec{e}_{\theta}$  is the peripheral unit vector,  $N_j(r, z)$  are nodal shape functions associated with mesh node  $j$  and (8) expresses  $N_j(r, z)$  in element  $k$  as a function of the coefficients  $a_j^{(k)}$ ,  $b_j^{(k)}$  and  $c_j^{(k)}$ .  $N_j(r, z)^{(k)}$  features a quadratic dependence on  $r$  such that a homogeneous electric field can be represented exactly on the mesh [9].

## SENSITIVITIES OF THE RESONANCE FREQUENCY

As will become clear below, highly accurate sensitivities of the cavity eigenmode with respect to geometric parameters are of paramount importance for studying microphoning and Lorentz detuning and for a stochastic analysis or optimisation of the design. The sensitivities of the eigenfrequency  $\omega_p$  of eigenmode  $(\omega_p, \mathbf{u}_p)$  with respect to the geometric parameters  $\zeta_q$  are obtained directly from the eigenvalue solver by [10–12]

$$\frac{d\omega_p}{d\zeta_q} = \frac{1}{2\omega_p} \frac{\mathbf{u}_p^H \left( \frac{d\mathbf{K}_{\alpha}}{d\zeta_q} - \omega_p^2 \frac{d\mathbf{M}_{\beta}}{d\zeta_q} \right) \mathbf{u}_p}{\mathbf{u}_p^H \mathbf{M}_{\beta} \mathbf{u}_p} \quad (9)$$

# REALISTIC 3-DIMENSIONAL EIGENMODAL ANALYSIS OF ELECTROMAGNETIC CAVITIES USING SURFACE IMPEDANCE BOUNDARY CONDITIONS

Hua Guo\*, Peter Arbenz†, Computer Science Department, ETH Zurich, Zurich, Switzerland  
Benedikt Oswald‡, Paul Scherrer Institute, Villigen, Switzerland

*Abstract*

The new X-ray Free Electron Laser (SwissFEL) at the Paul Scherrer Institute (PSI) employs, among many other radio frequency elements, a transverse deflecting cavity for beam diagnostics. Since the fabrication process is expensive, an accurate 3-D eigenmodal analysis is indispensable. The software package Femaxx has been developed for solving large scale eigenvalue problems on distributed memory parallel computers. Usually, it is sufficient to assume that the tangential electric field vanishes on the cavity wall (PEC boundary conditions). Of course, in reality, the cavity wall is conductive such that the tangential electrical field on the wall is nonzero. In order to more realistically model the electric field we impose surface impedance boundary conditions (SIBC) arising from the skin effect model. The resulting nonlinear eigenvalue problem is solved with a nonlinear Jacobi–Davidson method. We demonstrate the performance of the method. First, we investigate the fundamental mode of a pillbox cavity. We study resonance, skin depth and quality factor as a function of the cavity wall conductivity. Second, we analyze the transverse deflecting cavity of the SwissFEL to assess the capability of the method for technologically relevant problems.

## FORMULATION OF THE PROBLEM

We wish to calculate the resonant frequencies and the corresponding field distribution in a dielectric electromagnetic cavity. The cavity wall  $\Gamma$  is assumed to be of arbitrary shape; there is no aperture or hole in  $\Gamma$ . The surface conductivity  $\sigma_s$  of  $\Gamma$  is large but finite. The interior  $\Omega$  of the cavity is assumed to be source-free, and is characterized by  $(\mu_0\mu_r, \varepsilon_0\varepsilon_r)$ .  $\mu_0$  and  $\varepsilon_0$  are the magnetic permeability and electric permittivity in free space.  $\mu_r$  and  $\varepsilon_r$  are relative magnetic permeability and relative electric permittivity, respectively. At microwave frequencies,  $\mu_r$  and  $\varepsilon_r$  can be assumed to be non-dispersive.

In the time-harmonic regime, after eliminating the electric field  $\mathbf{E}(\mathbf{x})$ , the magnetic field  $\mathbf{H}(\mathbf{x})$  satisfies

$$\begin{aligned} \nabla \times (\varepsilon_r^{-1} \nabla \times \mathbf{H}(\mathbf{x})) - k_0^2 \mu_r \mathbf{H}(\mathbf{x}) &= \mathbf{0}, \quad \mathbf{x} \in \Omega, \\ \nabla \cdot (\mu_r \mathbf{H}(\mathbf{x})) &= 0, \quad \mathbf{x} \in \Omega. \end{aligned} \quad (1)$$

Here,  $k_0 = \tilde{\omega} \sqrt{\mu_0 \varepsilon_0}$  is the *complex* wave number in free space,  $\tilde{\omega} = \omega + i\alpha$  is the *complex* angular frequency with  $\omega$  the angular frequency and  $\alpha$  the exponential decay rate.

\*hguo@inf.ethz.ch

†arbenz@inf.ethz.ch

‡benedikt.oswald@psi.ch

We use the surface impedance boundary condition (SIBC) on  $\Gamma$  [1]

$$\mathbf{n} \times (\mathbf{n} \times \mathbf{E}(\mathbf{x})) = Z_s \mathbf{n} \times \mathbf{H}(\mathbf{x}), \quad \mathbf{x} \in \Gamma. \quad (2)$$

Here,  $Z_s$  is the *complex* surface impedance and  $\mathbf{n}$  the surface normal vector pointing outwards.

We employ  $Z_s$  based on the theoretical skin effect model [2]

$$Z_s = \frac{1+i}{\sigma_s \delta}, \quad (3)$$

where  $\sigma_s$  is the surface conductivity, and  $\delta$  is the skin depth. The real part of  $Z_s$  is the surface resistivity, i.e.,

$$R_s = \text{Re}(Z_s) = \frac{1}{\sigma_s \delta}. \quad (4)$$

The skin depth  $\delta$  is [2]

$$\delta = \sqrt{\frac{2}{\omega \mu_0 \mu_r \sigma_s}}. \quad (5)$$

$\delta$  depends on the angular frequency  $\omega$ . Note that the skin effect model is appropriate only if  $\sigma_s$  is large enough such that (according to [2]): (1) the conduction current is given by Ohm's law and the net charge density is zero; (2) the displacement current is negligible in comparison with the current, i.e.,  $\omega \varepsilon_r \varepsilon_0 \ll \sigma_s$ . With the above two assumptions, we consider the conductor is good, and the loss of the cavity is small. In other words, the decay rate  $\alpha \ll \omega$ , and thus  $\omega \approx \tilde{\omega} = k_0 c$ , implying that

$$\delta \approx \sqrt{\frac{2}{k_0 c \mu_0 \mu_r \sigma_s}}. \quad (6)$$

The finite element method (FEM) is a suitable method for arbitrary geometrical scales. In order to apply the FEM we use the weak form of Eq (1), see [3],

Find  $k_0 \in \mathbb{C}$  and  $\mathbf{H} \in V$ ,  $\mathbf{H} \neq \mathbf{0}$ , such that for all  $\mathbf{f} \in V$  and all  $q \in W$

$$\begin{aligned} \int_{\Omega} \left[ \frac{1}{\varepsilon_r} \nabla \times \mathbf{H} \cdot \nabla \times \mathbf{f} - k_0^2 \mu_r \mathbf{H} \cdot \mathbf{f} \right] d\mathbf{x} \\ + ik_0 \frac{1}{Z_0} \int_{\Gamma} (\mathbf{n} \times \mathbf{E}) \cdot \mathbf{f} ds = 0, \quad (7) \\ \int_{\Omega} \mu_r \mathbf{H} \cdot \nabla q d\mathbf{x} = 0. \end{aligned}$$

Here,  $V$  denotes the functions in  $H(\text{curl}; \Omega)$  that satisfy the SIBC boundary conditions and  $W = H_0^1(\Omega)$  [1].  $Z_0 = \sqrt{\mu_0/\varepsilon_0}$  is the characteristic impedance of free space.



# DESIGN OF SRF CAVITIES WITH CELL PROFILES BASED ON BEZIER SPLINES\*

Bernard Riemann<sup>†</sup>, Thomas Weis, TU Dortmund University, Dortmund, Germany  
Axel Neumann, Helmholtz-Zentrum Berlin, Berlin, Germany

## Abstract

Elliptical cavities have been a standard in SRF linac technology for 30 years. In this work, we present a novel approach [1] using Bezier spline profile curves. By using different degrees of spline curves, the number of free parameters can be varied to suit a given problem (endcell tuning, basecell figures of merit), thus leading to a high flexibility of the spline approach. As a realistic example, a cubic spline SRF multicell cavity geometry is calculated and the figures of merit are optimized for the operational mode. We also present an outline for HOM endcell optimization that can be realized using available 2D solvers.

## INTRODUCTION

In modern ring-based and linac facilities, high acceleration gradients and duty cycles are achieved using superconducting radio frequency (SRF) cavities. To protect these cavities from quenching and RF breakdown, a sufficiently small ratio of peak surface electric field and accelerator gradient  $E_{surf}/E_{acc}$  is required. Therefore the shapes must not contain edges, and thus a smooth profile curve for the figure of rotation is needed.

As had been done in normal-conducting cavities, edges of cylindrical/iris-loaded cavities were rounded off in a first step. To further enhance performance, the rounding circles were substituted by ellipses [2] (Fig. 1), leading to modern SRF “re-entrant”, “low-loss” and “TESLA-shape” [3] cavities, in which resonant multipacting of secondary electrons is highly suppressed in contrast to cylindrical shapes. While elliptical shapes have shown superior performance, this parameterization is used by historical contingency, as to the authors’ knowledge, no other parameterizations of similar smoothness (modulated sinusoid curves, splines) have been researched for ultra-relativistic particles.

### Spline Geometry Parameters

The spline cavity geometry is such an alternative shape with additional desirable properties like continuous curvature, and a number of free parameters that can be chosen lower than for elliptical shapes (but may be arbitrarily increased).

\* this work is supported by BMBF contract 05K10PEA

<sup>†</sup> bernard.riemann@tu-dortmund.de

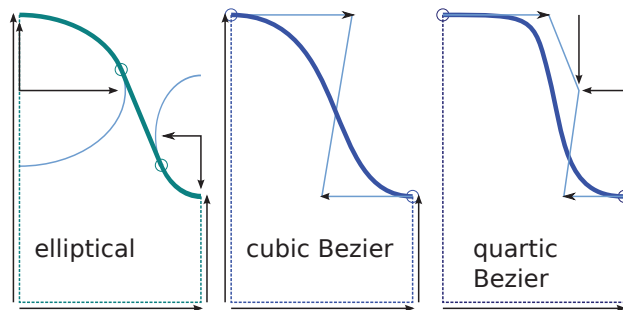


Figure 1: Sketch and cavity parameters (arrows) for different cavity shape parameterizations.

A Bezier spline is a parameterized curve [4]

$$\vec{s}(t) = \vec{a}_0 + \vec{a}_1 t + \vec{a}_2 t^2 + \dots = \sum_{n=0}^N \vec{s}_n b_{n,N}(t) \quad (1)$$

with Bernstein polynomials  $b_{n,N}$  and  $t \in [0, 1]$ . The  $N + 1$  points  $\vec{s}_n$  define the so-called control polygon and contain the free parameters of the spline. Let us consider the simplest possible case of a cubic ( $N = 3$ ) Bezier spline as shown in Fig. 1. The 8 geometry parameters are reduced by a) zero slope of the curve at iris and equator radius of the cavity, and b) fixed relation of the coordinate system to the equator plane. 5 cavity parameters remain, compared to 7 for an elliptical cavity.

Applying two further elementary RF problem constraints c) operation frequency and d) transit-time factor (cell length is  $\beta\lambda/2$ ), only three optimization parameters remain for the specific application. Instead of specifying these constraints, the low dimensionality of the remaining problem allows to scan the remaining parameter space, thus creating a “map” for the cubic Bezier cavity that can be used to speed up complex design optimization tasks.

## IMPLEMENTATION

For the single cell computations with periodic boundary conditions, the 2d code SUPERFISH [5] was employed. Since splines are not implemented in SUPERFISH, a small wrapper for MATLAB was developed. The spline geometry was discretized by calculating a 200 point (halfcell) polygon from its parameters (Fig. 2), which was then used as input in SUPERFISH, also specifying a special localized mesh that matches the polygon discretization accuracy.

# TOOLS FOR ANALYSIS AND IMPROVEMENT OF LINAC OPTICS DESIGN FOR HIGH BRIGHTNESS ELECTRON BEAMS

S. Di Mitri<sup>#</sup>, M. Cornacchia, C. Scafuri, Sincrotrone Trieste S.C.p.A., Basovizza, 34149, Italy

## Abstract

The optics design of single pass high brightness electron linacs usually aims at the preservation of the transverse emittance. Collective effects mainly impose constraints to the optics design such as at the low-beta interaction points in colliders and magnetic compressors in free electron lasers (FELs). Other constraints are from the trajectory correction scheme, performance of diagnostics, collimation systems and physical space limitations. Strong focusing is typically prescribed for all the aforementioned cases, although it may hamper the main goal of emittance preservation through the excitation of optical aberrations. Strong focusing also potentially leads, through focusing errors, to large beam optics mismatch. Based on these sometimes conflicting requirements, we have developed tools for the analysis and improvement of electron linac optics. They are based on the Elegant code [1] and allow the user to identify: i) local sources of phase space distortions and emittance dilution, ii) lattice areas particularly sensitive to focusing errors, iii) poor trajectory steering. The analysis does not require massive particle tracking since it deals with the single particle motion in the normalized phase space.

## ELEGANT ON-LINE

In order to use Elegant as an on-line machine model [2], we have developed a set of utilities for interfacing the simulator with the accelerator. We have exploited the Elegant capability to read and write a set of element parameters from a file in SDDS format via the `load_parameters` and `write_parameters` commands. The SDDS file is filled in with the actual parameters of the running accelerator by means of a dedicated utility which examines the SDDS files and maps the requested parameters to the appropriate control system variables by means of database tables. The requested variables are then acquired from the control system and scaled if necessary, e.g. converting beam position monitors (BPM) readings from millimeter to meter). The reverse path is followed for setting parameters: Elegant writes the new values to the SDDS files, another dedicated utility reads the new parameters from the SDDS file, maps them to control variables and set the values via standard control system calls. Since Elegant works with normalized machine physics quantities, we have developed a set of specialized control system servers, called Tango devices [3], which perform the conversion from engineering quantities (e.g. current) to machine physics quantities (e.g. quadrupole strength) by means of calibration tables. Such tables are directly handled by the Tango server.

<sup>#</sup>simone.dimitri@elettra.trieste.it

## OPTICS MATCHING

The goal of optics matching is to impose the design values of the Twiss functions to the electron beam. This is typically done with at least four quadrupole magnets. For beam energies lower than  $\sim 100$  MeV, the beam optics cannot be predicted with sufficient accuracy in Elegant since the particles move in the space-charge dominated regime. For this reason, it is very important to measure the beam optics at the *end* of the injector, where the electron spatial distribution is frozen to any practical purpose. The matching loop is illustrated in Fig. 1.

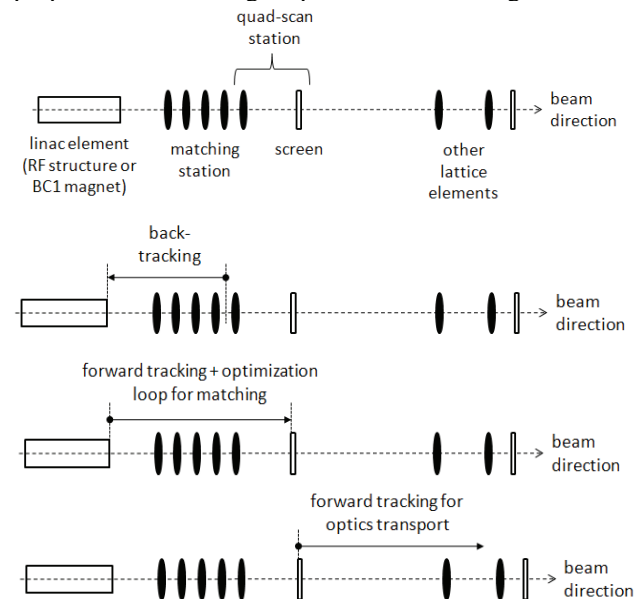


Figure 1: Illustration of the optics matching loop [2]. From top to bottom: i) the beam Twiss parameters are measured with the quadrupole scan technique [4] at the entrance of the last quadrupole magnet of the matching station; ii) the present machine configuration is read by Elegant and the measured Twiss parameters are back-tracked to a point upstream of the matching station; iii) starting from the present machine configuration, Elegant starts optimizing the quadrupole strengths to match the beam Twiss parameters to the design values; iv) once the matching has been performed, the beam is transported through the downstream lattice.

The matching loop has been coded in MATLAB [5] and a Graphical User Interface (GUI) is available as a standard control room application. A theoretical betatron mismatch parameter is defined as follows [6]:

$$\xi = \frac{1}{2} (\bar{\beta}\gamma - 2\bar{\alpha}\alpha + \bar{\gamma}\beta) \quad (1)$$

# ANALYTICAL PRESENTATION OF SPACE CHARGE FORCES\*

S. Andrianov<sup>†</sup>, SPbSU, St. Petersburg, Russia

## Abstract

This paper presents an analytical description of space charge forces generated by charged particle beams. Suggested approach is based on some set of models for particle distribution function. All necessary calculations have analytical and closed form for different models for beam density distributions. These model distributions can be used for approximation of real beam distributions. The corresponding solutions are included in general scheme of beam dynamics presentation based on matrix formalism for Lie algebraic tools. Computer software is based on corresponding symbolic codes and some parallel technologies. In particular, as computational tools we consider GPU graphic card NVIDIA. As an example, we consider a problem of beam dynamics modelling for microprobe focusing systems.

## INTRODUCTION

Most of space charge modelling methods are based on numerical methods and corresponding programming technologies. In particular, matrix processors became very popular in the last time for numerical evaluations (i. e. using the Particle-in-Cell method). But for long time beam evolution problems these methods demonstrate rather low effectiveness. The nature of the corresponding beam dynamics needs effective algorithms for space charge field reconstruction during the beam evolution along the reference orbit (with coordinate  $s$ ). For this purpose in this paper we consider the following two methods: a beam with elliptical form in transverse four-dimensional phase space (*unbunched beam model*) and a beam presented as six-dimensional ellipses (*bunched beam model*). For the both models we use Ferrer's integrals method [1]. This method allows to derive corresponding formulae for beam generated field in symbolic forms. Similar presentation is compatible with presentation of the corresponding beam dynamics using Lie algebraic tools formalism [2]. In this paper we demonstrate evaluation method of electrical field generated by different distribution functions of beam particles. The analytical presentation of corresponding solutions is matched with matrix formalism for Lie algebraic tools [3]. Furthermore this approach can be realized for solution of Maxwell–Vlasov equations [4].

\* Work supported by Federal Targeted Program "Scientific and Scientific-Pedagogical Personnel of the Innovative Russia in 2009-2013" (Governmental Contract no. p 793)

<sup>†</sup> sandrianov@yandex.ru

## DISTRIBUTION FUNCTION IN PHASE SPACE

In this section we demonstrate basic idea of our approach using the first models – the unbunched beam model in four-dimensional space with following coordinates  $\{x, p_x, y, p_y\}$ . The corresponding distribution function  $f(x, p_x, y, p_y, s)$  can be presented as a function of  $\mathcal{X}^2 = \mathbf{X}^T \mathbb{A} \mathbf{X}$ , where  $\mathbf{X} = (x, y, p_x, p_y)^T$  and  $\mathbb{A}$  is a symmetric nonsingular matrix. Let us consider some popular functions to present space charge distribution.

1) *Uniform distribution:*

$$\varphi(\mathcal{X}^2) = \frac{2\sqrt{\det \mathbb{A}}}{\pi^2} \Theta(1 - \mathcal{X}^2), \quad \Theta(x) = \begin{cases} 1, & x \geq 0, \\ 0, & x < 0. \end{cases}$$

2) *Vladimirov–Kapchinsky (microcanonical) distribution:*

$$\varphi(\mathcal{X}^2) = \frac{\sqrt{\det \mathbb{A}}}{\pi^2} \delta(1 - \mathcal{X}^2).$$

3) *Normal (Gauss) distribution:*

$$\varphi(\mathcal{X}^2) = \frac{\sqrt{\det \mathbb{A}}}{4\pi^2} \exp\left(-\frac{\mathcal{X}^2}{2}\right).$$

Of course, three indicated types of distributions don't exhaust all variety of admissible distributions family. But these distributions are interesting from point of view of configuration distributions of charge density in the configuration space (in the next we omit the variable  $s$  for reduction).

$$\rho(x, y) = \int_{R^2} f(x, p_x, y, p_y) dp_x dp_y.$$

Indeed, practically, it is very difficult to measure the function  $f(\mathbf{X})$ , but the distribution  $\rho(x, y)$  can be obtained with measurement accuracy. More over, only function  $\rho(x, y)$  defines the electrical potential (or electrical field) which is necessary for beam dynamics evaluation. Let present the matrix  $\mathbb{A}$  in a block matrix form

$$\mathbb{A} = \begin{pmatrix} \mathbb{A}^{11} & \mathbb{A}^{12} \\ \mathbb{A}^{21} & \mathbb{A}^{22} \end{pmatrix}, \quad \mathbb{A}^{kk} = (\mathbb{A}^{kk})^T, \quad \mathbb{A}^{21} = (\mathbb{A}^{12})^T,$$

then we can write

$$\mathcal{X}^2 = \mathbf{X}^T \mathbb{A} \mathbf{X} = \mathbf{X}_1^T \mathbb{A}^{11} \mathbf{X}_1 + \mathbf{X}_1^T \mathbb{A}^{12} \mathbf{X}_2 + \mathbf{X}_2^T \mathbb{A}^{21} \mathbf{X}_1 + \mathbf{X}_2^T \mathbb{A}^{22} \mathbf{X}_2,$$

where  $\mathbf{X}_1 = (x, y)^T$ ,  $\mathbf{X}_2 = (p_x, p_y)^T$ . After some evaluations one can obtain the following equalities.

1) *Uniform distribution:*

$$\rho(x, y) = \frac{2qN_0}{\pi} \sqrt{\frac{\det \mathbb{A}}{\det \mathbb{A}^{22}}} (1 - \mathcal{X}_r^2) \Theta(1 - \mathcal{X}_r^2),$$

# DYNAMICS OF ENERGY LOSS OF A BUNCH INTERSECTING A BOUNDARY BETWEEN VACUUM AND DIELECTRIC IN A WAVEGUIDE\*

T. Yu. Alekhina<sup>#</sup> and A. V. Tyukhtin, St. Petersburg State University, St. Petersburg, Russia

## Abstract

We analyze radiation of a small bunch crossing a boundary between two dielectrics in a cylindrical waveguide. The main attention is paid to investigation of dynamics of a charge energy loss and the effect of the boundary on the electromagnetic field (EMF). Algorithms of computations for the field and the energy loss are founded upon certain transformations of integration path. We consider two instances in detail: the bunch is flying from dielectric into vacuum and from vacuum into dielectric. In both cases we compare the energy losses by transition radiation (TR) and by Cherenkov one (CR). Our investigation shows, for example, that energy loss is negative at certain segments of the bunch trajectory.

## INTRODUCTION

One of the problems being important for the wakefield acceleration technique and for new methods of generation of microwave radiation consists in analysis of effect of the boundary on the wave field when a bunch flies into a dielectric structure or from one. It should be noticed that energetic characteristics of TR at a single boundary in a waveguide and in the case of a dielectric plate were investigated in papers [1,2]. However, the most attention was paid to study the energetic spectrums of generated modes. Dynamics of an energy loss as well as an EMF structure has not been analyzed.

Our research is based on original approach used previously for the case of the vacuum-plasma boundary [3]. But Cherenkov radiation is not generated in such situation; therefore it varies radically from the case under consideration. The electromagnetic field structure of the point charge was partially investigated in our works [4,5]. Now we analyze dynamics of the energy losses which allows of better understanding physical phenomena in this situation.

We consider a point charge  $q$  moving in a metal circular waveguide of radius  $a$  along its axis ( $z$ -axis) and intersecting the boundary ( $z=0$ ) between two homogeneous isotropic non-dispersive dielectrics with permittivity  $\varepsilon_1$  ( $z < 0$ ) and  $\varepsilon_2$  ( $z > 0$ ) at the moment  $t=0$ . The charge passes uniformly with a velocity  $\vec{v} = c\beta\vec{e}_z$  ( $c$  is a light speed in vacuum).

The analytical solution of the problem is traditionally found for the spectral harmonics of the vector potentials as an expansion into a series of eigenfunctions of the transversal operator [3,6]. Expressions for components of the EMF can be easily derived from the formulae for the

general case of the boundary between two arbitrary homogeneous isotropic media [3].

We investigate the dynamics of the charge energy loss per unit length of the charge motion:

$$W = -qE_z \Big|_{r \rightarrow 0}^{z \rightarrow \beta ct}. \quad (1)$$

As it follows from general expressions for EMF the charge energy losses in both media have two summands:  $W_{1,2} = W_{1,2}^q + W_{1,2}^b$ . The first one ( $W_{1,2}^q$ ) is connected with so-called by V. L. Ginzburg [7] “forced” field that is EMF of the charge in a regular waveguide. It contains CR if  $\beta > \beta_{C1,2}$ ,  $\beta_{C1,2} = \varepsilon_{1,2}^{-1/2}$ . The second summand ( $W_{1,2}^b$ ) is connected with the “free” field that is determined by the influence of the boundary and includes TR. Each summand is decomposition in an infinite series of normal

modes: 
$$W_{1,2}^{q,b} = \sum_{n=1}^{\infty} W_{n1,2}^{q,b}. \quad (2)$$

The charge energy loss in a regular waveguide with homogeneous filling analysed in many papers is equal to [8]

$$W_{n1,2}^q = \begin{cases} 2q^2 (a^2 \varepsilon_{1,2} J_1^2(\chi_{0n}))^{-1}, & \beta > \beta_{C1,2} \\ 0, & \beta < \beta_{C1,2} \end{cases}, \quad (3)$$

where  $\chi_{0n}$  is the  $n^{\text{th}}$  zero of the Bessel function  $J_0(x)$ .

For analysis of the charge energy loss by TR ( $W_{n1,2}^b$ ) we use the exact integral representation. We investigate it with analytical and computational methods. Analytical research is an asymptotic investigation with the steepest descent technique. Computations are based on original algorithm using some transformation of the integration path.

We study two cases in detail: the bunch is flying from dielectric ( $\varepsilon_1 > 1$ ) into vacuum ( $\varepsilon_2 = 1$ ) and from vacuum ( $\varepsilon_1 = 1$ ) into dielectric ( $\varepsilon_2 > 1$ ).

## THE CASE OF FLYING FROM DIELECTRIC INTO VACUUM

### Numerical Approach

Efficient algorithm used for numerical calculation is based on a certain transformation of the initial integration path in the complex plane of  $\omega$ . Earlier such an algorithm was used for calculating of the forced field in different dispersive media [9] and in a waveguide with the boundary between vacuum and cold plasma [3]. We demonstrate this method for the vacuum area.

\*Work supported by St.-Petersburg State University

<sup>#</sup>tanya@niirf.spbu.ru

# DESIGN AND APPLICATIONS OF THE BMAD LIBRARY FOR THE SIMULATION OF PARTICLE BEAMS AND X-RAYS\*

D. Sagan, Wilson Laboratory, Cornell University, Ithaca, NY, 14853, USA

## Abstract

The open-source Bmad software library has been developed for simulating both charged particle beams and X-rays. Owing to its modular, object-oriented design, Bmad has proved to be versatile, and is currently used in a number of programs at Cornell's Laboratory for Elementary-Particle Physics. This paper will discuss the design of the Bmad library and how features such as the ability to simulate overlapping elements, the ability to define the action of control-room "knobs," and the ability to select among different tracking algorithms, have all contributed to a flexible simulation environment that eases the task of both programmers and users alike. Also discussed are the uses that Bmad has been put to, including machine control and the integration of particle beam and X-ray simulations.

## INTRODUCTION

Bmad, an open-source software library for simulating both charged particle beams and X-rays, has been in development at Cornell beginning in the 1990s[1]. Originally, the syntax for the lattice files for Bmad was patterned after the syntax of the MAD program[2]. Since, at that time, only a subset of the MAD language was used, the name "Baby MAD" or "Bmad" for short was chosen.

The initial purpose for developing Bmad was modest: Simply to be able to compute Twiss parameters and the closed orbit, and to provide a standard lattice description format. As Bmad evolved, the scope of Bmad expanded so that currently Bmad can simulate such things as spin, X-ray photons, coherent synchrotron radiation, intra-beam scattering, Touschek effect, etc., etc.

Bmad has proved to be versatile and, as a result, is now used in a number of programs at Cornell. Experience with Bmad has shown that there are a number of design features that have made Bmad especially useful. The purpose of this paper is to discuss this and to discuss some of the applications that Bmad has been used for. Finally, plans for the future of Bmad will be presented.

## DESIGN PHILOSOPHY

The aim of the Bmad project is to:

- Cut down on the time needed to develop programs.
- Minimize computation times.
- Cut down on programming errors.
- Provide a simple mechanism for lattice function calculations from within programs.

- Provide a flexible and powerful lattice input format.
- Standardize sharing of lattices between programs.

To maximize code reuse, Bmad, written in Fortran, is designed to be object oriented from the ground up. For example, it takes only one line of executable code to parse a lattice file:

```
type (lat_struct) lat
call bmad_parser('lat.bmad', lat)
```

The call to `bmad_parser` in this example causes the file named "lat.bmad" to be parsed and the information to be stored in a variable named `lat` of type `lat_struct` (equivalent to a C++ class). For communication with C++ code, Bmad defines a set of C++ classes and there are interface routines to convey information between between the Fortran structures and the C++ classes.

From the beginning, Bmad development has been driven by the need to solve the practical problems arising from the requirements of machine simulation, lattice design and machine control. As a result, one emphasis of Bmad development has been on minimizing the bookkeeping tasks of both programmer and user. There are a number of features that have proved to be especially useful in this regard, and some are discussed below: The ability to superimpose elements on top of other elements, the ability to slice elements into pieces, the ability to define controller elements that control the attributes of other elements, and the ability to choose the algorithm used for particle tracking.

## Superposition of Elements

"Superposition" is the ability to overlap lattice elements spatially. Figure 1 shows an example which is a greatly simplified version of the IR region of Cornell's CESR storage ring when CESR was an e+/e- collider. As shown in Fig. 1A, two quadrupoles named `q1w` and `q1e` are partially inside and partially outside the interaction region solenoid named `c1eo`. In the lattice file, the IR region layout is defined to be

```
cesr: line = (... q1e, dft1, ip, dft1, q1w ...)
c1eo: solenoid, l = 3.51, superimpose, ref = ip
```

The line named `cesr` ignores the solenoid and just contains the interaction point marker element named `ip` which is surrounded by two drifts named `dft1` which are, in turn, surrounded by the `q1w` and `q1e` quadrupoles. The solenoid is added to the layout on the second line by using superposition. The "ref = ip" indicates that the solenoid is placed relative to `ip`. The default, which is used here, is to place the center of the superimposed `c1eo` element at the center of the `ip` reference element. Within a program, the representation of the lattice in the `lat_struct` structure that Bmad creates will contain two lists: One list,

\* Work supported by the National Science Foundation under contract PHY-1002467.

# SPACE CHARGE EFFECTS AND FOCUSING METHODS FOR LASER ACCELERATED ION BEAMS

P. Schmidt, O. Boine-Frankenheim, V. Kornilov, P. Spädtke, GSI, Darmstadt, Germany

## Abstract

Within the scope of the LIGHT-Project [1] high intense beams of laser accelerated ions and co-moving electrons are produced. We are interested in methods for the controlled deneutralization of the beam, e.g. using a thin metal foil to absorb the electrons. Those beams show high initial divergence angle and velocity spread [1]. Therefore methods of focusing and collimating the beam are indispensable. Hence the focusing with a pulsed power solenoid is discussed.

## INTRODUCTION

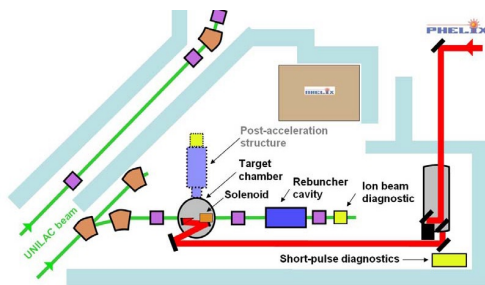


Figure 1: Setup of the LIGHT-Project.

Currently the LIGHT-Project (Laser Ion Generation, Handling and Transport)[1] is performed at the Helmholtzzentrum für Schwerionenforschung Darmstadt (former GSI) (Germany). Within this project, high intense ion beams are generated by laser acceleration, using GSI's PHELIX-Laser. A sketch of the used setup is given in Fig. 1. Referring to the TNSA mechanism [2], one can expect, that the generated beam is quasi-neutral, composed of protons and co-moving electrons. We are therefore interested in methods for the controlled deneutralization of the beam to get clean experimental conditions. This can be done by using a thin metal foil to absorb the electrons<sup>1</sup>. The properties of this thin metal foil should be such that all electrons are removed, keeping the velocity -and density distribution of the protons being unaffected. The position of the foil is determined so that space charge has no effect behind the foil. A criterion in terms of beam parameters is worked out, by which one can decide how important space charge is. Following this foil, the beam is focused and carried towards a re-buncher-cavity (see Fig. 1). The focusing with a pulsed power solenoid (see Fig. 1) is discussed.

<sup>1</sup>The foil is not yet implemented in the setup.

## BEAM MODEL

For the determination of space charge effects, we will use a rather simple beam model. Nevertheless it turns out, that this leads to general criterion, which only depends on the beam parameters. Let us assume we have a uniform cylindrical bunch with radius  $r_0$  and length  $l_b$ , containing  $N_0$  protons<sup>2</sup>. The charge number is  $Z = 1$  and charge of each particle is  $q = e$ . Furthermore the beam has a longitudinal velocity  $\vec{v}_{\parallel}$  with a velocity spread  $\Delta v_{\parallel}$  and a transversal velocity  $\vec{v}_{\perp} = v_{\parallel} r/r_0 \tan(\vartheta)$ , where  $\vartheta$  is the divergence angle. In the simplest case the bunch length is then given by the transversal velocity spread:  $l_b(z) = l_0 + \Delta v_{\parallel}/v_{\parallel} z$ , where  $z$  is the longitudinal coordinate and  $l_0$  the initial length of the bunch. Neglecting edge effects, one finds the following envelope equation for the beam:

$$\partial_{zz}^2 \sigma = K(z)/\sigma \quad (1)$$

Here  $\sigma = r/r_0$  is the envelope radius, normalized by the initial radius. The model and geometry independent parameter

$$K(z) = \frac{Z^2 \rho}{\beta_{\parallel}^2 c^2 \gamma^3 m_p} \frac{e^2}{2\epsilon_0} \quad (2)$$

is called perveance. With the particle density  $\rho$ ,  $\beta_{\parallel} = v_{\parallel}/c$ ,  $c$  the speed of light,  $\gamma$  the Lorentzian factor and  $m_p$  the ion mass. As one can see from Fig. 2, the result from eq. 1 is in good agreement with PIC Simulations done with VORPAL<sup>©</sup>[3].

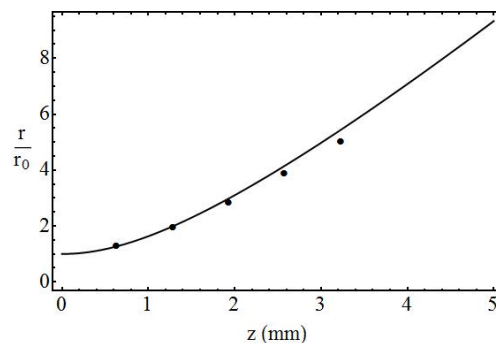


Figure 2: Beam radius from eq. 1 (black line) and simulation (dots) with VORPAL<sup>©</sup>[3].

## SPACE CHARGE EFFECTS

The perveance from eq. 2 only depends on beam parameters and is a measure for the strength of space charge

<sup>2</sup>As one will see, the criterion can be applied for any ion.

# MATRIX FORMALISM FOR LONG-TERM EVOLUTION OF CHARGED PARTICLE AND SPIN DYNAMICS IN ELECTROSTATIC FIELDS

A. Ivanov\*, S. Andrianov, Saint-Petersburg State University, Russia

## Abstract

The matrix formalism as a numerical approach for solving of ODE equations is considered. It is a map method and has several advantages over classical step-by-step integration methods. This approach allows to present the solution as set of numerical matrices. A complete derivation of the equations this method is based on will be shown. Problems of symplectification and computing performance are discussed. We have developed an application that provides a tool for differential equations solving. The developed program allows to generate the final programming codes on C++, Fortran, MATLAB, C#, Java languages. The given approach is applied to long-term evolution of charged particle and spin dynamics in electrostatic fields.

## MATRIX FORM OF ODE

Let's introduce a nonlinear system of ordinary differential equations

$$\frac{d}{dt}X = F(t, X). \quad (1)$$

Under the assumptions of  $F(0, X_0) = 0$  the system (1) can be presented in the following form

$$\frac{d}{dt}X = \sum_{k=0}^{\infty} P^{1k}(t)X^{[k]}, \quad (2)$$

where  $X^{[k]}$  is kronecker power of vector  $X$ , matrices  $P^{1k}$  can be calculate as

$$P^{1k}(t) = \frac{1}{(k)!} \frac{\partial^k F(t, X_0)}{\partial (X^{[k]})^T}, \quad k = 1, 2, \dots$$

Note that vector  $X$  is equal to  $(x_1^{k_1}, \dots, x_n^{k_n})$ , where  $x_i$  means  $i$ th component of state,  $(k)! = k_1! \dots k_n!$

## NUMERICAL IMPLEMENTATION

Solution of system (2) can be written in form

$$X = \sum_{k=0}^{\infty} R^{1k}(t)X_0^{[k]}. \quad (3)$$

Elements of matrices  $R^{1k}$  are depended on  $t$  and can be calculated in symbolic mode [1]. But such algorithms are quite complex. In this paper we propose a numerical implementation of it. In this case matrices  $R^{1k}$  are evaluate in the specific time.

\* 05x.andrey@gmail.com

After differentiating the equation (3) and taking into account (2) we get

$$\begin{aligned} \frac{dX}{dt} &= \sum_{k=0}^{\infty} \frac{dR^{1k}(t)}{dt} X_0^{[k]}, \\ \sum_{k=1}^{\infty} \frac{dR^{1k}(t)}{dt} X_0^{[k]} &= \sum_{k=1}^{\infty} P^{1k}(t)X^{[k]}. \end{aligned}$$

The partial derivatives of this equations with respect to  $X_0^{[j]}$  are equal to

$$\begin{aligned} \frac{dR^{10}(t)}{dt} &= \sum_{k=1}^{\infty} P^{1k}(t)(R^{1k})^{[k]}, \\ \frac{dR^{1j}(t)}{dt} &= \sum_{k=1}^{\infty} P^{1k}(t) \frac{\partial X^{[k]}}{\partial (X_0^{[j]})^T}, \quad k = 1, 2, \dots \end{aligned} \quad (4)$$

and define the system of ordinary differential equations. Solution of this system is deterined matrices  $R^{1k}$ .

For integration of equations (4) numerical approach can be used. Note that step-by-step integration use only for map building. After that the solution that corresponds to the initil point  $X_0$  can be calculate with the same map (3). In the research we use symplectic 2 stage Runge-Kutta scheme of 4 order (see [2]).

## SYMPLECTICATION

The relation (3) can be presented as map transformation

$$X = R \circ X_0. \quad (5)$$

This map  $R$  is symplectic if

$$M^*JM = J, \forall X_0, \quad (6)$$

where  $M = \partial X / \partial X_0$  and  $M^*$  is the transpense of  $M$ ,  $E$  is identity matrix,

$$J = \begin{pmatrix} 0 & E \\ -E & 0 \end{pmatrix}. \quad (7)$$

Relation (6) in case of numerical matrices  $R^{1k}$  leads to a system of equations

$$a_0 + A_1 \mathbf{X}_0^{[1]} + \dots + A_k \mathbf{X}_0^{[k]} = 0,$$

where  $A_i$  is a numerical vector. Note that this equation must be satisfied for any  $X_0$ . It means that the coefficients of each polynom are equal to zero and in this way appropriate corrections of the elements of the matrices  $R^{1k}$  can be found.

# EM SIMULATIONS IN BEAM COUPLING IMPEDANCE STUDIES: SOME EXAMPLES OF APPLICATION

C. Zannini, CERN, Geneva Switzerland and EPFL, Lausanne, Switzerland

G. Rumolo, CERN, Geneva, Switzerland

## Abstract

In the frame of the SPS upgrade an accurate impedance model is needed in order to predict the instability threshold and if necessary to start a campaign of impedance reduction. Analytical models, 3-D simulations and bench measurements are used to estimate the impedance contribution of the different devices along the machine. Special attention is devoted to the estimation of the impedance contribution of the kicker magnets that are suspected to be the most important impedance source in SPS. In particular a numerical study is carried out to analyze the effect of the serigraphy in the SPS extraction kicker. An important part of the devices simulations are the ferrite model. For this reason a numerical based method to measure the electromagnetic properties of the material has been developed to measure the ferrite properties. A simulation technique, in order to account for external cable is developed. The simulation results were benchmarked with analytical models and observations with beam. A numerical study was also performed to investigate the limits of the wire method for beam coupling impedance measurements.

## INTRODUCTION

The aim of this paper is a description of the simulation studies performed in the frame of an improvement of the SPS impedance model. The simulations were performed mostly using the Wakefield solver of the 3-D commercial code CST Particle Studio.

### SPS KICKER IMPEDANCE MODEL

A kicker is a special type of magnet designed to abruptly deflect the beam off its previous trajectory, for instance to extract the beam to a transfer line or to a beam dump. Among all the SPS elements, the kickers are suspected to contribute to a significant amount of the transverse impedance of the SPS.

#### Simple Models

In a very simple approximation an SPS ferrite loaded kicker can be modelled as two parallel plates of ferrite (see Fig. 1). For this simple geometrical model all the impedance terms (longitudinal, driving and detuning horizontal and vertical impedances) are calculated in [1, 2, 3]. Simulation results were found in very good agreement with the existing models [1, 2] and exactly predicted the detuning (also called quadrupolar) impedance of these devices [3]. The perfect agreement between analytical model and numerical simulations

shown in [4] can be read as an important benchmark for the simulation code in the correct solution of electromagnetic problem involving dispersive materials such a ferrite.

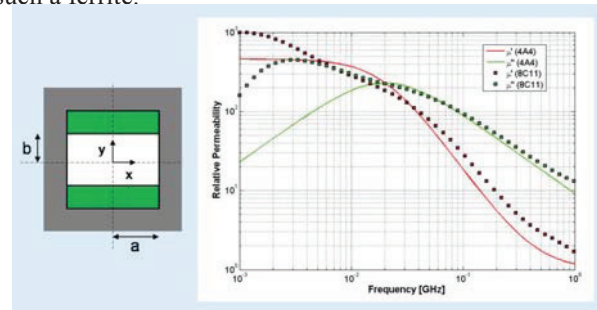


Figure 1: Tsutsui model on the left: ferrite in green, PEC in gray and vacuum in white; complex permeability of the ferrite 4A4 and 8C11 on the right.

In the frame of an improvement of the kicker impedance model we performed a simulation study step by step to allow a good understanding of the different contributions to the kicker impedance. First, a device of finite length inserted in the vacuum tank and equipped with an inner conductor can support propagation of a quasi-TEM mode when interacting with the beam. The device behaves as a transmission line formed by the vacuum tank and the inner conductor which are continued on the external cables and closed on the appropriate circuit terminations. The TEM mode affects the impedance below a certain frequency (when the field penetration in the ferrite becomes comparable to the magnetic circuit length). This behaviour disappears as soon as we allow for 2-D geometries (infinite in the longitudinal direction) because the transverse TEM mode arises at the discontinuities which in this case are moved to infinity. In order to consider this aspect a circuit model was developed and benchmarked with CST 3-D simulations [5]. The good agreement between theoretical model and CST simulations is an ulterior proof of reliability of the code.

#### Realistic Models

In order to approach a more realistic model other aspects have to be considered: the longitudinal segmentation (see Fig. 2), internal circuits, non ideal terminations etc. An important simulation effort was devoted to the estimation of the impedance contribution of the SPS extraction kickers. Due to heating issues the original design of these kickers was modified. Interleaved fingers were printed by serigraphy directly on the ferrite (see Fig. 3). At the

# NUMERICAL CALCULATION OF BEAM COUPLING IMPEDANCES IN THE FREQUENCY DOMAIN USING FIT\*

U. Niedermayer<sup>#</sup> and O. Boine-Frankenheim

Technische Universität Darmstadt, Institut für Theorie Elektromagnetischer Felder (TEMF),  
Schlossgartenstraße 8, 64289 Darmstadt, Germany

## Abstract

The transverse impedance of kicker magnets is considered to be one of the main beam instability sources in the projected SIS-100 at FAIR and also in the SPS at CERN. The longitudinal impedance can contribute to the heat load, which is especially a concern in the cold sections of SIS-100 and LHC. In the high frequency range, commercially available time domain codes like CST Particle Studio serve to calculate the impedance but they are inapplicable at medium and low frequencies which become more important for larger size synchrotrons. We present the ongoing work of developing a Finite Integration Technique (FIT) solver in frequency domain which is based on the Parallel and Extensible Toolkit for Scientific computing (PETSc) framework in C++. Proper beam adapted boundary conditions are important to validate the concept. The code is applied to an inductive insert used to compensate the longitudinal space charge impedance in low energy machines. Another application focuses on the impedance contribution of a ferrite kicker with inductively coupled pulse forming network (PFN).

## INTRODUCTION

For the SIS100 synchrotron which will be built in the framework of the FAIR project, especially the coasting beam and the high intensity proton bunch are susceptible to impedance driven coherent transverse instabilities. Since SIS100 is a cryogenic (< 20 K) machine, the beam induced heat load is an important issue. In the relevant frequency range of several kHz to 2 GHz impedance sources are mainly given by the thin stainless steel beam pipe [1] and ferrite components. Above the cut-off frequency of the beam pipe, wake fields are traveling off-phase with the beam such that no net interaction takes place in long bunches. Additionally to the necessary ferrite kickers and their supply networks, also an inductive ferrite insertion to compensate the negative inductive longitudinal space charge impedance has been proposed. The longitudinal and transverse impedances of these objects have to be quantified in order to ensure a stable high intensity beam by designing instability countermeasures.

Usually coupling impedances are defined as the Fourier transform of the wake function. The wake function can be calculated by commercial software such as CST Particle Studio [2]. At low frequencies, which become more

important for large hadron synchrotrons, this technique is inapplicable. From Küpfmüller's uncertainty principle  $\Delta t \Delta f \geq 1$  with some definition of the time-duration and bandwidth [3] one finds that 300 km of wake-length have to be integrated in order to obtain a frequency-resolution of 1 kHz. Therefore at low and medium frequencies a frequency domain (FD) approach is pursued. The problem of determining coupling impedances in the frequency domain has already been addressed by Doliwa et al. [4] using a Neumann series approach with a Python implementation. The new implementation described here is supposed to carry on this work on a more general C++ platform with properly defined interfaces to the PETSc [5] framework on modern 64-bit machines.

The following will give a definition of the coupling impedances directly in FD. By convention underlined symbols emphasize complex variables. This also serves to distinguish between time domain (TD) and frequency domain (FD) fields. The beam with total charge  $q$  in a synchrotron is modeled as a disc with radius  $a$  of uniform surface charge density  $\sigma$  traveling with velocity  $v$ . The transverse displacement  $d_x$  of the beam (i.e. a coherent dipole oscillation) is approximated to first order by

$$\sigma(\varrho, \varphi) \approx \frac{q}{\pi a^2} [\Theta(a - \varrho) + \delta(a - \varrho) d_x \cos \varphi] \quad (1)$$

$$=: \sigma_{\parallel} \Theta(a - \varrho) + \sigma_{\perp} \delta(a - \varrho) \quad (2)$$

where  $\Theta$  is the unit step and  $\delta$  is its generalized derivative. The beam's volume charge density is given by  $\varrho(\vec{r}, t) = \sigma(\varrho, \varphi) \delta(z - vt)$  and it reads in frequency domain

$$\underline{\varrho}(\vec{r}, \omega) = \int_{-\infty}^{\infty} \varrho(\vec{r}, t) e^{-i\omega t} dt = \frac{1}{v} \sigma(\varrho, \varphi) e^{-i\omega z/v}. \quad (3)$$

The beam current density in frequency domain is

$$\underline{J}_{s,z}(\varrho, \varphi, z; \omega) = \sigma(\varrho, \varphi) e^{-i\omega z/v} =: \underline{J}_{\parallel} + \underline{J}_{\perp} \quad (4)$$

where  $\underline{J}_{\parallel}$  and  $\underline{J}_{\perp}$  are the monopole and dipole components, as in Eq. (2), respectively. The coherent force due to beam induced electromagnetic fields acting back on the beam is described by the coupling impedance [6]

$$\underline{Z}_{\parallel}(\omega) = -\frac{1}{q^2} \int_{\text{beam}} \underline{\vec{E}} \cdot \underline{\vec{J}}_{\parallel}^* dV \quad (5)$$

$$\underline{Z}_{\perp,x}(\omega) = -\frac{v}{(qd_x)^2 \omega} \int_{\text{beam}} \underline{\vec{E}} \cdot \underline{\vec{J}}_{\perp}^* dV. \quad (6)$$

The electric field  $\underline{\vec{E}}$  is to be calculated from Maxwell's equations. Instead of the cosine distribution for dipolar excitation in Eq. (2) one can also use a twin wire approximation, as described in [7].

\* Work supported by GSI

<sup>#</sup>u.niedermayer@gsi.de

# ELECTROMAGNETIC CHARACTERIZATION OF MATERIALS FOR THE CLIC DAMPING RINGS

E. Koukovini-Platia\*, G. De Michele†, C. Zannini\*, G. Rumolo,  
CERN, Geneva, Switzerland

## Abstract

The performance of the Compact Linear Collider (CLIC) damping rings (DR) is likely to be limited by collective effects due to the unprecedented brilliance of the beams. Coating will be used in both electron (EDR) and positron damping rings (PDR) to suppress effects like electron cloud formation or ion instabilities. The impedance modeling of the chambers, necessary for the instabilities studies which will ensure safe operation under nominal conditions, must include the contribution from the coating materials applied for electron cloud mitigation and/or ultra-low vacuum pressure. This advocates for a correct characterization of this impedance in a high frequency range, which is still widely unexplored. The electrical conductivity of the materials in the frequency range of few GHz is determined with the waveguide method, based on a combination of experimental measurements of the complex transmission coefficient  $S_{21}$  and CST 3D electromagnetic (EM) simulations.

## INTRODUCTION

The EM characterization of the material properties up to high frequencies is required for the impedance modeling of the CLIC DR components. Layers of coating materials such as amorphous carbon (aC) and Non-Evaporable Getter (NEG) are necessary for e-cloud mitigation and ultra-high vacuum. The waveguide method is used to characterize the properties of those coating materials in a range of frequencies of few GHz. The reliability of this method is tested in the range of 9-12 GHz using a standard X-band waveguide before trying to measure in the range of 325-500 GHz using a Y-band waveguide. The electrical conductivity of the material is obtained from the measured transmission coefficient  $S_{21}$  and 3D EM simulations with CST Microwave Studio® (CST MWS) [1].

## WAVEGUIDE METHOD

An X-band copper (Cu) waveguide of 50 cm length and the same Cu waveguide coated with NEG are the devices under study during the experiment. Using a network analyzer, the transmission coefficient is measured over a frequency range from 9-12 GHz. The experimental method's setup is displayed in Fig. 1. The  $S_{21}$  coefficient is related to the attenuation due to the finite conductivity of the material.

\* also affiliated at EPFL

† also affiliated at EPFL and PSI

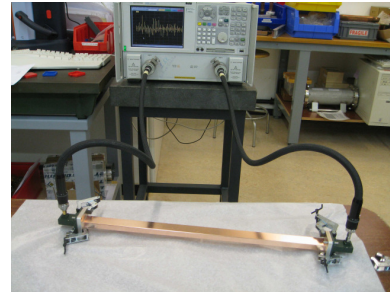


Figure 1: Measurements setup: using a network analyzer, the transmission coefficient  $S_{21}$  of an X-band waveguide is measured.

## NEG Coating Procedure

NEG coating is necessary to suppress fast ion instabilities in the EDR. A Cu X-band waveguide is coated with a Ti-Zr-V thin film by magnetron sputtering using two cathodes, each of them made of elemental wires inter-twisted together [2]. The coating was targeted to be as thick as possible in order to increase the sensitivity of the measurements. From x-rays measurements, the thickness is assumed to be  $9 \mu\text{m}$ . The real profile of the coating thickness will be implemented in the simulations as soon as more detailed profile measurements will be available.

## SIMULATIONS WITH CST

The CST MWS is used to simulate a waveguide made from Cu and a NEG coated one with the same dimensions as the real ones (see Fig. 2). With the Transient Solver of CST, the experimental setup used for the measurements can be simulated in real time domain.

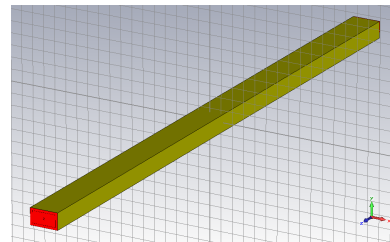


Figure 2: X-band Cu waveguide simulated with CST MWS of 50 cm length.

For each frequency from 9-12 GHz the output of the 3D EM simulations is the  $S_{21}$  parameter as a function of conductivity. The relative permittivity  $\epsilon_r$  and permeability  $\mu_r$  of the material are assumed to be equal to one while the conductivity  $\sigma$  is the unknown parameter which is scanned

# THE DARK CURRENT AND MULTIPACTING CAPABILITIES IN OPAL: MODEL, BENCHMARKS AND APPLICATIONS

C. Wang\*, Z.G. Yin, T.J. Zhang, CIAE, Beijing, China  
 A. Adelmann†, PSI, Villigen, Switzerland

## Abstract

Dark current and multiple electron impacts (multipacting), as for example observed in radio frequency (RF) structures of accelerators, are usually harmful to the equipment and the beam quality. These effects need to be suppressed to guarantee efficient and stable operation. Large scale simulations can be used to understand causes and develop strategies to suppress these phenomenas.

We extend OPAL, a parallel framework for charged particle optics in accelerator structures and beam lines, with the necessary physics models to efficiently and precisely simulate multipacting phenomenas. We added a Fowler-Nordheim field emission model, two secondary electron emission models, developed by Furman-Pivi and Vaughan respectively, as well as efficient 3D boundary geometry handling capabilities. The models and their implementation are carefully benchmark against a non-stationary multipacting theory for the classic parallel plate geometry. A dedicated, parallel plate experiment is sketched.

## INTRODUCTION

Dark current and multipacting phenomena have been observed in various accelerator RF structures, e.g. in electron guns, due to field emission caused by strong accelerating fields [1], and multipacting is also appearing in high-Q RF cavities of cyclotrons [2, 3]. These phenomena are usually harmful to the equipment and beam quality, as they will cause galvanic etching on the surface of the cavity and thus cause RF breakdown.

Multipacting in cyclotron cavities is a very disturbing phenomenon. The seed electrons will impact the cavity surface, and produce an avalanche of new electrons. Under certain conditions (material, geometry of the RF structure, frequency and level of the electromagnetic field), the secondary emission yield (SEY) coefficient will be larger than one and lead to exponential multiplication of electrons. This kind of discharge will limit the power level, until the surfaces are cleaned through a conditioning process. However, this process is very time-consuming [2, 3].

Large scale dark current and multipacting simulations based on reliable data of surface material, full size geometry model of RF structures and parallel computing capabilities, allow more thorough analysis and a deeper understanding of these phenomena, even in early design stages of RF structures.

To make OPAL [4] a feasible tool for performing large scale dark current and multipacting simulations, we imple-

ment a 3D particle-boundary collision test to minimise particle searching during the tracking process. In a subsequent step we add surface physics models including an analytic Fowler-Nordheim field emission model and two secondary emission models, developed by Furman-Pivi and Vaughan respectively. The above mentioned models and their implementation in OPAL have been benchmarked against a non-stationary theory [5]. A nano-second time resolved multipacting experiment is ongoing.

## MODELS

### Geometry Handling

Testing particle-boundary collisions is crucial to both dark current and multipacting simulations. Since complex 3D geometries are hard to be accurately parameterized by simple functions, we use triangulated surfaces, which are extracted from a volume mesh generated by GMSH [6], to represent the complex geometries. Subsequently we can make use of efficient 3D line segment-triangle intersection (LSTI) tests to identify particle-boundary collisions.

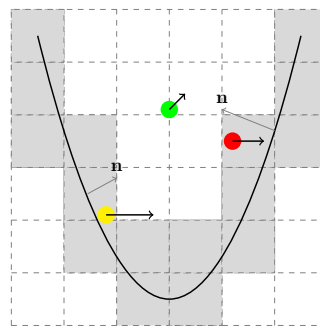


Figure 1: Schematic view of the particle-boundary early rejection strategy. The dark black line represents the boundary surface, particles are coloured dots with an attached momenta arrow. Gray arrows visualize inward normals of the boundary.

Our LSTI test algorithm is based on [7], and the detailed introduction to our implementation can be found in our previous paper [8]. Early rejection strategies skip particles far away from the boundary and with equal direction of momenta and boundary normal vectors (see Figure 1)

### Surface Physics Models

Electron field emission is a major source of both dark current particles and primary incident particles in secondary emission. We employ the Fowler-Nordheim (F-N)

\* cwang@ciae.ac.cn

† andreas.adelmann@psi.ch

# EFFICIENT MODELING OF LASER-PLASMA ACCELERATORS USING THE PONDEROMOTIVE-BASED CODE INF&RNO\*

C. Benedetti<sup>†</sup>, C.B. Schroeder, E. Esarey, W.P. Leemans, LBNL, Berkeley, CA 94720, USA

## Abstract

The ponderomotive force approximation enables efficient modeling of laser-plasma accelerators. It allows simulation in cylindrical geometry which captures relevant 3D physics at 2D computational cost. INF&RNO (INtegrated Fluid & paRticle simulation cOde) is an efficient 2D cylindrical code based on the envelope model for the laser, a PIC or fluid description for the plasma, and the ponderomotive force approximation to describe the effect of the laser pulse on the plasma. These and other features, such as an improved laser envelope solver, a dynamical resampling of the phase space distribution to reduce on-axis noise, and a Lorentz boosted frame modeling capability, allow for a speedup of several orders of magnitude compared to standard (explicit) full PIC simulations while still retaining physical fidelity. The code has been benchmarked against analytical solutions and 3D PIC simulations. In this paper we report on the latest developments of the code, focusing in particular on the improved laser envelope solver, and we discuss its performance.

## INTRODUCTION

Numerical modeling of a laser-plasma accelerator (LPA) [1], where a short and intense laser pulse interacts with an underdense plasma over distances ranging from a few millimeters/centimeters (yielding  $\sim 0.1/1$  GeV electron energy [2, 3]) up to several tens of centimeters (as in the BErkeley Lab Laser Accelerator experiment (BELLA) [4] where  $\sim 10$  GeV electrons are expected), is a computationally challenging task. A 3D “full” (*i.e.*, where the fast oscillations of the plasma electrons in the laser field are taken into account) PIC simulation requires  $10^4 - 10^5$  CPU hours using today’s supercomputers for a millimeter-scale plasma and  $\sim 10^6$  CPU hours for a centimeter-scale plasma. The simulation of a  $\sim 10$  GeV stage as required by BELLA would necessitate several tens of millions of CPU hours and are practically impossible to perform with standard simulation tools and today’s computational resources. However, numerical modeling plays a central role in the understanding and optimization of LPAs. Simulations are required since the physics of the laser-plasma interaction is highly nonlinear and, consequently, analytical solutions are lacking.

Two approaches have been proposed to overcome these limitations and allow for the simulation of multi-GeV LPA

stages: *i.* use reduced models [5, 6, 7]; *ii.* run the simulation in an optimal Lorentz boosted frame (LBF) [8] instead of in the laboratory frame. Codes based on reduced models allow for a significant speedup compared to full PIC simulations either because of dimensionality reduction (*e.g.*, 2D cylindrical instead of full 3D cartesian) or because of approximations in the physical description of the system (*e.g.*, quasi-static instead of fully dynamic plasma response, ponderomotive approximation instead of full Lorentz force, etc.). Even if they may lack important elements of the physics (*e.g.*, a quasi-static code can not describe self-injection), their use has been proven to be successful in several relevant scenarios [5, 9, 10, 11]. The use of an LBF has been strongly pursued by several groups [12, 13, 14, 15]. The advantage of running a simulation in an LBF relies on the fact that, if backward propagating waves (*e.g.*, Raman backscattering) can be neglected, and this is generally true for LPAs, then it has been shown [8] that the unbalance between the maximum and minimum physical scales involved in a simulation, which contribute to set the computational complexity of the problem, is not invariant under Lorentz transformation. It turns out that, in general, the laboratory frame is not the optimal choice to run the simulation, while running it in a boosted frame can considerably reduce the scale unbalance, shortening (also by several orders of magnitude) the simulation length.

The INF&RNO computational framework [6, 16], is a 2D cylindrical ( $r - z$ ) code that adopts an envelope model for the laser pulse and makes use of the (time-averaged) ponderomotive force approximation to describe the interaction of the laser pulse with the plasma. The plasma can be modeled using either a PIC or a fluid description. Both PIC and fluid modalities are integrated in the same computational framework allowing for staged simulations (*e.g.*, PIC for injection and fluid for acceleration). The adoption of the cylindrical geometry allows the description of 3D physics (laser evolution, electromagnetic field structure) at 2D computational cost. The code features an improved laser envelope solver which enables an accurate description of the laser pulse evolution deep into depletion even at a reasonably low resolution. This new algorithm overcomes some of the limitations reported in other implementations of the laser envelope solver [7]. For the PIC part, a dynamical resampling of the phase space distribution is implemented in order to reduce the on-axis noise which affects, in some cases, 2D axisymmetric codes when the computational grid is loaded with a constant number of particles per cell. Finally, an LBF modeling capability has been introduced within the (noiseless) fluid framework. The employment of the LBF by the user is transparent since

\*Work supported by the Office of Science, Office of High Energy Physics, of the U.S. Department of Energy under Contract No. DE-AC02-05CH11231.

<sup>†</sup>cenedetti@lbl.gov

# MAD-X PROGRESS AND FUTURE PLANS

L. Deniau, CERN, Geneva, Switzerland

## Abstract

The design efforts for the High Luminosity upgrade of the Large Hadron Collider (HL-LHC) will require significant extensions of the MAD-X code widely used for designing and simulating particle accelerators. These changes are framed into a global redesign of the MAD-X architecture meant to consolidate its structure, increase its robustness and flexibility, and improve its performance. Some examples of recent extensions to MAD-X like the RF-Multipole element will be presented. Improvement for models and algorithms selection providing better consistency of the results and a wider range of use will be discussed. The computation efficiency will also be addressed to profit better of modern technologies. In this paper, we will describe the last improvements and the future plans of the project.

## INTRODUCTION

The Methodical Accelerator Design (MAD) project has a long history, aiming to be at the forefront of computational physics in the field of particle accelerator design and simulation. The MAD scripting language is de facto the standard to describe particle accelerators, simulate beam dynamics, and optimize beam optics.

MAD-X is the successor of MAD-8 and was first released in June 2002 [1]. It offers most of the MAD-8 functionalities, with some additions, corrections, and extensions [2]. The most important of these extensions is the Polymorphic Tracking Code (PTC) of E. Forest [3].

A decade after its first release, MAD-X is still the main tool used to design and simulate accelerators at CERN. But its original design was mainly focusing on the urgent needs for the LHC, and a large part of the code was inherited from old software written in the 80's. The framework of the LHC upgrade studies is a good opportunity to reorganize and upgrade the overall core of MAD-X to support recent hardware (64 bit, multicores) and new needs. In parallel, the project must continue to incorporate new functionalities in the legacy code, like the two recent optical elements added for modeling thin RF-Multipoles and thin non-linear lenses with elliptical magnetic potential.

The long-term evolution of MAD-X is an essential aspect of the project, because many users around the world consider the application as one of the most flexible and accurate for optics design, as mentioned in comparisons of optics codes [4, 5]. Moreover, MAD-X with PTC is often taken as the reference for benchmarking other codes, and seen by the community of particle accelerator physicists as a key tool that is poised to evolve.

In this paper we expose four different aspects of the project, namely the project improvements and the feature

extensions performed during the past year, and the physics and application improvements that are planned for the next couple of years. Each of these aspects addresses different concerns of the project, which are of equal importance from our point of view for the future of MAD-X.

## PROJECT IMPROVEMENT

### Motivations

The MAD-X project falls into the category of middle-size complex projects. The size of the source code ( $\approx 165\text{K SLOC}^1$ ) and the number of features provided is not very large but most of the features rely on very complex knowledge difficult to implement and support. In this kind of project, *simplicity and discipline* should have been the rule of thumb during the development process, because the complexity comes inevitably from the implementation of the provided features. Presumably due to priority issues, these rules were not strictly followed during the first decade of development of MAD-X and the drift resulting from the added complexity has led to the untidy feeling perceived by the users. The usual software metrics based on the number of SLOC under-evaluates the complexity of the application. As a consequence, a new improvement process has been set out (Fig. 1), starting from the outside layers of the project to emphasize the restoration of some cross-platform invariants (e.g. build and test system), and to simplify the development process (e.g. code organization) before important new developments is launched.

### Global Redesign

The need for a global redesign of MAD-X became obvious with time, as the amount of resources required to implement new features became exponential or equivalently, the time to completion with constant resources became logarithmic. The observable behavior of the application was not always matching the users expectations, and the feedback from the active MAD community has been collected during the past decade and recorded into a project tracker.

After some attempts to improve locally the implementation, it became clear that the process would not converge to a stable solution because some undecidable and coupled bugs were found.

**Undecidable bugs** occur for example, when memory must be managed in the absence of proper reference handling or garbage collection: freeing the faulty object crashes the application while not freeing the object provokes significant memory leaks that will crash the application later. This latter kind of bug can be painful for ap-

<sup>1</sup>Source Line Of Code

# BEAM DYNAMICS SIMULATIONS USING GPUS

J. Fitzek, S. Appel, O. Boine-Frankenheim, GSI, Darmstadt, Germany

## Abstract

PATRIC is a particle tracking code used at GSI to study collective effects in the FAIR synchrotrons. Due to the need for calculation-intensive simulations, parallel programming methods are being explored to optimize calculation performance.

Presently the tracking part of the code is parallelized using MPI, where each node represents one slice of the particles that travel through the accelerator. In this contribution different strategies will be presented to additionally employ GPUs in PATRIC and exploit their support for data parallelism without major code modifications to the original tracking code. Some consequences of using only single-precision in beam dynamics simulations will be discussed.

## PATRIC SIMULATION CODE

The international FAIR facility with its new accelerators will be built at GSI, using the existing linac and SIS18 synchrotron as injectors. PATRIC is a particle tracking code that has been developed at the GSI accelerator physics department over many years and that is used to study collective effects in the circular accelerators within the FAIR facility. For more information on PATRIC see also [1].

### Structure of the Code

Besides others, the PATRIC simulation code mainly consists of the Pic class as representation of the particles, the SectorMap class for ion optical elements like magnets including their transfer matrix, and the BeamLine class to group SectorMaps to form the accelerator (see also Figure 1). The main program takes care of the object creation, distribution of the calculation, and time measurement.

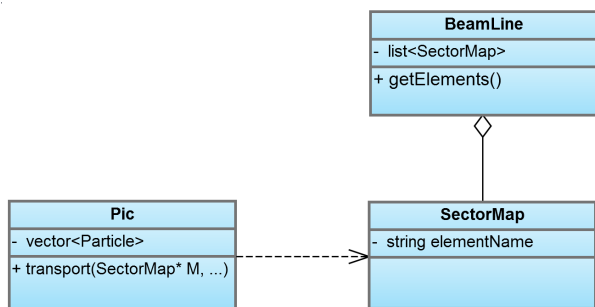


Figure 1: Structure of the PATRIC simulation code.

### Existing Problem Division

Presently the tracking part of the code is parallelized using MPI, where each node represents one slice of the particles that travel through the accelerator. For tracking many thousand particles, a large number of identical calculations has to be performed on different data. Therefore the decision was to divide the problem by the data.

Dividing the data can be done in many different ways. As basis for PATRIC, the particles were divided longitudinally in slices and assigned to MPI nodes as shown in Figure 2. Because particles that interact with each other reside on the same node, this distribution allows to include the calculation of these effects locally on the MPI node. By dividing the problem as described, PATRIC is enabled for distributed computing, which already gives a good performance gain.

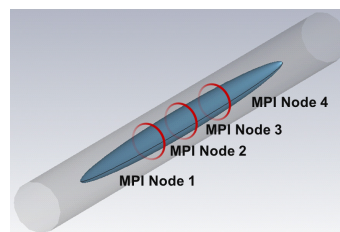


Figure 2: Structure of the existing parallelization using MPI: Each node processes one longitudinal slice of particles (figure created with CST EM Studio).

Due to the need for even more calculation-intensive simulations for FAIR, parallel programming methods are being explored to optimize the calculation performance of the PATRIC simulation code beyond the possibilities of MPI. In the context of a diploma thesis different strategies are being investigated to additionally employ GPUs in PATRIC and exploit their support for data parallelism without major code modifications to the original tracking code.

### Parallelization with GPUs

Today all end user computers contain powerful GPUs with remarkable floating point performance. GPUs are specialized on graphics processing and therefore support massively parallel calculations. Since they are affordable and nowadays equipped with a general purpose programming interface, they are more and more used to solve calculation-intensive problems. Especially their support for data parallelism makes them suit for the calculations that have to be performed during particle simulations.

# AN OpenMP PARALLELIZATION OF REAL-TIME PROCESSING OF CERN LHC BEAM POSITION MONITOR DATA

H.Renshall, L.Deniau, CERN, Geneva, Switzerland

## Abstract

SUSSIX is a FORTRAN program for the post processing of turn-by-turn Beam Position Monitor (BPM) data, which computes the frequency, amplitude, and phase of tunes and resonant lines to a high degree of precision. For analysis of LHC BPM data a specific version run through a C steering code has been implemented in the CERN Control Centre to run on a server under the Linux operating system but became a real time computational bottleneck preventing truly on-line study of the BPM data. Timing studies showed that the independent processing of each BPMs data was a candidate for parallelization and the Open Multiprocessing (OpenMP) package with its simple insertion of compiler directives was tried. It proved to be easy to learn and use, problem free and efficient in this case reaching a factor of ten reductions in real-time over twelve cores on a dedicated server. This paper reviews the problem, shows the critical code fragments with their OpenMP directives and the results obtained.

## THE PROBLEM

SUSSIX is a FORTRAN program for the post processing of turn-by-turn Beam Position Monitor (BPM) data, which computes the frequency, amplitude, and phase of tunes and resonant lines to a high degree of precision through the use of an interpolated Fast Fourier Transform (FFT). Analysis of such data represents a vital component of many linear and non-linear dynamics measurements.

For analysis of LHC BPM data a specific version *sussix4drive*, run through the C steering code *Drive God Lin*, has been implemented in the CERN Control Centre (CCC) by the beta-beating team. Analysis of all LHC BPMs, however, represents a major real time computational bottleneck in the control room, which has prevented truly on-line study of the BPM data. In response to this limitation an effort has been underway to decrease the real computational time, with a factor of 10 as the target, of the C and FORTRAN codes by parallelising them.

## SOLUTIONS CONSIDERED

Since the application is run on dedicated servers in the CCC the obvious technique is to profit from the current multi-core hardware: 24 cores are now typical. The initial thinking was to parallelise the FFT code.

The first attempts were to try a parallelised FFT from the Numerical Algorithms Group (NAG) `fs16i2dc1`

library for SMP and multicore processors together with the Intel 64-bit FORTRAN compiler and the Intel maths kernel library recommended by NAG. This library uses the OpenMP technology.

Various NAG examples of enhanced routines were run (but not the multi-dimensional FFTs) and all slowed down in real time using more cores. This was not surprising since the examples only take milliseconds, comparable to the overhead to launch a new thread. Also it was found that the SUSSIX application calls `cfft` (D704 in the CERN program library), which maps onto NAG `c06ecf`, which had not yet been enhanced. This led to making a detailed central processing unit (CPU) profiling of the application.

Profiling the application (with `gprof`) showed that in fact only 7.5% of the CPU time was spent in `cfft` while 70% was spent in a function `zfunsr` searching for the maximum of the Fourier spectra with large numbers of executions of an efficient inner loop of BPM data over many turns. This loop could not be improved (maxd turns of a BPM data is typically 1000):

```
double complex zp, zpp, zv
zpp=zp(maxd)
do np=maxd-1,1,-1
  zpp=zpp*zv+zp(np)
enddo
```

It was decided to try and parallelise SUSSIX directly using the OpenMP implementation supported by the Intel and GCC compilers. The home web site is [www.openmp.org](http://www.openmp.org) and an excellent tutorial at [computing.llnl.gov/tutorials/openMP](http://computing.llnl.gov/tutorials/openMP) was the main reference. Examination of the code granularity revealed that the highest level of independent code execution was over the processing of individual BPM data.

The pure FORTRAN offline version was parallelised first by adding OpenMP parallelisation directives around the main BPM loop. In this version each BPMs data is in a separate physical file hence they could be opened and read in parallel:

```
!$OMP PARALLEL DO PRIVATE(n,iunit,
                          filename,nturn)
!$OMP& SHARED (isix,ntot,narm,iana,...,
              iicf)
do n=1,ntot ! Parallel loop over BPM
  call datspe(iunit,idam,ir,nt1,nt2,
             nturn,...,iana)
  call ordres(eps,narm,nrc,idam,n,nturn)
enddo
!$OMP END PARALLEL DO
```

# SOME COMPUTATIONAL CHALLENGES IN THE MODELING OF ACCELERATORS AND THEIR SOLUTIONS IN THE SIMULATION CODE WARP

J.-L. Vay\*, C. Benedetti, LBNL, USA  
D.P. Grote, R.H. Cohen, A. Friedman LLNL, USA

## Abstract

This paper presents an overview of the Particle-In-Cell accelerator code Warp's capabilities, summarizing recent original numerical methods that were developed within Warp, including a large-timestep "drift-Lorentz" mover for arbitrarily magnetized species, a relativistic Lorentz invariant leapfrog particle pusher, an electromagnetic solver with tunable numerical dispersion and efficient stride-based digital filtering, Particle-In-Cell with Adaptive Mesh Refinement, and simulations in Lorentz boosted frames.

## INTRODUCTION

The Particle-In-Cell (PIC) Framework Warp [1] was originally developed to simulate space-charge-dominated beam dynamics in induction accelerators for heavy-ion fusion (HIF) [2]. In recent years, the physics models in the code have been generalized, so that Warp can model beam injection, complicated boundary conditions, denser plasmas, a wide variety of accelerator lattice components, and the non-ideal physics of beams interacting with walls and plasmas. The code now has an international user base and is being applied to projects both within and far removed from the HIF community. Ongoing or recent examples of applications outside HIF include the modeling of plasma traps for the production of anti-Hydrogen [3], Paul traps [4, 5], non-conventional Penning-Malmberg micro-trap [6], transport of electron beams in the UMER ring [7], ECR ion sources [8], capture and control of laser-accelerated proton beams [9], and fundamental studies of multipacting [10]. It is also applied to the study and design of existing and next generation high-energy accelerators including the study of electron cloud effects [11], coherent synchrotron radiation [12] and laser wakefield acceleration [13].

These studies have necessitated the introduction or development of advanced numerical methods, including methods to model multiple-species effects in accelerators and chambers, efficient ensemble methods, particle advance algorithms that allow a longer time step, and adaptive mesh refinement (AMR).

## NOVEL ALGORITHMS

### Hybrid Drift-Lorentz

It was observed in [14] that the Boris pusher causes particles to gyrate with spuriously large radius for time steps that are large compared to the gyroperiod, albeit with the

correct drift velocities (provided the gradients are still sampled adequately). A new solver that interpolates between the Boris velocity push and a drift kinetic advance was developed and implemented in Warp [15, 17]; it reproduces both the correct drift velocity and gyroradius for an arbitrarily large ratio of time step  $\delta t$  relative to cyclotron period  $\tau_c$ , as well as correct detailed orbit dynamics in the small-timestep limit. The pusher has provided an order of magnitude or more saving in computing resources in the simulations of electron cloud effects in the HCX experiment [15, 16]. An implicit time-advance scheme incorporating drift-Lorentz interpolation has also been developed [17].

### Lorentz Invariant Advance

The relativistic version of the Boris (or Hybrid Lorentz-Drift) particle pusher does not maintain strict Lorentz invariance, resulting eventually in unacceptably large inaccuracies when modeling the transport of ultra-relativistic beams in accelerators. To this effect, an alternative to the Boris pusher that conserves strict Lorentz invariance (to machine precision) was developed and implemented in Warp, and its effectiveness demonstrated on the modeling from first principles of the interaction of a 500 GeV proton beam with a background of electrons [18]. The pusher has subsequently been implemented by others and has also proven useful for correctly capturing the drift speed of electrons of a highly magnetized relativistic electron-ion flow in astrophysical simulations using the code TRISTAN [19].

### Electromagnetic Solver

Warp's electromagnetic solver is based on the Non-Standard Finite-Difference (NSFD) technique [20, 21], which is an extension of the Finite-Difference Time-Domain technique to larger stencils in the plane perpendicular to the direction of the finite difference. This gives the user some control on the numerical dispersion and Courant time step limits which do depend on those parameters. As shown in [22], for a given set of parameters, and for cubic cells, the Courant time step multiplied by the speed of light equals the cell size, and the numerical dispersion vanishes along the main axes. More details on the solver implementation and characteristics for several sets of coefficients are available in [23]. Also described in [23] are the implementation of Perfectly Matched Layers for the absorption of waves at grid boundaries and of Friedman's damping algorithm for noise control [24]. In the same paper, it is shown that introducing a stride in the usage of standard linear filtering allows for construction of efficient iterative sideband

\*jlvay@lbl.gov

# BEAM DYNAMICS STUDIES FOR PARTICLE DRIVEN PLASMA WAKEFIELD ACCELERATION EXPERIMENTS AT PITZ

M. Khojuyan\*<sup>†</sup>, M. Gross, G. Klemz, G. Koss, M. Krasilnikov, A. Oppelt, F. Stephan, DESY, Zeuthen, Germany

## Abstract

The Photo Injector Test Facility at DESY, Zeuthen site (PITZ) is developing and optimizing high brightness electron sources for linac based free electron lasers such as FLASH and the European XFEL. The high quality of the 25 MeV electron beam together with the availability of a highly flexible photocathode laser system makes the PITZ injector a perfect facility for variety of experimental studies. Two approaches are of great interest for future applications in the context of particle driven plasma wakefield acceleration experiments: self-modulation and transformer ratio studies. In both cases a high density electron beam is interacting with plasma which has a density of about  $10^{15} \text{ cm}^{-3}$ . ASTRA [1] simulations were done to study the e-beam density along the existing PITZ beamline, especially at two different possible longitudinal positions of the planned plasma cell, in order to reach the particle density required for occurrence of self-modulation. The results of the beam dynamics studies are presented and discussed in this paper.

## MOTIVATION

Plasma is a promising medium for high gradient acceleration of charged particles. It can sustain orders of magnitude higher fields compared to conventional accelerators. Large amplitude plasma waves can be excited either by powerful lasers [2] or by charged particle beams [3]. In both cases either the pulse length of the intense laser or the temporal length of the particle beam should be in the order of the plasma wavelength. In a particle driven wakefield acceleration scheme, the fields generated by the drive bunch / bunches are used to accelerate a witness bunch. The transformer ratio  $R \equiv W_w^+ / W_d^-$  (maximum energy gain of the witness bunch divided by maximum energy loss of the drive bunch) is an important parameter which in general is limited to two [4], except in special cases when the bunch has an asymmetric current profile [5]. The most successful experiment in concept of particle driven plasma wakefield acceleration was performed at Stanford Linear Accelerator Center (SLAC), by doubling the energy of an ultra-short (50fs) 42 GeV electron beam [6]. Although two order of magnitudes higher accelerating gradients compared to RF accelerators were demonstrated, the experimental results revealed the limitation of the transformer ratio. An other idea was to accelerate an electron beam up to hundreds of GeV by using high energy ultra-short proton beams as

a driver [7]. The plasma in this case will play the role of a medium, which transfers the energy of the protons to the energy of the electrons. As currently available high energy proton beams are tens of centimeters long, the self-modulated regime for long proton beams was afterwards suggested to excite large amplitude wakefields in plasma [8]. When a long particle beam (bunch length is long compared to the plasma wavelength) enters the plasma, it is radially modulated by the periodic focusing/defocusing forces and the beam density modulation provides a positive feedback for the instability to grow [9]. For the case of the CERN 450 GeV proton driver beam, simulations show that an injected 10 MeV witness electron beam can be accelerated to an energy of several hundred MeV after a few meters propagation in a  $7 \cdot 10^{14} \text{ cm}^{-3}$  density plasma [10]. For beams which are longer than the plasma wave period, where self-modulation occurs, the wakefield properties are strongly affected by the drive beam dynamics [11]. PITZ is a known facility for generating and characterizing high brightness electron sources. Recently PITZ has become a very attractive facility for different challenging experiments due to the excellent transverse beam properties such as the transverse emittance which turned out to be unique over a wide range of bunch charges [12]. PITZ can make an important contribution to the questions related to self-modulation by measuring the longitudinal phase space properties of a relatively long 25 MeV electron beam after interaction with a  $10^{15} \text{ cm}^{-3}$  dense plasma. The basic observation would be to detect electron beam energy modulation  $> 1\%$ , which should be possible with the recently available PITZ diagnostics [13]. In this work two possible longitudinal positions of the planned plasma cell arranged into the PITZ linac are considered. Beam dynamics studies were done predicting the possibility of high beam densities required for the self-modulation process.

## INTRODUCTION: BEAM PARAMETERS FOR SIMULATIONS

An overview of the current PITZ setup is shown in Fig. 1. The highly flexible laser system at PITZ, which was developed by the Max-Born institute, produces flat-top laser pulses with sharp rise and fall times [14]. High brightness electron beams are generated using a  $\text{Cs}_2\text{Te}$  photocathode and are accelerated in an L-band RF gun cavity up to 7 MeV (low energy section). The electron beam gets its final energy of about 25 MeV by the cut disc structure (CDS) booster cavity. A dipole can be used to deflect the beam by  $180^\circ$  for different studies, particularly for the fi-

\* martin.khojuyan@desy.de

<sup>†</sup> On leave from ANSL, Yerevan, Armenia

# GLOBAL SCAN OF ALL STABLE SETTINGS (GLASS) FOR THE ANKA STORAGE RING\*

M. Streichert<sup>†</sup>, N. Hiller, E. Huttel, V. Judin, B. Kehrer, M. Klein<sup>‡</sup>,  
 S. Marsching, C. Meuter, M.J. Nasse, A.-S. Müller, M. Schuh, N.J. Smale  
 Karlsruhe Institute of Technology (KIT), Karlsruhe, Germany

## Abstract

The design of an optimal magnetic optics for a storage ring is not a simple optimization problem, since numerous objectives have to be considered. For instance, figures of merit could be tune values, optical functions, momentum compaction factor, emittance, etc. There is a technique called “GLobal scan of All Stable Settings” (GLASS)[1], which provides a systematic analysis of the magnetic optics and gives a global overview of the capabilities of the storage ring. We developed a parallel version of GLASS, which can run on multi-core processors, decreasing significantly the computational time. In this paper we present our GLASS implementation and show results for the ANKA lattice.

## INTRODUCTION

ANKA is the synchrotron light source of the Karlsruhe Institute of Technology (KIT)[2]. It consists of 4 super periods with two double bend achromats each. Each DBA structure contains 2 bending magnets, 5 quadrupole families and two chromatic sextupole families to control the vertical and horizontal chromaticity. We want to study all linear stable settings of ANKA at 2.5 GeV by scanning all possible quadrupole settings. At the moment, ANKA is operated in three different modes, in low-emittance with the natural emittance of 50 nm rad[3], low- $\beta_y$  mode with vertical beta value of 1.9 m in the straight sections[4] and low- $\alpha_c$ -mode with reduced momentum compaction factor.[5].

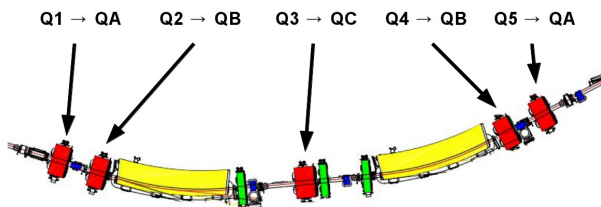


Figure 1: One half of the super period showing the reduced number of quadrupole families.

For our studies, we considered a symmetric super period by reducing the number of quadrupole families from

\* This work has been supported by the Initiative and Networking Fund of the Helmholtz Association under contract number VH-NG-320.

<sup>†</sup> max.streichert@student.kit.edu

<sup>‡</sup> now at SOLEIL, Gif-sur-Yvette, France

5 down to 3 (see Fig. 1), which allowed us to decrease the computation time. Since the ANKA storage ring consists of 4 identical super periods, we need to consider only one super period to check for linear stability of each set of quadrupole settings. The linear stability criterion is given by

$$|\text{tr}(M_{x,y})| < 2, \quad (1)$$

where  $M_{x,y}$  is the transversal transfer matrix of one super period.

We also considered fringe field integrals and quadrupole components in bending magnets to get a realistic model at 2.5 GeV[6]. To decrease the computation time, we implemented a parallel C++ code using OpenMP.

## GLASS SCAN

The quadrupole strength scan was performed in the range of  $-2.4$  to  $2.4 \text{ m}^{-2}$  with a resolution of  $0.02 \text{ m}^{-2}$  for the ANKA magnets corresponding to the maximum possible current. The compiled C++ code checked the linear stability criterion of  $240^3$  quadrupole settings in only 11 seconds on 12 cores and filtered out all unstable settings. Only 3% of all possible quadrupole settings are stable for the ANKA lattice at 2.5 GeV, but not all of them are feasible for the real machine. Therefore, we considered only the settings that satisfy the following constraints:

- $\beta_{x,y} < 40 \text{ m}$ ,  $|\eta_x| < 2 \text{ m}$ ,  $J_x, J_s > 0$ ,
- no tune resonance up to the 2<sup>nd</sup> order,

where  $\beta_{x,y}$  is the transversal beta function,  $|\eta_x|$  the horizontal dispersion function and  $J_x, J_s$  are the damping partition numbers. The constraints were checked with the Accelerator Toolbox (AT)[7] for MATLAB, which took 28 hours on a single core. Then, we queried the resulting database with stable solutions and computed the corresponding emittance for each of them. In Figure 2 all stable settings are shown in the quadrupole-strength-space, classified by different colors into three emittance ranges. As shown in Figure 2, we found two islands of stable settings but only the one with the positive quadrupole strengths for QA family and negative for QB family contains emittance values lower than 100 nm rad. The other island has emittance values that are greater than 770 nm rad. Hence this region is not interesting for further studies on low-emittance optics.

We were also interested in low beta values in the straight sections. Since there are three insertion devices installed in

## EMISSION STUDIES OF PHOTOCATHODE RF GUN AT PITZ

J. Li\*+, G. Asova‡, I.V. Isaev, M. Groß, L. Hakobyan, Y. Ivanisenko, M. Khojoyan‡+, G. Klemz, G. Kourkafas, M. Krasilnikov, K. Kusoljariyakul‡‡, M. Mahgoub, D. Malyutin, B. Marchetti, A. Oppelt, B. Petrosyan, S. Rimjaem‡‡, A. Shapovalov, F. Stephan, G. Vashchenko, DESY, 15738 Zeuthen, Germany  
 G. Feng, DESY, 22607 Hamburg, Germany  
 L. Shang, University of Science and Technology of China, 230029 Hefei, China  
 D. Richter, HZB, 12489 Berlin, Germany

### Abstract

The Photo Injector Test facility at DESY, Zeuthen site (PITZ), was built to develop and optimize electron sources for linac based Free Electron Lasers (FELs) like FLASH and the European XFEL. For the value of the bunch charge extracted from a photocathode, discrepancy has been observed between the data measured at PITZ and simulation results from the ASTRA code. As a factor which could explain the discrepancy, a Schottky-like effect is considered. Meanwhile, the PARMELA code was applied to the emission studies on the PITZ gun as benchmark. Since PARMELA cannot be used to simulate Schottky-like effects with its own modules, MATLAB scripts have been developed to implement this feature of the photoemission in an RF gun.

### INTRODUCTION

With the aim to produce beams with high density, low transverse emittance and short bunch length, the PITZ characterizes the RF photocathode electron sources for FLASH and the European XFEL. Considering it is one of the most sensitive components for high quality beams in an XFEL facility, detailed research should be done on the electron gun.

Measurement of the accelerated charge downstream of the gun as a function of the beam launch phase, which is called phase scan or Schottky scan, is a basic experiment to study the emission properties of the PITZ gun. A Space Charge Tracking Algorithm (ASTRA) [1], originally developed at DESY and extensively used in photo injector design and benchmarking of experimental data [2], has been used to simulate the phase scans. The measured extracted charge is not consistent with the simulation results. One of the possible reasons is a Schottky-like effect. In order to justify this hypothesis, Phase and Radial Motion in Electron Linear Accelerators

(PARMELA) [3], which is widely applied to linac design and dynamic analysis, has been used to simulate the emission process of the PITZ gun. Simulations have been done considering Schottky-like effects with ASTRA and PARMELA, respectively.

### BACKGROUND AND MOTIVATION

#### PITZ Gun

The electron gun is a 1.6-cell copper cavity with resonance frequency of 1.3 GHz. The Cs<sub>2</sub>Te photocathode is inserted into the backplane of the cavity by a load-lock system. The cavity is surrounded by a pair of solenoids: the main solenoid, used to focus the beam, counteracting its expansion due to the space charge force, and the bucking one, used to compensate the field of the main solenoid on the photocathode surface to ensure that the electron bunch leaves the magnetic focusing region without any remaining average angular momentum [4].

#### Discrepancy for Higher Charge

When specific machine settings were directly used in ASTRA, it was not possible to produce 1 nC at the gun operation phase, whereas 1 nC and even higher charge is experimentally detected. ASTRA phase scans have different shapes as compared to the experimentally measured data in Fig. 1, in which zero phases are the Maximum Mean Momentum Gain (MMMGM) phases. Initial parameters are shown in Tab. 1.

As a factor which could explain this discrepancy, field enhancement was considered, such as Schottky-like effect.

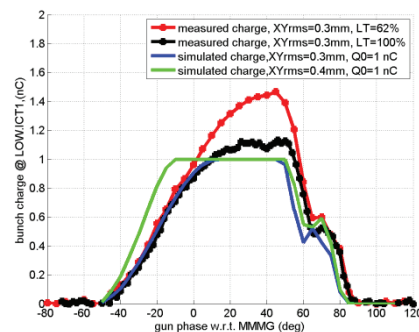


Figure 1: Measured and simulated (ASTRA) phase scans.

\* ji.li@desy.de

+ On leave from USTC/NSRL, Hefei, China

‡ On leave from INRNE, Sofia, Bulgaria

‡+ On leave from ANSL, Yerevan, Armenia

‡‡ Currently at Chiang Mai University, Chiang Mai, Thailand.

# LUMPED EQUIVALENT MODELS OF COMPLEX RF STRUCTURES\*

T. Flisgen<sup>†</sup>, J. Heller, U. van Rienen, Universität Rostock, IAE, IEF, 18059 Rostock, Germany

## Abstract

The prediction of RF properties of complex accelerating structures is an important issue in computational accelerator physics. This paper describes the derivation of state space equations for complex structures based on real eigenmodes of sections of the decomposed complex structure. The state space equations enable the calculation of system responses due to port excitations by means of standard ordinary differential equation solvers. Therefore, the state space equations are referred to as lumped equivalent models of such complex RF structures. Besides fast computation of system responses, the equivalent models enable the calculation of secondary quantities such as external quality factors. The present contribution discusses theoretical aspects by means of a validation example.

## INTRODUCTION

The investigation of complex radio frequency (RF) structures is a crucial task in the design of particle accelerators. Often the treatment of these complex and large RF devices exceeds the capabilities of modern workstation computers. Therefore, many problems are tackled by means of cluster computers in combination with suitable parallel simulation codes (e.g. ACE3P [1]). In this contribution a proof of principle for an alternative approach is presented. Here, the complex structure is decomposed into segments likewise it is proposed by the method of Coupled S-Parameter Calculations (CSC) [2, 3]. This decomposition has the following advantages:

- The separate treatment of the segments is less time- and memory-consuming.
- The properties of equal segments need to be computed only once.
- If sections show symmetries their treatment can be further simplified.
- If Maxwell's equations can be solved analytically for sections their numerical treatment is not needed.
- If parameter studies are of interest only the properties of sections with free parameter(s) need to be recalculated.

After decomposition of the complex structure, state space equations in an impedance formulation for the segments are created by a 3D eigenmode expansion [4, 5, 6]. These impedance state space equations are also referred to

as lumped equivalent models of the segments as they describe the dependency of the transient modal voltages on transient modal currents at the segment's waveguide ports. By employing a modification of the CSC scheme, the state equations of the segments are combined to obtain the state space equations of the complete structure. These equations allow for the computation of transient system responses as well as frequency domain transfer functions. Furthermore, secondary quantities such as external quality factors can be derived from the lumped model. In addition, the field distribution inside the full structure is also available as the state equations for the individual segments are obtained by a 3D eigenmode expansion.

In comparison to [6] where the coupling scheme is introduced and the focus lies on theoretical derivations, this paper presents a more sophisticated application example for the creation of lumped equivalent models of complex RF structures.

## APPLICATION EXAMPLE AND CREATION OF ITS LUMPED MODEL

A third harmonic cavity with three cells (see [7] for geometric details) and simplified higher order mode (HOM) couplers<sup>1</sup> is chosen as an application example. The entire structure is considered to be lossless and the beam pipes are shortcut with perfect electric conducting (PEC) walls. Fig. 1 shows the structure under test and its decomposition into segments. The entire structure is comparably small and not complex such that the direct numerical calculation of its properties like the transfer function is easily feasible for the sake of comparison and validation. To model these sections, five different state space equations of the form

$$\frac{\partial}{\partial t} \mathbf{x}_r(t) = \mathbf{A}_r \mathbf{x}_r(t) + \mathbf{B}_r \mathbf{i}_r(t), \quad (1)$$

$$\mathbf{v}_r(t) = \mathbf{B}_r^T \mathbf{x}_r(t). \quad (2)$$

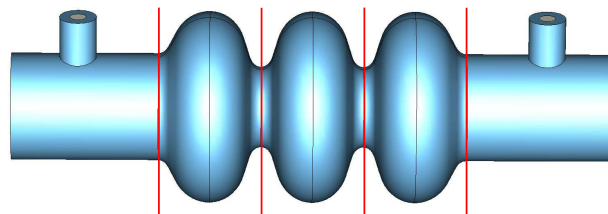


Figure 1: Lossless third harmonic cavity with two end cells, one middle cell and two simplified HOM couplers and its decomposition into five segments (left coupler, left end cell, middle cell, right end cell and right coupler).

\* partially funded by EU FP7 Research Grant No. 227579

<sup>†</sup> Thomas.Flisgen@Uni-Rostock.de

<sup>1</sup>An antenna tip protruding into the beam pipe.

# EIGENMODE COMPUTATION FOR FERRITE-LOADED CAVITY RESONATORS \*

K. Klopfer\*\*, W. Ackermann, T. Weiland

Technische Universität Darmstadt, Institut für Theorie Elektromagnetischer Felder (TEMF)  
Schlossgartenstraße 8, 64289 Darmstadt, Germany

## Abstract

For acceleration of charged particles at the heavy-ion synchrotron at the GSI Helmholtzzentrum für Schwerionenforschung in Darmstadt two ferrite-loaded cavity resonators are installed within the ring. Their eigenfrequency can be tuned by a properly chosen bias current and thereby modifying the differential permeability of the ferrite material. The goal of the presented work is to numerically determine the lowest eigensolutions of accelerating ferrite-loaded cavities based on the finite integration technique (FIT). The newly developed solver includes two subcomponents: Firstly, a magnetostatic solver supporting nonlinear material for the computation of the magnetic field which is excited by the specified bias current. This enables to linearize the constitutive equation for the ferrite material at the current working point, at which the differential permeability tensor is evaluated. Secondly, a Jacobi-Davidson type eigensolver for the subsequent solution of the nonlinear eigenvalue problem. Particular emphasis is put on the implementation to enable efficient distributed parallel computing. First numerical results for biased ferrite-filled cavity resonators are presented.

## INTRODUCTION

Within the heavy-ion synchrotron at GSI two ferrite-loaded cavity resonators are operated to continuously accelerate the injected charged particles. Inside the cavity housing ferrite ring cores are installed around the beam pipe. A magnetic field is established in these rings by means of two different current windings: Firstly, a field constant in time due to the bias current, and, secondly, an additional time-harmonic component induced via radio frequency coupling. During the acceleration phase the resonance frequency has to be adjusted to reflect the increasing speed of the heavy ions. This can be achieved by properly choosing a bias current and thereby modifying the differential permeability of the ferrite material. For the SIS 18 ferrite cavity, biasing enables to alter the resonance frequency in a range from about 0.6 MHz to 5.0 MHz. A detailed description of the SIS 18 ferrite cavity can be found in [1].

In this paper, the main aspects of the applied numerical approach are briefly summarized followed by helpful remarks on efficient parallel computing. After that, the functionality of the solver is demonstrated based on two different simple examples.

\* Work supported by GSI

\*\* klopfer@temf.tu-darmstadt.de

## COMPUTATIONAL APPROACH

The relevant fundamental relations used for the calculation of eigenmodes of biased ferrite-loaded cavity resonators as well as the applied approach for the numerical computation were already discussed in [2]. Hence, here the most important aspects are picked up and summarized.

The dependence of the eigenmodes on the differential permeability leads to several consequences: The static magnetic field generated by the bias current has to be calculated beforehand by means of a nonlinear magneto-static solver. The constitutive equation is then linearized at the specified working point. Moreover, the frequency dependence of the permeability tensor results in a nonlinear eigenvalue problem. A dedicated solver for parallel computing has been developed to meet the tight requirements. Presently, only Hermitian eigenvalue problems are supported. Consequently, the current version of the solver is applicable for loss-less materials as well as models discretized on equidistant grids.

## PARALLEL COMPUTING

The realization of the solver should allow an efficient computation on distributed memory machines. To this end, it aims at a high computation to communication ratio as well as a good load balancing. Regarding the first aspect, the degrees of freedom (DOFs) of the FIT are arranged such that all matrices have only few non-zero components in their far off-diagonal regions. This directly leads to reduced communication between the individual processes and thus to a better parallel efficiency. For illustration, the effect of the re-ordering is shown with the structure of the system matrix of the eigenvalue problem on the left of Fig. 1. Having in mind that the number of computations one processing unit has to perform is approximately proportional to the number of non-zeros of the system matrix which are owned by this process, it can also be seen from this figure that the load balancing is rather poor. The reason for this is that many variables are included that in fact are zero in the FIT because they are allocated on elements outside the computation domain (including perfect electric conductor cells) or due to boundary conditions. Consequently, in the current implementation all the pseudo DOFs are completely removed beforehand and therefore very good load balancing is obtained.

The reduction of the system size automatically results in further benefits, not only for parallel computing. In fact, the beneficial impact on the memory allocation at the time

# PRELIMINARY STUDY OF SINGLE SPIKE SASE FEL OPERATION AT 0.26 NANOMETERS WAVELENGTH FOR THE EUROPEAN XFEL

B. Marchetti<sup>#</sup>, M. Krasilnikov, F. Stephan, DESY, Zeuthen, Germany  
 M. Dohlus, Y. Kot, I. Zagorodnov, DESY, Hamburg, Germany  
 J. Roensch-Schulenburg, University of Hamburg, Hamburg, Germany

## Abstract

The production of ultra-short (fs or sub-fs long), high power radiation pulses in the X-ray spectral region, showing a single spike spectrum, represents a challenge for many existent SASE-FELs [1] [2].

In order to realize single spike operation the length of the electron bunch after compression must be extremely small [3] (less than a micrometer) and the consequent degradation of its emittance has not to suppress the radiation production.

Several technical restrictions, such as limits of diagnostics for small charges, RF jitter and micro-bunching instabilities play an important role in the choice of the operation working point.

In this paper we are going to study the feasibility of single spike or few spikes lasing for bunches with a charge of tens of pC in the European XFEL facility [4] giving some preliminary results concerning the choice of the working point.

## INTRODUCTION

### Single Spike Condition

The radiation produced by Free Electron Lasers (FELs) working in the Self Amplified Spontaneous Emission (SASE) configuration is characterized by an energy spectrum constituted by many spikes. The number of the spikes depends on the longitudinal properties of the electron bunch. In fact, once the bunch is injected into the undulator, the radiation emitted by the electrons located in a certain longitudinal position can be amplified only by other electrons placed within a fixed longitudinal distance (in the forward direction) from them. This distance is proportional to the cooperation length, defined as a radiation slippage in one power gain length [3]. The cooperation length depends on the emitted radiation's wavelength  $\lambda$ , according to:

$$L_c = L_{cld}(1 + \eta), \quad (1)$$

where the parameter  $\eta$ , defined as in [5], takes into account transverse effects and beam energy spread, and  $L_{cld}$  is the one-dimensional cooperation length, defined as:

$$L_{cld} = \frac{\lambda}{\sqrt{3} \cdot 4\pi\rho}, \quad (2)$$

with  $\rho$  being the one dimensional FEL parameter.

<sup>#</sup>barbara.marchetti@desy.de

Every longitudinal slice in the bunch whose length is  $2\pi L_c$  contributes to a different spike in the energy spectrum of the produced radiation, thus in order to have a single spike, the e-bunch must be shorter than  $2\pi L_c$ .

It is very difficult to satisfy this condition in X-rays FELs where, according to equations (1) and (2),  $2\pi L_c$  becomes very small, typically a fraction of  $\mu\text{m}$ .

### Single Spike at the European XFEL

Several methods have been proposed in order to achieve short e-bunch lengths and thus sub-fs radiation pulses (see for example [2] and its references).

In this paper we start from the very simple case of strong compression of electron bunches having a charge of tens of pC. We characterize different compression setups considering the most recent layout of the European XFEL. Our aim is to give a starting point for further optimization. The principal effects influencing the electron beam acceleration and transport, such as RF wakefields and coherent synchrotron radiation (CSR) effects inside magnetic compressors have been included. Space charge force has been fully included in the injector, while only longitudinal space charge force has been considered in the rest of the linear accelerator.

## BUNCH COMPRESSION AT XFEL

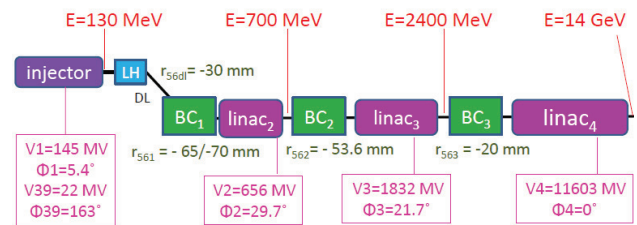


Figure 1: Scheme of the European XFEL layout including the parameters used in the following simulations. The three magnetic bunch compressors (BCs) have a variable curvature radius and thus a variable dispersion ( $R_{56}$ ); in the work described in this paper the curvature radius in BC<sub>1</sub> has been changed in order to scan the bunch properties around the maximum compression point.

### Layout Description

In Fig. 1 a scheme of the layout of the European XFEL is shown. Through the use of a third harmonic RF-cavity placed in the injector region, the correction of the non-linearity in the longitudinal phase space distribution of the e-bunch is possible. The laser heater (LH) can mitigate the effect of micro-bunching instability. The electron bunch compression starts in the dogleg and is

## RECONSTRUCTION OF VELOCITY FIELD\*

Dmitri A. Ovsyannikov, Elena D. Kotina, St. Petersburg State University, St. Petersburg, Russia

### Abstract

In this paper we suppose that the distribution density of particles in phase space is known. Using Liouville's equations the problem of finding velocity field is considered as a minimization problem. Thus the problem of determination of velocity field is reduced to solving of elliptic system of Euler-Lagrange equations.

### INTRODUCTION

Different inverse problems of electrodynamics have been the subject of attention of many researchers. In particular, solving of inverse problems of electrodynamics, where by pre-assigned motions (given velocity field) electromagnetic fields were determined, had been investigated in works of G.A.Grinberg, A.R.Lucas, B.Meltzer, V.T.Ovcharov, V.I.Zubov, E.D.Kotina [1-9]. It should be noted, that the problem of determination of velocity field is a separate task. In particular, the task of determination of velocity field could be considered as the problem of the optimal control theory [10]. In this case it is needed to find the velocity field securing necessary beam dynamics. In this paper we suppose that the distribution density of particles in phase space is known. The problem of finding the velocity field is considered as a minimization problem. Similar problem is widely discussed in the literature for image processing based on the so-called optical flow. This approach was also used for the motion correction for radionuclide tomographic studies [11]. In this work the problem of determining the velocity field in solving the problem of charged particle beam formation in a stationary magnetic field is also considered.

### PROBLEM STATEMENT

Let the dynamical system be given by a differential equation

$$\frac{dx}{dt} = f(t, x), \quad (1)$$

where  $t$  is independent variable further referred to as time,  $x$  is  $n$ -vector of the phase coordinates  $x_1, x_2, \dots, x_n$ ,  $f$  is  $n$ -dimensional vector function.

We assume that  $f(t, x)$  is defined and, together with the partial derivatives  $\partial f / \partial x$  it is continuous with respect to the variables  $t, x$  on  $T_0 \times R^n$ , where  $T_0 = [t_0, T] \subset R^1$ , the number  $t_0, T$  are fixed. We assume that solution  $x = x(t, t_0, x_0)$  is defined on the entire interval  $T_0$  for any  $x_0 \in R^n$ .

Let us consider together equation (1) the following equation:

$$\frac{\partial \rho}{\partial t} + \frac{\partial \rho}{\partial x} f + \rho \cdot \operatorname{div}_x f = 0, \quad (2)$$

under initial condition

$$\rho(t_0, x) = \rho_0(x), \quad (3)$$

where  $\rho_0(x)$  – given function and  $\rho = \rho(t, x)$ .

We will consider arbitrary region  $G_{t_0} \subset R^n$ . Suppose that, by the system (1),  $G_t$  is the image set of  $G_{t_0}$ . Using the equation (2) we obtain

$$\int_{G_t} \rho(t, x_t) dx_t = \int_{G_{t_0}} \rho_0(x_0) dx_0, \quad t \in T_0. \quad (4)$$

If for some nonnegative scalar function  $\rho(t, x)$  the equality (4) holds for any  $G_{t_0} \subset R^n$ , then let us say that the system (1) has integral invariant of order  $n$ . The function  $\rho(t, x)$  is called the kernel or the density of the integral invariant [7]. From physical point of view the equality (4) may be treated as conservation of the particle (charge) mass along the trajectories of the system (1). The equation (2) is called the transport equation [10]. Note that the equation (2) is also called the generalized Liouville equation or Liouville's equation when the system (1) is given in canonical conjugate variables, here  $\operatorname{div}_x f(t, x) = 0$ .

Suppose that the phase trajectory family equation (1) corresponds to the set of random initial values of the coordinates with the density of probability distribution (3) and moreover  $\int_{M_0} \rho_0(x_0) dx_0 = 1$ . The function  $\rho(t, x)$  may

be treated as the variation of the density of probability distribution in time, and in the phase space of coordinates of the dynamical system (1). In this case the equation (2) is called the Fokker-Planck-Kolmogorov equation.

Further we suppose that given function  $\rho(t, x)$  satisfies the transport equation (2). The problem is to restore the velocity field of the system (1), i.e. to find function  $f(t, x)$ . In common case, this is ill-posed problem [12]. So we will use the method of regularization. Let us fix some moment  $t$  and formulate the problem of determination function  $f(t, x)$  as a minimization problem. We will now introduce the functional

\*Work supported by SPbGU, grant 9.39.1065.2012

# ON ACCELERATOR DRIVEN SUBCRITICAL REACTOR POWER GAIN

Anna G. Golovkina, Dmitri A. Ovsyannikov, SPbSU, St. Petersburg, Russia  
 Igor V. Kudinovich, Krylov Shipbuilding Research Institute, St. Petersburg, Russia

## Abstract

The accelerator driven system (ADS) with subcritical reactor is considered. Such systems demonstrate high safety, due to the fact, that the reactor operates at subcritical level. The problem of the reactor power rate maximisation on fixed values of effective multiplication factor and the external neutron source (neutron generating target) intensity is studied. In this paper the main attention is paid to the reactor core optimisation. Some ways of ADS power rate gain and optimised reactor core parameters are proposed.

## INTRODUCTION

Since the early 1990's, accelerator driven systems (ADS - subcritical reactors with external neutron source generated by proton accelerators through a spallation target) have been proposed [1] for addressing certain missions in advanced nuclear fuel cycles. Institutes throughout the world have conducted numerous programs evaluating the role of ADS in nuclear waste transmutation and energy production. The interest is induced by a number of ADS different applications, for example:

- Transmuting selected isotopes present in nuclear waste (e.g., actinides, fission products) to reduce the burden these isotopes place on geologic repositories.
- Generating electricity and/or process heat.
- Producing fissile materials for subsequent use in critical or sub-critical systems by irradiating fertile elements.

There are needed high energy proton beams for transmutation problems. Such beams could be obtained only in large and expensive accelerators. So using them in ADS designed for power generation isn't economical effective. There should be used cheaper accelerators with lower output beam energy, so some other ways to increase reactor power rate are needed to be found.

## EXTERNAL NEUTRON SOURCE AMPLIFICATION

In the general case the neutron flux  $\Phi(r, E)$  in subcritical reactor is described by equation:

$$\mathbf{M}\Phi(r, E) = -\mathbf{M}_1\Phi(r, E) - q(r, E),$$

$$r \in V, E_T \leq E \leq E_f; \quad (1)$$

$$\Phi(r_S, E) = 0, r_S \in S,$$

where  $\mathbf{M}$  - operator describes transport, slowing-down and absorption of neutrons,

$\mathbf{M}_1$  - operator describes fission neutron source,

$q(r, E)$  - intensity of the external neutron source,

$E_f$  - thermal neutron energy;

$E_T$  - fission neutron energy

The multiplication factor of the reactor core  $k_{\text{eff}}$  does not depend on the external neutron source intensity and it is defined for critical fictitious system by equation:

$$\mathbf{M}\Phi_0(r, E) = -\frac{1}{k_{\text{eff}}}\mathbf{M}_1\Phi_0(r, E), \quad (2)$$

$$\Phi_0(r_S, E) = 0, r_S \in S$$

Eq. (2) can be written as:

$$\mathbf{M}\Phi_0(r, E) = -\mathbf{M}_1\Phi_0(r, E) - \frac{1-k_{\text{eff}}}{k_{\text{eff}}}\mathbf{M}_1\Phi_0(r, E). \quad (3)$$

Equations (1) and (3) are the same if spatial and energy distribution of the external source is:

$$q(r, E) = \frac{1-k_{\text{eff}}}{k_{\text{eff}}}\mathbf{M}_1\Phi_0(r, E), \quad (4)$$

where  $\Phi_0(r, E)$  is the solution of Eq. (3).

A source with the spatial and energy distribution given by Eq. (4) is called a reference source [3].

The full intensity of the external neutron source is defined by

$$Q_1 = \int_V \int_{E_T}^{E_f} q(r, E) dE dV,$$

and fission neutron generation intensity for sub-critical system:

$$Q_f = \int_V \int_{E_T}^{E_f} \mathbf{M}_1\Phi(r, E) dE dV.$$

Then thermal power rate of reactor ( $N_0$ ) is:

$$N_0 = \frac{P_f Q_f}{\nu},$$

where  $P_f$  - energy, released per fission,  $\nu$  - mean number of neutrons per fission.

The relation of  $Q_f$  and  $Q_1$  for reference source is:

$$\left(\frac{Q_f}{Q_1}\right)_{\text{ref}} = \frac{k_{\text{eff}}}{1-k_{\text{eff}}} \quad (5)$$

In case of arbitrary spatial and energy distribution of external neutron source the efficiency of its amplification in the core can be estimated:

$$k_{\text{ampl}} = \left(\frac{Q_f}{Q_1}\right) / \left(\frac{Q_f}{Q_1}\right)_{\text{ref}}$$

# SIMULATION OF MULTIBUNCH INSTABILITIES WITH THE HEADTAIL CODE

N. Mounet, E. Métral and G. Rumolo (CERN, Geneva, Switzerland)

## Abstract

Multibunch instabilities due to beam-coupling impedance can be a critical limitation for synchrotrons operating with many bunches. To study these instabilities, the HEADTAIL code has been extended to simulate the motion of many bunches under the action of wake fields. All the features already present in the single-bunch version of the code have remained available, in particular synchrotron motion, chromaticity, amplitude detuning due to octupoles and the ability to load any kind of wake fields through tables. The code has been then parallelized in order to track thousands of bunches in a reasonable amount of time, showing a linear scaling with the number of processors used. We show benchmarks against Laclare's theory in simple cases, obtaining a good agreement. Results for bunch trains in the LHC and comparison with beam-based measurements are also exhibited.

## INTRODUCTION

Transverse coupled-bunch instabilities occur in general when several bunches interact with their surroundings, creating wake fields that act back on the bunch train in such a way as to give rise to an exponentially growing oscillation. To evaluate the rise times of such instabilities, several theories exist, such as Sacherer's [1], Laclare's [2] and Scott Berg's [3], as well as a macroparticle simulation code, MTRISM [4]. All have some limitations: MTRISM and Scott Berg's theory do not take into account quadrupolar impedance which is quite significant in e.g. the LHC due the high-impedance flat collimators [5]; Sacherer's and Laclare's formalisms assume a machine entirely filled with equidistant bunches, which is not the case in e.g. the LHC and even less in the SPS where only about 30% of the machine is filled to produce the nominal LHC beam. Therefore, to be able to study multibunch instabilities in the LHC and the SPS, we chose to extend the single-bunch macroparticle code HEADTAIL [6]. A first simplified version, accounting only for rigid bunch oscillations with no longitudinal motion, was already developed in Ref. [7]. We present here a new extension that can handle both multibunch and intrabunch motion, benchmarking it with respect to theory, and showing various results in the case of the LHC. Finally, we compare HEADTAIL simulations using the LHC impedance model with beam-based experiments.

## DESCRIPTION OF HEADTAIL MULTIBUNCH

HEADTAIL is a macroparticle simulation code where each individual macroparticle  $i$  is tracked through a ring

subdivided into several kick sections. After initialization with Gaussian (or uniform) distributions, with the possibility to enforce longitudinal matching, macroparticles are tracked in mainly three steps per kick section: 1) the bunches are sliced longitudinally, 2) wake fields kicks are applied to each macroparticles, and 3) their transverse phase space coordinates are linearly transported to the next kick section. Once per turn, the synchrotron motion update is applied, separately for each bunch. For the second step, the kicks  $\Delta x'_i$ ,  $\Delta y'_i$  and  $\Delta \delta_i$  are computed as

$$\begin{aligned}\Delta x'_i &= \mathcal{C} \sum_{z_S > z_{S_i}} n_S W_x(z_{S_i} - z_S, x_S, y_S, x_{S_i}, y_{S_i}), \\ \Delta y'_i &= \mathcal{C} \sum_{z_S > z_{S_i}} n_S W_y(z_{S_i} - z_S, x_S, y_S, x_{S_i}, y_{S_i}), \\ \Delta \delta_i &= \mathcal{C} \sum_{z_S \geq z_{S_i}} n_S W_{||}(z_{S_i} - z_S),\end{aligned}$$

where  $\mathcal{C} = -\frac{e^2}{E_0 \beta^2 \gamma}$ ,  $\gamma$  being the Lorentz factor,  $\beta = \sqrt{1 - \gamma^{-2}}$ ,  $E_0$  the rest mass of the elementary particles (protons or electrons) and  $e$  the elementary charge.  $S_i$  is the slice containing the macroparticle  $i$ , and  $n_S$ ,  $x_S$ ,  $y_S$ ,  $z_S$  are the number of particles, and the transverse and longitudinal positions of each slice  $S$  ( $z$  decreases when going toward the tail of the bunches). In the above expressions the sums run over all slices and bunches before the slice of the macroparticle considered, neglecting thus any wake emitted in the forward direction. The sums continue up to a certain number of turns, i.e. the wakes of preceding turns are taken into account.  $W_{||}(z)$  is the longitudinal wake function, while  $W_x(z)$  and  $W_y(z)$  are given by

$$\begin{aligned}W_x(z, x_S, y_S, x_{S_i}, y_{S_i}) &= W_x^{dip}(z)x_S + W_{xy}^{dip}(z)y_S \\ &+ W_x^{quad}(z)x_{S_i} + W_{xy}^{quad}(z)y_{S_i},\end{aligned}\quad (1)$$

$$\begin{aligned}W_y(z, x_S, y_S, x_{S_i}, y_{S_i}) &= W_y^{dip}(z)y_S + W_{xy}^{dip}(z)x_S \\ &+ W_y^{quad}(z)y_{S_i} + W_{xy}^{quad}(z)x_{S_i},\end{aligned}\quad (2)$$

where *dip* stands for "dipolar" and *quad* for "quadrupolar". Note that coupled terms – i.e. linear wakes in the  $x$  direction but proportional to the  $y$  position and vice versa, are taken into account. The wake functions above ( $W_x^{dip}(z)$ ,  $W_x^{quad}(z)$ , etc.) are provided in a table given in input.

The code has been parallelized over the bunches, which is quite efficient since all bunches can be treated almost independently, the only requirement being that after each slicing the processors exchange for all the bunches the positions and number of particles of each slice, such that the wakes can be computed in all bunches. This represents a limited amount of data since the number of slices usually does not exceed a few hundreds. Indeed, Fig. 1 shows

# CALCULATION OF LONGITUDINAL INSTABILITY THRESHOLD CURRENTS FOR SINGLE BUNCHES \*

P. Kuske, Helmholtz-Zentrum Berlin für Materialien und Energie, Germany

## Abstract

Based on the publication by M. Venturini, et al. [1] a computer program has been developed that solves the Vlasov-Fokker-Planck equation numerically on a two dimensional grid. In this code different types of longitudinal interactions and their combinations are implemented. Calculations have been performed for the 1.7 GeV storage ring BESSY II and the 600 MeV ring MLS using the wake created by the shielded coherent synchrotron radiation (CSR). The results are compared with measurements on both rings which were based on the observation of the onset of time dependent fluctuations ("bursts") of CSR [2, 3]. Fair agreement is found between theory and experiment. The theoretical results complement calculations performed by Bane, et al. [4] for this type of interaction. The new results emphasize the resistive nature of the CSR-interaction, especially in regions where shielding effects are small or the resonance-like features of this wake are important. It is found that in these regions the instability is weak and thresholds depend on the damping time.

## INTRODUCTION

The longitudinal stability of a single bunch of charged particles circulating in a storage ring is still a domain of active experimental and theoretical research. On the experimental side the observation of CSR has supplemented the conventional RF-techniques and extended the region of observation frequencies into the THz part of the bunch spectrum. Thus the time resolution reaches the fs-region. Already the first observations of the time dependent CSR at BESSY II created the desire to compare theoretical and experimental results [2]. On the theoretical side the most advanced semi-analytical approach has been introduced by Oide and Yokoya [5], however, predictions based on their approach are ambiguous. Multi particle tracking codes suffer from the rather high shot noise and therefore a numerical solution of the Vlasov-Fokker-Planck (VFP) equation was chosen for the theoretical modelling [2,6].

## THEORETICAL MODEL

The ensemble of electrons is described by a distribution function,  $\psi(q,p,\tau)$ , which can be written in terms of the normalized phase-space coordinates:  $q=z/\sigma_z$ ,  $p=(E_0-E)/\sigma_E$ , and  $\tau$ , in units of the synchrotron period,  $1/\omega_s$ . The low current rms bunch length,  $\sigma_z$ , and the natural energy spread,  $\sigma_E$ , are related by:  $\omega_s\sigma_z/c=\alpha\sigma_E/E_0$  with  $c$ , the speed of light, and  $\alpha$ , the momentum compaction factor. The VFP equation describes the evolution of the

distribution which depends on the radiation excitation and damping and the interaction of the particles [1]:

$$\frac{\partial\psi}{\partial\tau} + p\frac{\partial\psi}{\partial q} - [q + F_c(q,\tau,\psi)]\frac{\partial\psi}{\partial p} = \frac{2}{\omega_s t_d} \frac{\partial}{\partial p} \left( p\psi + \frac{\partial\psi}{\partial p} \right)$$

The r.h.s. is the Fokker-Planck-term which introduces damping and diffusion and  $t_d$  is the longitudinal damping time. The coefficient in the square brackets is the approximated linear restoring force of the RF-potential and  $F_c$  is the collective force from the interaction of the charge distribution with itself and its metallic surrounding. This force or the induced voltage is obtained by the convolution of the longitudinal charge density with the wake function. The charge density,  $\lambda(q,\tau)$ , is given by  $\lambda(q,\tau)=\int dp \psi(q,p,\tau)$ . The wake function depends on the types of interactions studied.

## Numerical Solution of the VFP-Equation

Warnock, et al [7] and Venturini, et al [1] proposed two different numerical algorithms to find the distribution function on a two dimensional grid as a function of time. In both cases the required extrapolation of the distribution function to off-grid points can lead to unrealistic negative values for  $\psi(q,p,\tau)$ . Therefore, a kind of wave function,  $g(q,p,\tau)$ , is introduced so that the probability to find electrons is given by  $\psi(q,p,\tau)=g^2(q,p,\tau)$  and always larger than zero. As a result only the Fokker-Planck-term needs to be modified in the VFP equation for  $g(q,p,\tau)$ :

$$\frac{\partial g}{\partial\tau} + p\frac{\partial g}{\partial q} - [q + F_c] \frac{\partial g}{\partial p} = \frac{2}{\omega_s \tau_1} \left( \frac{g}{2} + p\frac{\partial g}{\partial p} + \frac{1}{g} \left( \frac{\partial g}{\partial p} \right)^2 + \frac{\partial^2 g}{\partial p^2} \right)$$

This equation is solved by splitting the time step,  $\Delta\tau$ , of the temporal evolution of the wave function,  $g(q,p,\tau)$ , into smaller steps [1]:

$$\begin{aligned} g_1(q,p,\tau) &= g_0(q-p\cdot\Delta\tau/2,p,\tau) \\ g_2(q,p,\tau) &= g_1(q,p+(q+F_c(q,g_0))\cdot\Delta\tau,\tau) \\ g_3(q,p,\tau) &= g_2(q-p\cdot\Delta\tau/2,p,\tau) \\ g_4(q,p,\tau+\Delta\tau) &= g_3(q,p,\tau) + \text{diffusion} + \text{damping} \end{aligned}$$

The code uses a fourth order polynomial in order to interpolate to off-grid points. The interpolation is performed between the grid points  $g(x-2\Delta)$ ,  $g(x-\Delta)$ ,  $g(x)$ ,  $g(x+\Delta)$  and  $g(x+2\Delta)$  and thus is more symmetric relative to the central point compared to a cubic Hermite interpolation [1].  $x$  stands for the  $p$  or  $q$  coordinate and  $\Delta$  is the distance between grid points. The first step coded in BASIC looks like this:

```
For ip = -iqmax To iqmax: For ip = -ipmax To ipmax
  g0 = gold(ip, ip)
  If Abs(g0) > .000001 Then
    dQ = - ip *deltaP/deltaQ* dtau / 2
    gmm = gold(ip - 2, ip): gm = gold(ip - 1, ip)
```

\*Work supported by the BMBF and the Land Berlin

# COMPUTATIONAL NEEDS FOR RF DESIGN OF SUPERCONDUCTING CAVITIES\*

A. Lunin<sup>#</sup>, T. Khabiboulline, S. Yakovlev, Fermilab, Batavia, IL 60510, USA

## Abstract

The computational approaches assure essential guidance and order for the design of superconducting cavities and cryomodules. The nature of superconductivity requires the precise computation of surface electromagnetic fields in order to design the cavity shape with a maximum accelerating gradient. At the same time, the thickness of the cavity shell is limited by the ability to cool it down to the temperature of liquid He, which makes the mechanical stability of a cavity and a liquid He vessel assembly extremely important. Hence, a self-consistent electro-mechanical optimization is required in order to minimize microphonics and/or Lorentz force detuning phenomena. Some specific challenges are estimation of the amount of RF losses caused by the interaction of the passing beam with SC cavity and a multipactor analysis in the SC cavity and RF coupler. Finally, the irregular time structure of a beam train with its own dense spectra may stochastically induce High Order Mode (HOM) fields in a cavity which results in beam emittance dilution.

The study of these effects leads to specification of the SC cavity and cryomodule and can significantly impact the efficiency and reliability of superconducting linac operation.

## INTRODUCTION

SRF cavities are widely used today for various applications in high energy physics, nuclear physics and material science requiring an acceleration of charged particles [1][2][3]. New projects such as Accelerator Driven Subcritical systems (ADS), high intensity proton accelerator (Project X), Facility for Rare Isotope Beams (FRIB) and Next Generation Light Source Facility (NGLS) are under development [4][5][6][7]. Because of such diversity, designs of SRF cavities cover wide range of particles velocities ( $\beta \sim 0.05 - 1$ ), operating frequencies (0.072 - 4 GHz), beam currents (1mA - 100mA) and suitability for pulsed and continuous operation regimes. Besides, the SRF cavity is a complicated electro-mechanical assembly and consists of: bare cavity shell with power and HOM couplers, stiffening elements (ring, bars), welded LHe vessel, slow and fast frequency tuners and vacuum and coupler ports. A mechanical design of SRF cavity is illustrated in Figure 1 [8]. Therefore, the development of SRF cavity requires a complex, self-consistent electro-mechanical analysis in order to minimize microphonics and/or Lorentz force detuning phenomena and preserve good cavity tenability simultaneously.

\* Operated by Fermi Research Alliance, LLC under Contract No. DE-AC02-07CH11359 with the U.S. Department of Energy.  
#lunin@fnal.gov

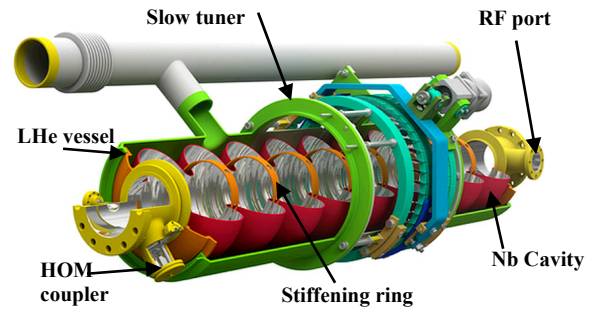


Figure 1: ILC 1.3 GHz 9-cell cavity.

The following aspects need to be taken into account during the design process:

- Cavity acceleration efficiency, including minimization of surface field enhancement factors (both electric and magnetic) and choosing optimum beta value for multiple cavities in the linac section.
- High gradient pulsed operation and minimizing of Lorentz force detuning coefficient.
- Operation with small beam current and narrow cavity bandwidth, particularly suppressing microphonics and preserving good cavity tenability simultaneously.
- HOM dumping in order to minimize cryogenic losses, preserving good beam emittance and excluding any transverse or longitudinal beam instabilities.
- Analyzing field emission effects including multipactor and dark current simulations.

We discuss all these issues and possible solutions below

## SRF CAVITY EM ANALYSIS

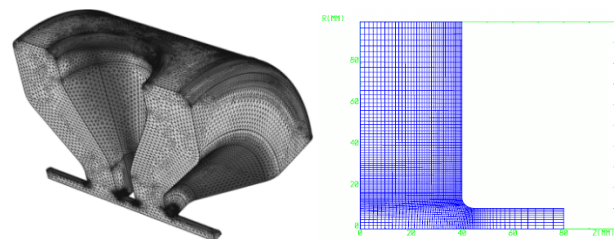


Figure 2: Meshing approaches in 3D (left) and 2D (right) domains.

Superconducting resonators suffer from both high magnetic field, which causes a thermal quench if it goes above critical value, and high electrical field, because it initiates surface field emission which produces additional cryolosses and may result in strong x-rays as well. Thus, the SRF cavity EM design requires precise surface

# ARBITRARY HIGH-ORDER DISCONTINUOUS GALERKIN METHOD FOR ELECTROMAGNETIC FIELD PROBLEMS\*

K. Papke<sup>†</sup>, C. R. Bahls, U. van Rienen, Universität Rostock, IAE, IEF, 18059 Rostock, Germany

## Abstract

In this paper, we present a time integration scheme applied to the Discontinuous Galerkin finite element method (DG-FEM, [1]) for the computation of electromagnetic fields in the interior of three-dimensional structures. This approach is also known as Arbitrary High-Order Derivative Discontinuous Galerkin (ADER-DG, [2, 3]). By this method, we reach arbitrary high accuracy not only in space but also in time. The DG-FEM allows for explicit formulations in time domain on unstructured meshes with high polynomial approximation order. Furthermore, the Discontinuous Galerkin method in combination with the arbitrary high order time integration scheme is well suited to be used on massively parallel computing architectures. Moreover the method can be extended for local time stepping to become more efficiently by reducing the computation time [4].

## INTRODUCTION

For the design and optimization of Higher-Order-Mode Coupler (Fig. 1), used in RF accelerator structures, numerical computations of electromagnetic fields as well as scattering parameter are essential. These computations can be carried out in time domain. In this work the implementation and investigation of a time integration scheme based on the Discontinuous Galerkin Finite-Element Method (DG-

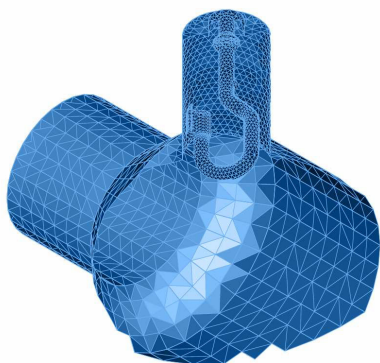


Figure 1: Tapered beam pipe with Higher-Order-Mode Coupler. The aspect ratio of such a grid is relatively high, due to the filigree structure of the antenna. Therefore, such a model is well suited for the application of local time stepping schemes.

FEM) with arbitrary order in space and time is demonstrated for solving 3-D electromagnetic problems in time domain.

## THE NUMERICAL SCHEME

With known initially and boundary conditions it is sufficient to describe classic electromagnetic phenomena only by AMPERE's and FARADAY's law of MAXWELL equations. The partial differential equations can be written in the following general form:

$$\frac{\partial \mathbf{u}}{\partial t} + \mathcal{A}_1 \frac{\partial \mathbf{u}}{\partial x} + \mathcal{A}_2 \frac{\partial \mathbf{u}}{\partial y} + \mathcal{A}_3 \frac{\partial \mathbf{u}}{\partial z} = 0, \quad (1)$$

where

$$\mathbf{u}(x, y, z, t) = (E_x, E_y, E_z, H_x, H_y, H_z)^T. \quad (2)$$

The space-dependent Jacobian matrices  $\mathcal{A}_i$  determine the physical behavior of the equations. They contain material properties as well as the curl operator applied to E- and H-field. To solve this ordinary partial differential equation, a physical initial condition as well as boundary conditions are still needed.

For the numerical scheme the computational domain  $\Omega \in \mathbb{R}^3$  will be partitioned into conforming tetrahedral elements  $D^k$ . The approximate solution  $\mathbf{u}_h^k$  of (1) inside each tetrahedron  $D^k$  is given by:

$$\mathbf{u}_h^k = \sum_{i=1}^{N_p} \hat{\mathbf{u}}_i^k(t) \cdot \Phi_i^k(\mathbf{x}). \quad (3)$$

Here  $\Phi_i^k(\mathbf{x})$  are the nodal ansatz functions and  $\hat{\mathbf{u}}_i^k(t)$  are the time-dependent degrees of freedom which are allocated at the nodes of the element  $D^k$ .

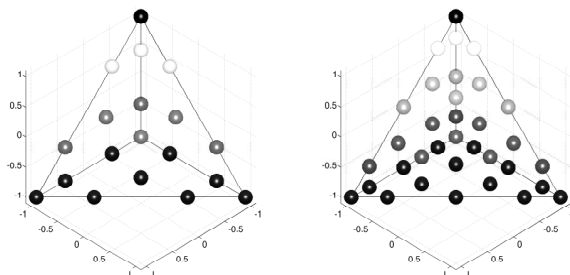


Figure 2: Reference element with the nodes on which the time-dependent degrees of freedom are defined. (left: 3rd order ansatz functions, right: 4th order ansatz functions)

\* Work supported by Federal Ministry for Research and Education BMBF under contract 05K10HRC

<sup>†</sup> kai.papke@uni-rostock.de

# STATUS OF THE HOM CALCULATIONS FOR THE BERLinPro MAIN LINAC CAVITY\*

A. Neumann<sup>†</sup>, W. Anders, J. Knobloch, Helmholtz-Zentrum Berlin, Berlin, Germany  
 B. Riemann, T. Weis, TU Dortmund University, Dortmund, Germany  
 K. Brackebusch, T. Flisgen, T. Galek, K. Papke, U. van Rienen  
 Rostock University, Rostock, Germany

## Abstract

The Berlin Energy Recovery Linac Project (BERLinPro) is designed to develop and demonstrate CW LINAC technology and expertise required to drive next-generation Energy Recovery Linacs (ERLs). Strongly higher order mode (HOM) damped multicell 1.3 GHz cavities are required for the main linac. The cavity under study is an integrated design of the Cornell base cell with JLab HOM waveguide couplers. Modifications to the end group design have also been pursued, including the substitution of one waveguide by a HZB-modified TTF-III power coupler. In this paper the progress in HOM calculations to avoid beam-breakup instabilities for the favored cavity structure will be presented.

## INTRODUCTION: THE BERLinPro PROJECT

The BERLinPro ERL will be a CW driven machine accelerating a 100 mA beam to 50 MeV while preserving a normalized emittance of better than 1 mm mrad at a pulse length of 2 ps [1]. For the different sections of the superconducting accelerator -SRF photo-injector, booster module and main linac in the recirculator- the operating boundary conditions for the cavity design vary from high current, high beam loading to a high current, zero net beam loading environment. Thus the requirements for quality factor and peak fields are quite different for these three cavity types as well as the HOM damping technique applied. Main emphasis of this paper will be the calculations for the main linac cavity.

The main linac cavity has to have strong HOM damping as it accelerates the beam during the first passage and decelerates the recirculated beam for energy recovery thus interacting with two 100 mA beams. The beam may excite a transverse acting mode, e.g. a TM<sub>10</sub> dipole mode, which deflects a following bunch. After recirculation, this bunch will arrive within the same structure affected now by an offset and, depending on the phase advance, possibly further exciting this dipole mode. This effect may add up from bunch to bunch until the beam will be lost - the so called beam break up (BBU) [2]. Equation 1 describes the dependence of the threshold current  $I_{th}$  for one cavity HOM on the mode's transverse shunt impedance  $R/Q_{\perp}$ , its external quality factor  $Q_{ext}$ , frequency  $\omega$  and the beam's energy  $\gamma$ , recirculating time  $t_r$  and the transfer matrix of the linear

beam optics  $M_{12}$ :

$$I_{th} = -\frac{2\gamma}{e} \frac{R}{Q_{\perp}} \frac{c}{Q_{ext}\omega M_{12}} \frac{1}{\sin(\omega t_r)}. \quad (1)$$

From the viewpoint of cavity design it means to minimize the HOM's  $R/Q_{\perp}$  and  $Q_{ext}$ . The HOM's spectrum and dispersion relation is mainly influenced by the mid-cell design, especially the cell-to-cell coupling via the iris diameter. By tuning the end-cells one achieves first of all field flatness for the fundamental TM<sub>010</sub>- $\pi$  mode and may avoid trapped modes within the center cells. The end-cell is mainly responsible to couple the HOMs to the loads or damping structures.

In this paper an update of the HOM calculations of the main linac cavity is given which was already introduced in [3]. Further a short outlook on ongoing activities is given of which more is described in [4].

## STRUCTURE DESIGN AND EIGENMODE CALCULATIONS

The baseline design so far consists of a seven cell structure using the Cornell's ERL design [5] and combining it with JLab style symmetric assembled waveguide HOM couplers [6] (see Figure 1). To allow for a flexible coupling, one group of HOM couplers is broken in symmetry by replacing one waveguide with a TTF-III type coaxial fundamental power coupler. This design combines the good peak field properties of the Cornell design with the advantage of waveguide couplers having a natural cutoff above the fundamental and further limiting the possibility of dust from ferrite beam tube absorbers propagating in the SC cavity.

Table 1 summarizes the figures of merit of the field-flatness tuned seven cell structure. The main task of this adapted design was to calculate its performance with respect to BBU, identify limiting HOMs and find means to tune them to lower  $Q_{ext}$  while preserving the fundamental's RF properties. Because of the influence of the couplers on the field distribution, most calculations done so far were carried out in 3D with CST MWS [7] making use of the given symmetry plane at the coaxial coupler and using both mesh types, tetrahedral and hexahedral, where the latter had to be used to calculate the  $Q_{ext}$ . In all results shown here mainly the Jacobi-Davidson-Method (JDM) was used. Figure 2 shows the calculated spectrum up to 3 GHz, mainly limited by mesh size versus computing power and time. Figure 3 depicts the corresponding  $Q_{ext}$ , demonstrating a rather good damping of the lowest order dipole

\*Work supported by Federal Ministry for Research and Education BMBF under contract 05K10HRC and 05K10PEA

<sup>†</sup> Axel.Neumann@helmholtz-berlin.de

# ASTRA BASED SWARM OPTIMIZATIONS OF THE BERLinPro INJECTOR

M. Abo-Bakr\*, B. Kuske, Helmholtz-Zentrum-Berlin, Germany

## Abstract

The Berlin Energy Recovery Linac Project *BERLinPro* is a compact ERL to develop the accelerator physics and technology required to generate and accelerate a 100-mA, 1-mm mrad normalized emittance beam. One of the project challenges is to generate a beam of this kind in the injector line of the machine. Extensive injector optimization studies have been done over the last years. A deep insight in the physics of high brilliance, low energy beams together with single parameter scans allowed for an efficient optimization, resulting in a layout, capable to deliver bunches of the needed charge and dimension. However, changes in the injector components' technical layout, as they are unavoidable in the current stage of the project, may require re-optimizations at any time, if necessary of the whole injector part. To support these work an ASTRA based 'swarm optimization' tool for massive parallel calculations on the institute's Linux computing cluster has been developed. Once the optimization wrapper code is written, results come for free and can help to extend the understanding of the underlying physics. Strategy, procedure and results of the 'swarm optimizations' will be presented in this paper.

## INTRODUCTION

*BERLinPro* [1] is a Energy Recovery Linac (ERL) Project of the "Helmholtz-Zentrum Berlin für Materialien und Energie", funded in 2011. ERLs combine the advantages of linear accelerators (linac) and storage rings: since in principle like linacs, the excellent beam properties of photo-injector electron sources, as they became available in the last years, can be used in an ERL in contrast to storage rings, where the beam parameters arise from an equilibrium state of excitation and damping processes. In addition adiabatic damping while acceleration as well as beam manipulation techniques (e.g. bunch compression) further improve the ERL's beam quality.

In contrast to storage rings, the complete beam energy is dumped in a linear accelerator, limiting the maximum average currents to small values. In ERLs the invested energy is recovered by re-passing the initially accelerating RF structures a second time on a decelerating phase, so that the beam energy restores the cavity fields. Average currents of cw operated ERLs, using super conducting RF technology, become thus comparable to those of storage rings.

*BERLinPro*'s primary function is to demonstrate a stable and reliable low emittance, high-current operation, proving the ERL to be suited for the variety of future applications, including 4<sup>th</sup> generation X-ray and Compton sources, EUV lithography and nuclear physics. The main *BERLinPro* parameter are listed in Table 1.

\*Michael.Abo-Bakr@helmholtz-berlin.de

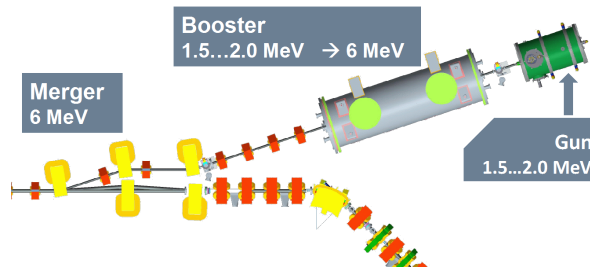


Figure 1: Layout of the *BERLinPro* Injector, including the modules of the photo cathode gun and the booster linac as well as a dipole dogleg, merging the injector beam onto the main linac / recirculator beam path.

Table 1: Main *BERLinPro* Parameters in "Standard Mode" Operation

Parameter	Value	Unit
Beam energy	50	MeV
Beam current @ 1.3 GHz	100	mA
Bunch charge	77	pC
Bunch length	~ 2	ps
Energy spread	0.5%	-
Emittance (norm.)	~ 1	mm mrad
Beam loss	< 10 <sup>-5</sup>	-

As the ERL bunch parameters a determined by those of the electron source the injector is one of an ERL's key aspects. To reach normalized emittances of about 1 π mm mrad and below not only a high performance gun is required but also a sophisticated injector setup for emittance conserving acceleration and transport of a strongly space charge (SC) dominated electron beam.

Injector beam line design aims for a trade-off in the bunch dimensions, minimizing the beam distortions due to SC effects, aberrations and RF-nonlinearities. In addition an effective emittance compensation scheme is mandatory.

Figure 1 shows a sketch of the *BERLinPro* injector, as presented in the Conceptual Design Report (CDR) [2]. Main components are

- a 0.6 cell gun cavity, followed by a sc solenoid also integrated in the gun module, the photo cathode laser has a uniform transverse and a Gaussian longitudinal profile,
- a three 2-cell booster cavities (cavity and module are based on a Cornell design), due to limited RF power at high currents one of the cavities will be operated only at "zero crossing",
- a three bend, 18° dogleg, with quadrupole magnets, both in front of the merger to control the transverse beam size and inside the merger to control the dispersion.

# HYBRID PROGRAMMING AND PERFORMANCE FOR BEAM PROPAGATION MODELING

Misun Min\*, Jing Fu, Azamat Mametjanov

Mathematics and Computer Science Division, Argonne National Laboratory, Argonne, IL 60439, USA

## Abstract

We examined hybrid parallel infrastructures in order to ensure performance and scalability for beam propagation modeling as we move toward extreme-scale systems. Using an MPI programming interface for parallel algorithms, we expanded the capability of our existing electromagnetic solver to a hybrid (MPI/shared-memory) model that can potentially use the computer resources on future-generation computing architecture more efficiently. As a preliminary step, we discuss a hybrid MPI/OpenMP model and demonstrate performance and analysis on the leadership-class computing systems such as the IBM BG/P, BG/Q, and Cray XK6. Our hybrid MPI/OpenMP model achieves speedup when the computation amounts are large enough to compensate the OMP threading overhead.

## INTRODUCTION

Multicore architectures are current trends for gaining improvement in computing power, instead of increased clock speed. To achieve scalable performance with minimal parallelization overhead on such platforms, we have explored incorporating multithreading frameworks into our existing MPI-only code NekCEM for beam propagation modeling. Specifically, we are using hierarchical parallelization frameworks based on MPI/OpenMP schemes for intranode operations of MPI programs using OpenMP directives around time-consuming loops that do not contain data dependencies, while leaving the source code unchanged.

NekCEM [1, 2, 3] is a freely available, massively parallel, scalable high-order code for electromagnetic device simulations. NekCEM has great potential for meeting the future computational needs of experimental and theoretical research at exascale, by using a fast communication kernel for efficiency and body-fitted hexahedral meshes that allow significant gains in accuracy. We previously conducted wakefield calculations using the spectral-element discontinuous Galerkin (SEDG) scheme [4, 5] with fourth-order Runge-Kutta time stepping, with favorable results in comparison with those from low-order methods.

Future-generation supercomputing systems will be memory-limited relative to the raw computational performance. Currently, per processor memory requirements for NekCEM scale roughly as 600 8-byte words per allocated gridpoint. The total memory requirements are  $n = EN^3$  points  $\times$  600 (words/point)  $\times$  8 (bytes/word). For example, with  $E=800K$  and  $N=16$ , the total memory requirements

are  $800K \times 16^3 \times 600 \times 8$ . Assuming that 200 MB of memory per core are available to the user, one can run this simulation with  $P > 786,432$  cores by setting the number of local elements more than 10. In the current parallel context, however, there will be an increasing memory penalty associated with two variables, the maximum number of cores and the upper bound on the total number of elements, as the problem size becomes very large at extreme scale. A hybrid MPI/share-memory framework can reduce the memory dependency on these two parameters.

## IMPLEMENTATION

Ultrarelativistic beam propagations are governed by Maxwell's equations,

$$\mathbf{Q} \frac{\partial \mathbf{q}}{\partial t} + \nabla \cdot \mathbf{F}(\mathbf{q}) = \mathbf{S}, \quad (1)$$

where we define the field vector  $\mathbf{q} = [\mathbf{H}, \mathbf{E}]^T$  and the flux  $\mathbf{F}(\mathbf{q}) = [\mathbf{F}_H, \mathbf{F}_E]^T$  with  $\mathbf{F}_H = \mathbf{e}_i \times \mathbf{E}$  and  $\mathbf{F}_E = -\mathbf{e}_i \times \mathbf{H}$ , and the source term  $\mathbf{S} = [0, \mathbf{J}]^T$ . The electric, magnetic, and current fields are represented by  $\mathbf{E} = (E_x, E_y, E_z)^T$ ,  $\mathbf{H} = (H_x, H_y, H_z)^T$ , and  $\mathbf{J} = (0, 0, J_z)^T$ , respectively. The material properties are defined as  $\mathbf{Q} = \text{diag}(\mu, \mu, \mu, \epsilon, \epsilon, \epsilon)$  with the free space permittivity  $\epsilon$  and free space permeability  $\mu$ . Initial fields in the presence of the Gaussian beam are obtained by solving the Poisson equation in transverse direction at the beam location in the longitudinal direction.

## Numerical Approach

We consider the computational domain  $\Omega$  with nonoverlapping hexahedral elements  $\Omega^e$  such that  $\Omega = \cup_{e=1}^E \Omega^e$ , and we define a weak formulation, introducing the numerical flux  $\mathbf{F}^*$  as in [4, 5]:

$$\left( \mathbf{Q} \frac{\partial \mathbf{q}}{\partial t} + \nabla \cdot \mathbf{F}(\mathbf{q}) - \mathbf{S}, \phi \right)_{\Omega^e} = (\hat{n} \cdot [\mathbf{F} - \mathbf{F}^*], \phi)_{\partial \Omega^e}. \quad (2)$$

The local solutions of the fields can be written as

$$q^N(\mathbf{x}, t) = \sum_{i,j,k=1}^N q_{ijk} \psi_{ijk}(\mathbf{x}), \quad (3)$$

where  $q_{ijk}$  is the solution at  $\mathbf{x}=(x_i, y_j, z_k)$  on  $\Omega^e$  and  $\psi_{ijk}=l_i(r)l_j(s)l_k(t)$  using the one-dimensional Legendre Lagrange interpolation polynomial  $l_i$  of degree  $N-1$  associated with the  $N$  Gauss-Lobatto-Legendre (GLL) quadra-

\* mmin@mcs.anl.gov

# COMPARISON OF EIGENVALUE SOLVERS FOR LARGE SPARSE MATRIX PENCILS \*

F. Yaman\*\*, W. Ackermann, T. Weiland, Technische Universität Darmstadt,  
Institut für Theorie Elektromagnetischer Felder (TEMF),  
Schlossgartenstraße 8, 64289 Darmstadt, Germany

## Abstract

Efficient and accurate computation of eigenvalues and eigenvectors is of fundamental importance in the accelerator physics community. Moreover, the eigensystem analysis is generally used for the identifications of many physical phenomena connected to vibrations. Therefore, various types of algorithms such that Arnoldi, Lanczos, Krylov-Schur, Jacobi-Davidson etc. were implemented to solve the eigenvalue problem efficiently. In this direction, we investigate the performance of selected commercial and freely available software tools for the solution of a generalized eigenvalue problem. We choose characteristic setups by considering spherical and billiard resonators next to a TESLA nine-cell cavity in order to test the robustness, accuracy, and computational speed as well as memory consumption issues of the recent versions of CST, Matlab, Pysparse, SLEPc and CEM3D. Simulations were performed on a standard personal computer and on a cluster computer to enable the handling of large sparse matrices in the order of hundreds of thousands up to several millions degrees of freedom (DOF). We obtain interesting comparison results with the examined solvers which is useful for choosing the appropriate solvers for a given practical application.

## INTRODUCTION

In this paper, we consider the numerical solution of the generalized eigenvalue problem

$$Ax = \lambda Bx \quad \text{for } B > 0 \quad (1)$$

for a given symmetric, real valued, large and diagonally dominant sparse matrix pencils A and B. The problem can be derived from Maxwell's equations for a source free bounded domain having perfectly conducting boundary condition on its surface. In principle, such a mathematical model coincides with a superconducting cavity which enclosures excited electromagnetic fields. Therefore, accurate calculation of eigenvalues  $\lambda$  has a critical importance and it leads to find the eigenfrequencies of several modes which are of fundamental importance for the acceleration of charged particles. In this context, performance of eigensolvers are always of interest in industry and scientific communities which constitutes the main motivation of our study.

Jacobi-Davidson method [1] which is based on iterative expansions of subspaces is recommended to solve eigenvalue problems dealing with diagonally dominant large

matrices in the literature [2, 3, 4]. Therefore, we select CEM3D, Pysparse and SLEPc solvers which all can employ Jacobi-Davidson implementation in their simulations. Here, we just mention the idea behind of the method shortly. Let  $V_k = \text{span}\{v_1, \dots, v_k\}$  be a subspace where  $v_k^T B v_j = \delta_{kj}$ . Then a Ritz pair  $(\theta_j, u_j)$  in  $V_k$ , can be obtained from the projected eigenvalue problem choosing the closest value to a given target  $\tau$ . In the next step, a convergence criteria

$$\|r\|_2 := \|(A - \theta B)u\|_2 < \epsilon. \quad (2)$$

is checked for  $\theta$  if it could be an eigenvalue for a selected  $\epsilon$ . Afterwards, the so-called correction equation

$$(I - Buu^T)(A - \theta B)(I - uu^T)z = -r \quad (3)$$

is solved iteratively with *tfqmr*s in CEM3D, with *bcgsl* in SLEPc and with *qmr*s in Pysparse for the unknown  $z$  where  $z \perp u$  and  $u^T$  is the transpose of  $u$ . Then we expand the subspace  $V_{k+1} = \text{span}\{v_1, \dots, v_{k+1}\}$  for the next iteration which starts finding approximate Ritz pairs for the updated subspace [5].

## NUMERICAL EXPERIMENTS

In the numerical tests, spherical and billiard resonators and a 9-cell TESLA cavity are considered. Structures are drawn and meshed with tetrahedrons having planar elements. Corresponding meshes are imported to CEM3D [6] in order to generate input sparse matrices for the eigenvalue solvers Pysparse [4], SLEPc [7] and Matlab [8]. Here, CEM3D is a parallel and a higher order FEM code which was implemented in our institute for the accurate calculations of eigenfrequencies for a given structure. Furthermore the same structures are used for the eigenvalue simulations in CST [9]. It is also noted that among these solvers only CEM3D and SLEPc have the capability to run on a distributed memory machine with multiprocessors in parallel.

For the comparison of different solver results, we first compute the eigenvalues of a spherical resonator from analytical expressions given in [10] by employing a root-finding algorithm which is simply explained in [11]. Eigenvalues are also calculated with SLEPc for different DOF and a relative error is calculated as,

$$\text{relative error} = \max_{i \in \text{DOF}} \frac{|\lambda^{\text{analytical}} - \lambda_i^{\text{numerical}}|}{\lambda^{\text{analytical}}} \quad (4)$$

by considering the worst computed degenerated mode eigenfrequency, see Figure 1.

\* Work supported by the DFG through SFB 634

\*\*yaman@temf.tu-darmstadt.de

# PIC SIMULATIONS OF LASER ION ACCELERATION VIA TNSA

Z. Lecz, O. Boine-Frankenheim, TU Darmstadt and GSI Darmstadt, Germany  
V. Kornilov, GSI, Darmstadt, Germany

## INTRODUCTION

The acceleration of ions with lasers up to energies of 60 MeV has been successfully demonstrated at different laser systems worldwide, including our facility: PHELIX [1]. The undergoing mechanism is understood as Target Normal Sheath Acceleration (TNSA) [2]. Due to the small transverse emittance and low installation cost laser-ion acceleration is a promising alternative to RF accelerators with the possible application in ion cancer therapy [3]. This contribution is devoted to the numerical investigation of the proton acceleration via the TNSA mechanism using 1D and 2D particle-in-cell electro-magnetic simulations. We employ the plasma simulation code VORPAL [4] and focus on the proton and electron phase-space distribution at the rear side of the target. The lack of knowledge about the thickness of hydrogen-rich contamination layer requires a detailed parameter study, which has been done in 1D. In this work we investigate the expansion and divergence of a thick proton layer from the rear side of the target using 2D simulations. In order to make sure that the results are physically correct and reliable we performed a detailed convergence study over the grid size and macro-particle charge.

## NUMERICAL HEATING IN 2D PIC SIMULATIONS

As we know, in 1D it is really easy to resolve the physical scale lengths (Debye-length) and we can use many macro-particles per cell in order to get better statistics and smoother plasma density. With resolution high enough we obtain results comparable to the fluid-hybrid codes, but the PIC code always gives us more data and realistic velocity phase-space distribution of particles. Therefore the PIC simulations are used to get insight into the smallest details of physical processes in plasma physics.

Very often in 2D we can not use the same high resolution. Because of the discretization of space and time we always have to be aware of the numerical errors which occur during field calculations and integration of equation of motion of particles. These errors can lead to increasing field amplitudes, consequently artificial particle acceleration. The main equations which are solved in the loop of a PIC code are the Faraday's and Ampere-Maxwell law:

$$\frac{\partial B}{\partial t} = -c\nabla \times E \quad (1)$$

$$\frac{\partial E}{\partial t} = c\nabla \times B - J \quad (2)$$

These equations are solved in the frequency domain by calculating the Fourier transform of the fields and then they

are transformed back, because the equation of motion is integrated in the time domain. This additional step speeds up the calculations significantly. Due to the granulated representation of the density, the Fourier transform of  $J$  can contain very high frequencies, which can not be resolved by the spatial grid. The high frequency noise can be reduced by increasing the grid resolution or increasing the number of particle per cell (PPC). However these two options are very expensive in terms of computing power and CPU time. A much better method is the implementation of higher order particle shapes and field interpolation which will smooth out the fields and current density in the simulation. Thus the noise disappears and the simulation will be more stable with correct energy conservation, but it does not mean that result is closer to the reality or that it is more reliable [5]. Very often the high frequency modulation of the density has a physical reason and in this case we exclude a part of the physical processes by applying a smoothing technique.

Interaction of high intensity laser with over-dense plasma requires a very high number of grid-cells in order to resolve the very small cold electron Debye-length ( $\lambda_{De}$ ). The usual length in both directions is a few tens of micrometers, while the Debye-length inside of the high density cold plasma is on the order of nanometers. In this case it is inevitable to use smoothing interpolations, which allows us to define grid cells larger than  $\lambda_{De}$ . In order to check the grid heating we performed several simulations with dense plasma ( $n_0=10^{27} \text{ m}^{-3}$ ) filling up completely the simulation box, which has periodic boundaries. The initial electron temperature was 1 keV. In Fig. 1 the simulation results are shown for 4 different grid resolution. Two simulations were done with linear interpolation and particle shape, which results in a very strong heating of the electrons. This numerical effect is not present if we switch to the cubic (third order) smoothing even if the grid size is 40 times larger than  $\lambda_{De}$ . A weak heating can be observed only for very small PPC, brown line.

Another important effect which can increase the electron temperature is the numerical Cherenkov emission. It is related to the Courant criteria [6], which defines the time step for a stable simulation. Discretizing the space automatically leads to a dispersion relation which says that the phase velocity of electro-magnetic waves propagating on the grid is smaller than the speed of light. If we have high energy electrons in the system they can have velocity close to the speed of light which means that they can travel faster than maximum phase velocity in the system. This situation results in the same effect what we observe in the reality: radiation into the medium. The emitted fields accelerate the electrons, thus their temperature is increasing. This effect

# INDEPENDENT COMPONENT ANALYSIS (ICA) APPLIED TO LONG BUNCH BEAMS IN THE LOS ALAMOS PROTON STORAGE RING\*

J. Kolski<sup>†</sup>, R. Macek, R. McCrady, X. Pang, LANL, Los Alamos, NM, 87545, USA

## Abstract

Independent component analysis (ICA) is a powerful blind source separation (BSS) method[1]. Compared to the typical BSS method, principal component analysis (PCA), which is the BSS foundation of the well known model independent analysis (MIA)[2], ICA is more robust to noise, coupling, and nonlinearity[3, 4, 5]. ICA of turn-by-turn beam position data has been used to measure the transverse betatron phase and amplitude functions, dispersion function, linear coupling, sextupole strength, and nonlinear beam dynamics[3, 4, 5]. We apply ICA in a new way to slices along the bunch, discuss the source signals identified as betatron motion and longitudinal beam structure, and for betatron motion, compare the results of ICA and PCA.

## INTRODUCTION

We apply BSS in a new way to slices along the bunch[6]. We digitize beam signals from the Los Alamos Proton Storage Ring (PSR) for a full injection-extraction cycle,  $\geq 1800$  turns. We divide the digitized signal into time slices of equal length using the 0.5 ns digitization bin length. The long digitized signal vector is stacked turn-by-turn to form the data matrix

$$\mathbf{x}(t) = \begin{pmatrix} x_1(1) & x_1(2) & \dots & x_1(N) \\ x_2(1) & x_2(2) & \dots & x_2(N) \\ \vdots & \vdots & \ddots & \vdots \\ x_M(1) & x_M(2) & \dots & x_M(N) \end{pmatrix}, \quad (1)$$

such that each row of  $\mathbf{x}$  is data from a single time slice for all  $N$  turns, and each column of  $\mathbf{x}$  is data from all  $M$  time slices for a single turn. The slices are located at a fixed longitudinal phase and position along the bunch. The last turn beam profile plotted in Fig. 1 is an example of the last column of  $\mathbf{x}$ .

ICA and PCA model  $\mathbf{x}$  as a linear combination of independent components (ICs) and principal components (PCs) respectively and yield respectively modes and patterns, describing the source signal's strength in space (along the bunch) and time.

### Principal Component Analysis (PCA)

PCA is the simplest of the BSS methods. Many other BSS methods use PCA for preprocessing and noise reduction. PCA was originally applied for beam analysis in the well known MIA.

\* Work supported by in part by United States Department of Energy under contract DE-AC52-06NA25396. LA-UR 12-24396

<sup>†</sup> Electronic address: jkolski@lanl.gov

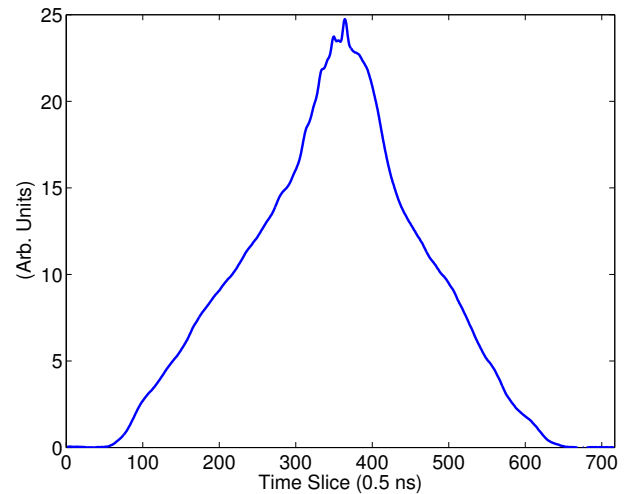


Figure 1: The last turn beam profile as an example of the last column of the data matrix  $\mathbf{x}$  in Eq. (1). The PSR's revolution period is 358 ns corresponding to 716 time slices.

PCA identifies patterns in data and expresses the high-dimensional data by highlighting the underlying structures represented as PCs. The PCs are used to compress data by reducing redundant dimensions without much loss of information. PCA minimizes the redundancy measured by covariance, maximizes the signal measured by variance, and results in uncorrelated PCs. Two random variable vectors  $\vec{y}_1$  and  $\vec{y}_2$  are uncorrelated if their covariance is zero,

$$\text{cov}(\vec{y}_1, \vec{y}_2) = \langle \vec{y}_1, \vec{y}_2 \rangle - \langle \vec{y}_1 \rangle \langle \vec{y}_2 \rangle = 0, \quad (2)$$

where  $\langle \dots \rangle$  is the expectation value. The core of PCA is singular value decomposition (SVD). SVD of the data matrix  $\mathbf{x}$  ( $M \times N$ ) yields eigenvectors  $\mathbf{U}$  ( $M \times M$ ) in column-space and  $\mathbf{V}$  ( $N \times N$ ) in row-space connected by a diagonal matrix of singular values (SVs)  $\mathbf{\Lambda}$  ( $M \times N$ ),

$$\mathbf{x} = \mathbf{U}\mathbf{\Lambda}\mathbf{V}^T. \quad (3)$$

The columns of  $\mathbf{U}$  span column-space, the  $M$ -dimensional space of time slice number, and are called spatial patterns. The columns of  $\mathbf{V}$  span row-space, the  $N$ -dimensional space of turn number, and are called temporal patterns. The PCs are ordered by their SVs, which represent their strength.

### Independent Component Analysis (ICA)

The objective of ICA is to calculate the  $L$  source signals  $\mathbf{s}$  ( $L \times N$ ) given the data matrix  $\mathbf{x}$  ( $M \times N$ ), but the mixing

# BIG DATA ANALYSIS AND VISUALIZATION: WHAT DO LINACS AND TROPICAL STORMS HAVE IN COMMON?

E.W. Bethel\*, S. Byna, J. Chou†, E. Cormier-Michel‡, C.G.R. Geddes,  
M. Howison, F. Li, P. Prabhat, J. Qiang, O. Rübel, R.D. Ryne, M. Wehner, K. Wu  
LBNL, Berkeley, CA 94720, USA

## Abstract

While there is wisdom in the old adage “the two constants in life are death and taxes,” there are unavoidable truths facing modern experimental and computational science. First is the growing “impedance mismatch” between our ability to collect and generate data, and our ability to store, manage, and gain understanding from it. The second is the fact that we cannot continue to rely on the same software technologies that have worked well for the past couple of decades for data management, analysis, and visualization. A third is that these complementary activities must be considered in a holistic, rather than Balkanized way. The inseparable interplay between data management, analysis, visualization, and high performance computational infrastructure, are best viewed through the lens of case studies from multiple scientific domains, where teams of computer and scientists combine forces to tackle challenging data understanding problems.

## INTRODUCTION

Big data and its attendant challenges—managing it and gaining insight into its secrets—are the subject of a substantial amount of research and development in industry, academia, and the broader scientific community. These challenges are often cited as being among the greatest barriers facing scientific knowledge discovery [1].

Within the high performance visualization and analysis community, several different but complementary approaches contribute solutions to these challenges. One approach focuses on increasing the capacity of the data analysis and visualization processing pipelines [2], and recent results have shown such techniques capable of scaling to extreme concurrency for both production [3] and research codes [4].

An alternative approach is to focus instead on limiting visualization and analysis processing to the subset of data of interest where presumably the interesting subset is much smaller in size than the original data. Projects in this space have focused on blending index and query technologies from scientific data management with visualization and analysis tools to implement what is known as *query-driven visualization* [5]. This class of solution has proven applicable to diverse problems ranging from forensic cybersecurity [6] to accelerator modeling [7].

\* Corresponding author ewbethel@lbl.gov

† jchou@cs.nthu.edu.tw

‡ ecormier@txcorp.com

The focus of this paper is on the nexus between those two approaches with an eye towards enabling scientific insight. Three case studies, one from climate modeling and two from accelerator modeling, show how high performance computing technology and advances in visualization and analysis software infrastructure combine to provide new scientific data understanding capabilities brought to bear on problems that can be characterized as “large data analysis and visualization.”

## CASE STUDY: TROPICAL CYCLONES AND CLIMATE MODELING DATA ANALYSIS

As with many computational science domains, the study of climate and climate change, benefits from increasingly powerful computational platforms. Modern climate codes, which model processes in the atmosphere, ocean, ice caps, and more, produce massive amounts of data. As discussed below, when modeling the atmosphere at 0.25° resolution for a period of about two decades of simulation time, the CAM5.1 code [8] produces approximately 100TB of model output. These data sizes will only grow in size with time.

One challenge facing this computational science community is a rich legacy of visualization and analysis tools that are serial in implementation, yet such tools are not capable of processing modern-sized data sets due to memory constraints. Worse, such tools are often incapable of performing the type of analysis required to gain understanding in ever-larger and ever-richer collections of data.

Output from codes like CAM5—which sample and discretize both space and time in a regular fashion and are often generated by ensemble simulation experiments for varying physical input parameters and initial conditions—exposes data parallelism in many different ways to analysis and visualization tasks. Many types of visualization or analysis codes can be run independently, and in parallel, across individual ensemble members, timesteps, spatial regions, and individual grid points.

There are several pressing needs and challenges within the climate modeling community. First is the growing “impedance mismatch” between their ability to collect or generate data, and their ability to perform analysis and visualization on massive data sets. Second is the need to be able to quickly and easily create and test a variety of different types of quantitative analysis activities, such as spatiotemporal feature detection, tracking, and analysis. Third is the ability to execute such capabilities on large, parallel